



UNIVERSITÀ DEGLI STUDI DI MILANO
**FACOLTÀ DI SCIENZE MATEMATICHE,
FISICHE E NATURALI**

CORSO DI LAUREA MAGISTRALE IN FISICA

Topological characterization of a Spin Glass transition in a Random Boolean Hopfield Network

Relatore:
Prof. Sergio Caracciolo
Correlatore:
Pietro Rotondo

Tesi di laurea di
Andrea Papale
Matr. 842151
P.A.C.S: 05.70.-a

ANNO ACCADEMICO 2014-2015

Mi è parso che in realtà il calcolo significhi molto poco e comunque non abbia affatto tutta l'importanza che gli attribuiscono molti giocatori. Certi se ne stanno seduti davanti a pezzi di carta rigata, segnano tutti i colpi, li contano, ne deducono le probabilità, fanno i loro calcoli e alla fine puntano e perdono proprio come noi, semplici mortali che giochiamo senza calcolare niente.

F. Dostoevskij, Il giocatore

Contents

Introduction	vii
1 Complex Systems	1
1.1 What is a complex system?	1
1.2 Power Law distributions: a description for scale-free systems	1
1.2.1 Maximum likelihood estimator	3
1.2.2 Scale-free invariance in power law distributions	6
1.3 Power Laws in complex systems: Dragon Kings and Black Swans	7
1.4 Scale-free Networks: the Barabási-Albert model	9
2 Random Boolean Networks	11
2.1 Neural Networks	11
2.2 Random Boolean Network model	11
2.3 The Topology of Random Boolean Networks	12
2.4 How to define a dynamics	14
2.5 Dynamical observables	16
2.6 Order and chaos: phase transition in Random Boolean Networks	17
2.6.1 Analytical solution for criticality with the annealed approximation	22
3 Spin Glass	25
3.1 The Sherrington Kirkpatrick model	25
3.1.1 Quenched disorder and frustration	26
3.1.2 Quenched, annealed averages and selfaveraging	27
3.2 The replica method	28
3.3 Phase transition	29
3.4 Complexity in Spin Glass Theory	31
4 The Hopfield Model	35
4.1 Thermodynamics	36
4.2 The limit of finite p	38
4.2.1 Low temperature phase	39
4.3 Limit of finite α : from the retrieval to Spin Glass phase	42
4.3.1 Symmetric replica solutions	47
4.3.2 Ferromagnetic solutions at $T = 0$	48
4.3.3 Spin Glass solutions at $T = 0$	49
4.3.4 Finite temperature solutions	50

5	Topological characterization of a Spin Glass transition	53
5.1	The Inherent Structure Approach	53
5.2	Zero temperature synchronous dynamics: Boolean Hopfield Networks	55
5.3	Topological observables: a transition from compact to scale free networks	57
5.3.1	Indegree: from compact support distributions to power laws .	58
5.3.2	Google Rank: a numerical approach	65
5.4	Conclusions	70
	Bibliography	73

Introduction

This Thesis aims to study Spin Glass systems in order to characterize the phase transitions they exhibits with a topological approach.

Benchmark models of Spin Glasses are the Sherrington-Kirkpatrick model [1, 2] and the Hopfield model [3], the last one being originally introduced in the context of associative neural networks.

The Hopfield model is a spin model originally proposed in 1982 by John Hopfield as a simple toy model describing the behavior of memory in the human brain. Each boolean spin interacts with all the others through coupling constants defined starting from a set of p configurations, quenched randomly chosen variables, called *memories*. In the original paper, Hopfield defined an asynchronous dynamics where one randomly chosen neuron changes his state at each time step according to the variation of energy. In the thermodynamic limit, varying α , the ratio between the number of memories and the total number of spins, the model exhibits a peculiar behavior with two phase transitions corresponding to critical values α_{crit1} and α_{crit2} . For $\alpha < \alpha_{crit1}$ the system shows a retrieving phase where memories are minima of the free energy and attractors of the dynamics. For $\alpha > \alpha_{crit2}$, there is a Spin Glass phase: there is a total collapse of the capabilities of the memory. The only ground state is the Spin Glass state. Replica symmetry is broken and as a consequence each state has the fine structure of a full ultrametric tree. In addition for $\alpha_{crit1} \leq \alpha \leq \alpha_{crit2}$ the ground state is the Spin Glass state but the retrieval is still efficient [4].

In the last decade topological aspects of real glasses have been elucidated through numerical simulations for small systems. In particular the *Inherent Structure Approach* [5] allows to model complex systems as networks: it combines the techniques of networks analysis to the usual techniques of complex systems theory in order to outline the global structure of potential energy landscapes. This method has been exhaustively used to investigate topological properties of classical particles interacting through Lennard-Jones potential [6]. For such kind of continuous systems, the potential energy landscape is a multi-dimensional configuration space where the potential energy is a function of the positions of all the atoms. The landscape of a system with many atoms will have a complex topography with higher-dimensional minima, saddles and barriers. According to this approach the landscape can be partitioned into basins of attraction surrounding each minima. Local minima can thus be organized in a graph (where they are represented as the vertices) and connected whenever a first order saddle-point exists connecting any couple of them. Interestingly this graph has the property to be *small-world* and with power-law degree distribution. The emergence of this complex network is probably an hallmark of the

complex nature of the glassy phase.

In discrete models of Spin Glass, such as Sherrington-Kirkpatrick or Hopfield, this topological approach is non-trivial to be generalized, lacking a well-defined notion of metric. In this thesis we try to overcome this problem in order to characterize phase transition through topological properties. The main idea is to define a synchronous dynamics on the discrete phase space of spin configurations. This space can be organized as a network where each configuration is a vertex directly connected to another one according to a deterministic dynamics. This step gives rise to a new class of Random Boolean networks, generalizing the ones introduced by Kauffman in the context of gene regulation and evolution [7].

This approach allows to define univocally a topology on the phase space which can be characterized through topological properties arising from such networks like the number of incoming connections of each node, the *indegree* or the *Google Rank*, a parameter describing the weight of each node compared to the entire network.

The main results are related to the Hopfield model with a zero temperature synchronous dynamics. This dynamics, according to the method inspired from the Inherent Structure Approach, generates the class of *Random Boolean Hopfield Networks*. For this kind of networks the distribution of the indegree shows clearly different properties varying the number of the initial memories of the system. In the phase characterized by a few number of memories the distribution exhibits a coexistence of a compact distribution and a peak. This kind of outlier is called *Dragon King* [8]: according to Sornette the presence of Dragon Kings in complex systems reveals the existence of mechanisms of self-organization that otherwise is not possible to observe from the distribution of the other events and could be associated to phase transitions. In this particular Random Boolean Network, the peak in the distribution of indegree is a consequence of a condensation of configurations which converge to a limited number of configurations, which results to be memories. In this particular case, Dragon King is present only at this stage and is reabsorbed by increasing the memories until it disappears completely in the full Spin Glass phase where the indegree distribution exhibits only a power law.

The number of configurations grows as 2^N and an exact enumeration of states is not realistic. Then it is necessary to introduce a new topological observable: the Google Rank.

The Google Rank has been developed in order to quantify numerically the relative importance of an element of network within the network itself in the context of web searching. A surfer is placed on a randomly chosen vertex of the network. Then its position is changed according to the following dynamics: for d times the surfer jumps to the neighboring vertex according to the synchronous spin dynamics. Then the surfer gets bored and starts again from a randomly selected vertex.

Even the Google Rank suggests the presence of a collective behavior characterized by the phase transition described so far. Again, in the ordered phase, the rank plot exhibits a distinct plateau consisting of configurations corresponding to the memories, and a compact distribution. This plateau is directly linked to the Dragon King in the distribution of indegree. Instead it shows a power law in the spin-glass phase.

It is important to underline how these topological considerations are sufficient to characterize qualitatively the phase transition in the contest of Random Boolean

Networks as a concrete alternative to the standard approach using overlap between configurations and local magnetization as order parameters. We will present strong evidences of the presence of a phase transition in the context of networks theory: Random Boolean Hopfield Networks exhibit a transition from *compact networks* in the regime of few memories to *scale free networks* in the Spin Glass phase. This transition will be characterized in terms of the distributions of connectivities: the properties of such systems change substantially varying α , the rate between the number of memories p and of spins N . The collective behavior originating from Hopfield model emerges clearly also in this approach of network analysis: transitions from compact distributions to power law distributions which are present both for indegrees and for Google Ranks are fundamental mainstay of this work. Dragon Kings in indegree distributions and plateaus obtained with Google Rank complete the description of the few memories phase: networks condenses to a regime where the most of configurations converges to a limited number of configurations, the memories. Memories are definitively the attractors of the dynamics and coincide to the absolute minima of the Hamiltonian. The resulting scale-free topology of the Spin Glass phase in Boolean Hopfield Networks suggests a reflection on global optimization, the task of locating the global minimum. In the Spin Glass phase attractors are also the minima of the Hopfield Hamiltonian and searching the global minimum is a NP-hard problem. As we will see, scale-free networks suggest that the correlation between the minimum of the Hamiltonian and the highest indegree as a possible inspiration for approach NP-hard problems.

In particular the thesis begins with an introduction to complex systems with a focus on power law distributions and on the concept of Dragon King. Then an exhaustive review of the properties of Random Boolean networks is reported: the main analytical results are presented and numerical results are replicated. The next chapter is dedicated to the general theory of Spin Glass, in particular of the Sherrington Kirkpatrick model with the replica approach by Parisi. Moreover the Hopfield model is widely discussed: the statistical mechanics properties, investigated by Amit, Gutfreund and Sompolinsky in the context of Spin Glass theory with the replicas approach, are deeply analyzed. The last chapter of the thesis is devoted to the topological characterization of Spin Glass transition in the Hopfield model. The distribution of indegree is obtained through an exact enumeration of states only for small systems ($N \leq 30$) for computational reasons while the Google Rank has been performed for bigger systems (up to $N = 500$).

Chapter 1

Complex Systems

1.1 What is a complex system?

Nowadays physics is able to describe a large number of phenomena with precision and simplicity. In many cases properties of individual elements can be exhaustively described but these results have a negligible role in predicting the behavior of large scale interconnected systems. In general the collective behavior of the interacting parts of a system cannot be inferred as a simple combination of the properties of the parts but arise as an emergent property of the system. This is the case of *complex systems* [9, 10].

The founding principle of the complex systems theory is well summarized by a famous quote from Aristotle taken from his *Metaphysica*: "the whole is more than the sum of its parts".

There is a large collection of real complex systems which cross the physical, biological and social worlds: interacting atoms or molecules, cars in traffic, interacting species in an ecosystem, the World Wide Web, interacting genes or cells, the neurons that make up the brain as we will see later in details.

In these examples and more in general in these disciplines, the complex systems approach brings to remarkable progresses and showed the limits of the usual approach: decomposing a system in parts in order to understand the behavior of the entire system in connection to the behavior of each component is no more enough to have a complete view [11]. In other words, the study of the basic principles cannot replace a detailed description of particular complex systems. However, universal principles and symmetries still simplify the study of the specific case.

One of the emergent properties of complex systems is that rare events occur with a finite non-negligible probability. Before deepening this last statement it is useful a short remark about power law distributions.

1.2 Power Law distributions: a description for scale-free systems

Many empirical observables converge to an expectation value. Ordinarily they have distributions which implies a negligible probability to be far from the typical value.

In nature, there are some kind of phenomena described by distributions which exhibits a totally different behavior which results difficult to be characterized starting from scientific observations.

This last property can be assumed as a sign of a self-organizing mechanisms at the origin of a hierarchy of scales in complex systems [11].

Among these distributions, *power law* deserves a deepening for its uncommon mathematical properties and the surprising physical phenomena [12]. This kind of distributions cannot be satisfactorily described only by an expectation value because their values typically vary by several order of magnitude in their own range.

Mathematically, an observable x which obeys a power law, has a probability distribution like

$$p(x) \propto x^{-\alpha},$$

where α is a the *exponent or scaling parameter*. This parameter typically varies in the range $2 < \alpha < 3$.

Few empirical phenomena exhibit power law for all values of x . More often the power law distribution is valid only for values greater than some minimum x_{min} . In this the case only the *tail* of the distribution is a power law.

Assuming now x as a continuous variable, then it is possible to describe a continuous power law through a probability density:

$$p(x) dx = Pr(x \leq X < x + dx) = Cx^{-\alpha} dx,$$

where X is the observed value and C the normalization constant. The last equation diverges as $x \rightarrow 0$ and clearly there must be a bound x_{min} . Then, assuming $\alpha > 1$, it is possible to evaluate the normalization constant after having integrate the distribution:

$$p(x) = \frac{\alpha - 1}{x_{min}} \left(\frac{x}{x_{min}} \right)^{-\alpha}.$$

In the discrete case, the probability distribution is proportional to the generalized or Hurwitz zeta function [12]:

$$\zeta(\alpha, x_{min}) = \sum_{n=0}^{\infty} (n + x_{min})^{-\alpha} \quad (1.1)$$

and the power law results:

$$P(x) = \frac{\zeta(\alpha, x)}{\zeta(\alpha, x_{min})} \quad (1.2)$$

Formulas of continuous distributions are usually simpler than those for the discrete distributions and exhibit a common behavior with discrete power law. So the continuous approximations for the discrete power law will be used in the following section.

Cumulative distributions with a power law form are sometimes said to follow *Zipf's law* or a *Pareto distribution* after two early researchers who championed their study. Since power law Cumulative distributions imply a power law form for the probability distributions, Zipf's law and Pareto distribution are effectively synonymous with power law distribution. Zipf's distribution and Pareto distribution differ from one another in the way the cumulative distribution is plotted - Zipf made

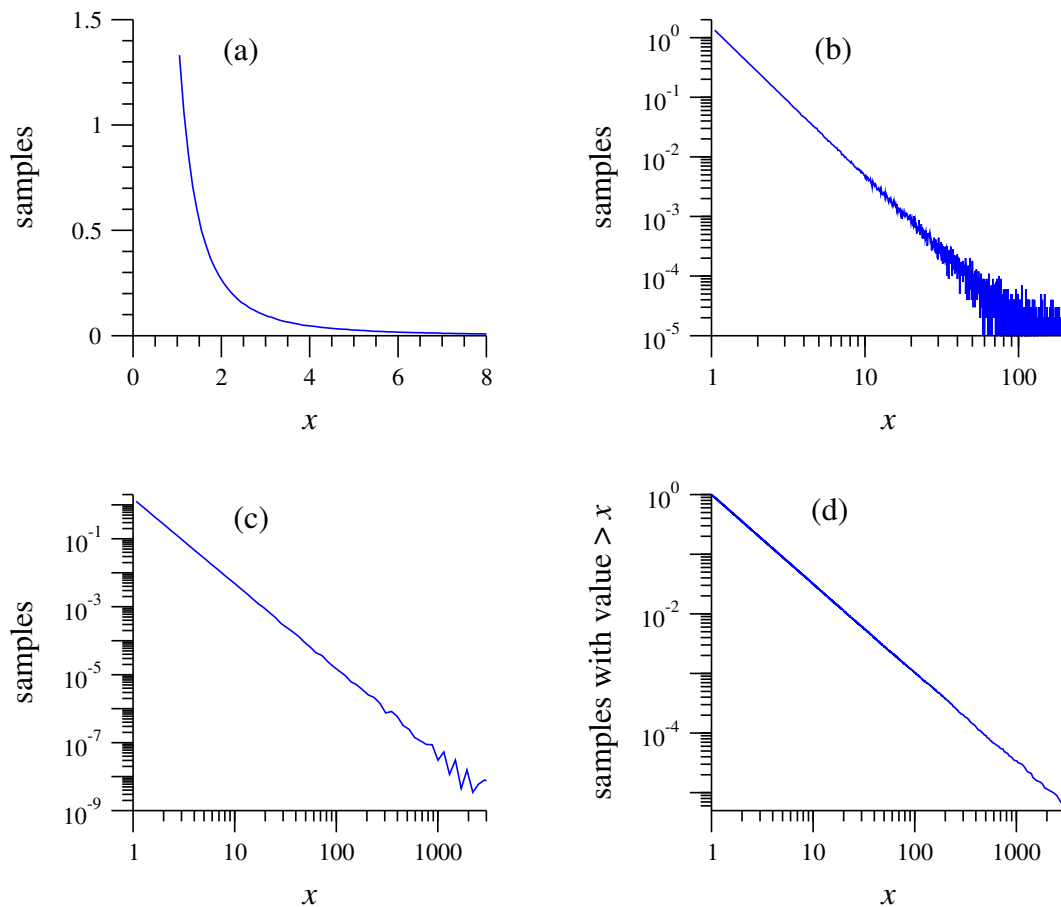


Figure 1.1: **Example of a power law distribution:** this example shows a set of 1 million random real number generated according to a power law probability distribution $p(x) = Cx^{-\alpha}$ with scaling parameter $\alpha = 2.5$. (a) Histogram obtained with the random data. (b) The same histogram on logarithmic scales. It is important to underline how the noise results to be relevant in the tail of the distribution. (c) Histogram of frequencies with a logarithmic binning. (d) A *Zipf*, a cumulative histogram of the same data. This cumulative distribution is again a power law with exponent $\alpha - 1 = 1.5$. This image is reproduced from [15].

his plots with x on the horizontal axis and $P(x)$ on the vertical one. Pareto did it the other way around.

1.2.1 Maximum likelihood estimator

Now let us consider the correct way to fit a power law distribution. Taking the logarithm of a power law distribution, $\ln p(x) = \alpha \ln x + \text{constant}$, the result will be a straight line in a logarithmic plot.

The typical approach to this problem is to construct a histogram of the data and to estimate the scaling parameter using the least squares linear regression on the linear form of the logarithmic histogram.

Unfortunately this kind of procedure is subject to systematic large errors: the

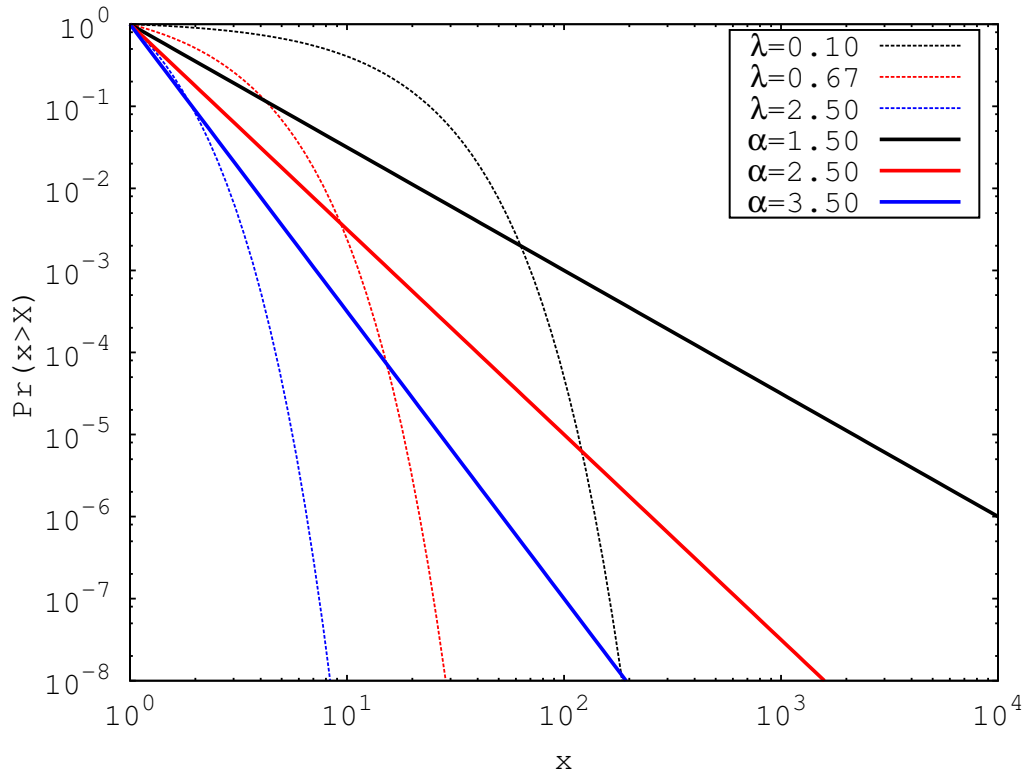


Figure 1.2: **Power law and exponential distributions:** this example shows a comparison between the different behavior of cumulative distributions in case of power law and exponential distributions for different values of parameters. The power law distributions are plotted with continuous lines while the exponential distributions with dashed lines. The normalization is such that $x \geq x_{min} = 1$.

assumption of linear regression implies that the dependent variable is affected by an independent, gaussian noise at each value of the independent variable. In the case of the power law, fitting the logarithm of a histogram, the noise is still independent but no more gaussian. In order to have gaussian fluctuations for $\ln p(x)$, it is necessary that $p(x)$ has log-normal fluctuations which violate the central limit theorem.

In conclusion linear regression formulas for the error are not applicable in this case.

An effective method to estimate the scaling parameter is then the *maximum likelihood estimator*. In order to estimate the most likely value of the scaling parameter α for the given data, let us consider again the continuous power law distribution,

$$p(x) = \frac{\alpha - 1}{x_{min}} \left(\frac{x}{x_{min}} \right)^{-\alpha},$$

and a set of n observations $x_i \geq x_{min}$. The probability that the data were described by the model is proportional to

$$p(x|\alpha) = \prod_{i=1}^n \frac{\alpha - 1}{x_{min}} \left(\frac{x}{x_{min}} \right)^{-\alpha}.$$

This probability is called *likelihood* of the given data. The data are most likely to have been generated by the model with scaling parameter α which maximize this function. Then we consider the logarithm of the likelihood \mathcal{L} which presents its maximum in the same value:

$$\begin{aligned}\mathcal{L} &= \ln p(x|\alpha) \\ &= \ln \prod_{i=1}^n \frac{\alpha - 1}{x_{min}} \left(\frac{x}{x_{min}} \right)^{-\alpha} \\ &= \sum_{i=1}^n \left[\ln(\alpha - 1) - \ln x_{min} - \alpha \ln \frac{x_i}{x_{min}} \right] \\ &= n \ln(\alpha - 1) - n \ln x_{min} - \alpha \sum_{i=1}^n \ln \frac{x_i}{x_{min}}.\end{aligned}$$

Let us set $\frac{\partial \mathcal{L}}{\partial \alpha} = 0$ in order to maximize the likelihood and solve for α . The estimate scaling parameter results:

$$\hat{\alpha} = 1 + n \left[\sum_{i=1}^n \ln \frac{x_i}{x_{min}} \right]^{-1}.$$

If the data are independent, identically distributed from a distribution with parameter α , then as $n \rightarrow \infty$, $\hat{\alpha} = \alpha$.

In order to evaluate the expected error let us rewrite the probability as

$$p(x|\alpha) = \left(\frac{\alpha - 1}{x_{min}} \right)^n e^{-b\alpha},$$

where $b = \sum_{i=1}^n \ln \left(\frac{x}{x_{min}} \right)$. Assuming again that $\alpha > 1$ in order to have a normalizable distribution, the mean and the mean square of α are given by:

$$\begin{aligned}\langle \alpha \rangle &= \frac{\int_1^\infty e^{-b\alpha} (\alpha - 1)^n \alpha d\alpha}{\int_1^\infty e^{-b\alpha} (\alpha - 1)^n d\alpha} \\ &= \frac{e^{-b} b^{-2-n} (n + 1 + b) \Gamma(n + 1)}{e^{-b} b^{-1-n} \Gamma(n + 1)} \\ &= \frac{n + 1 + b}{b}\end{aligned}$$

and

$$\begin{aligned}\langle \alpha^2 \rangle &= \frac{\int_1^\infty e^{-b\alpha} (\alpha - 1)^n \alpha^2 d\alpha}{\int_1^\infty e^{-b\alpha} (\alpha - 1)^n d\alpha} \\ &= \frac{e^{-b} b^{-3-n} (n^2 + 3n + b^2 + 2b + 2nb + 2) \Gamma(n + 1)}{e^{-b} b^{-1-n} \Gamma(n + 1)} \\ &= \frac{n^2 + 3n + b^2 + 2b + 2nb + 2}{b^2}.\end{aligned}$$

Then the variance of α results:

$$\begin{aligned}\sigma^2 &= \langle \alpha^2 \rangle - \langle \alpha \rangle^2 \\ &= \frac{n^2 + 3n + b^2 + 2b + 2nb + 2}{b^2} - \frac{(n + 1 + b)^2}{b^2} \\ &= \frac{n + 1}{b^2}.\end{aligned}$$

In conclusion, the error on α is

$$\sigma = \frac{\sqrt{n+1}}{b} = \sqrt{n+1} \left[\sum_i \ln \frac{x_i}{x_{min}} \right]^{-1} = \frac{\sqrt{n+1}}{n} (\alpha - 1)$$

An analogous result can be obtained for discrete variables.

1.2.2 Scale-free invariance in power law distributions

A power law distribution is sometimes called a *scale-free distribution* because is the only distribution which exhibits the property of *scale invariance*. This kind of probability distribution $p(x)$ has to satisfy the property that

$$p(bx) = g(b)p(x), \quad (1.3)$$

for any b . Changing the scale or the units of x by a constant factor b , the shape of the distribution has to remain unchanged, except for a multiplicative factor.

Therefore this property can be analyzed more clearly studying the logarithm of the likelihood \mathcal{L} :

$$\begin{aligned}\ln p(x) &= \ln \left[\frac{\alpha - 1}{x_{min}} \left(\frac{x}{x_{min}} \right)^{-\alpha} \right] \\ &= \ln [(\alpha - 1) x_{min}^{\alpha-1}] - \alpha \ln x \\ &= \ln C - \alpha \ln x.\end{aligned}$$

This result shows that a rescaling $x \rightarrow bx$ only shifts the power law up or down on a logarithmic scale. In practical terms, this means that the same principles or processes are at work no matter what the scale of analysis.

Moreover it is possible to demonstrate that a power law distribution is the only distribution which exhibits the scale free property. Let us consider again the equation (1.3), setting $x = 1$ gives $p(b) = g(b)p(1)$. Equation (1.3) can be written as

$$p(bx) = \frac{p(b)}{p(1)} p(x).$$

The differentiation respect to b , setting p' the derivate of p respect to its argument, gives:

$$xp'(bx) = \frac{p'(b)}{p(1)} p(x).$$

Now setting $b = 1$ gives:

$$x \frac{dp}{dx} = \frac{p'(1)}{p(1)} p(x).$$

This first-order differential equation has the solution

$$\ln p(x) = \frac{p(1)}{p'(1)} \ln x + \text{const.}$$

The exponential of the solution gives

$$p(x) = p(1) x^{-\alpha}$$

where $\alpha = -\frac{p(1)}{p'(1)}$. In conclusion this result asserts that the power law distribution is only function which satisfy the scale free property.

1.3 Power Laws in complex systems: Dragon Kings and Black Swans

There are several complex systems which are statistically characterized by power-law distributions. The population of cities, the intensities of earthquakes, the flux of meteorites, the area of fire or wildfire [13], relaxing times in spin glasses [14] or scale free networks are all characterized by a power law distribution.

As seen before, a power law distribution imply that extreme events are occurring with a finite non-negligible probability. From the opposite point of view, these extreme events has not more considered as particular cases: belonging to the same statistical distribution suggest that the physical process which generates them is the same of other events. In other words, if a given event with evident properties, like a great earthquake, belongs to a set of events described by a power law distribution, there are no possibilities to predict such a particular event because it shares all characteristic of other events. This concept is the foundation of the "Black Swan Theory" [16], which describe high impact rare events as unpredictable.

Now let us consider, as an example, the particular case of the population size of French cities [17] (see figure 1.3).

In general, the distribution of city sizes exhibits a power law distribution and France, is not an exception. Moreover French cities result to be a very peculiar case because the capital, Paris, is completely out of range. The size is several order larger than expected from the distribution of the rest of the population of cities. Sornette called this characteristic *Dragon King* [8]: it is been defined as the outlier which coexists with a power law distribution.

The rank-ordering plot of the sizes S of French cities (raised to the exponent $c=0.18$), ordered by descending sizes is plotted in figure 1.3 as a function of the city rank, in a logarithm scale.

The continuous black line is the exponential distribution $\exp[-(S/S_0)^c]$. Exponential distributions, in the limit when c is much smaller than 1, degenerate into power law distributions with finite scaling exponent.

In this case, the exponent $c = 0.18$ is small and can be shown that the resulting power law has a scaling exponent $\alpha \approx 2$ (see again [8] for details).

According to Sornette paper, Paris is not only a spurious outlier which could be ignored. Paris has historically covered a important role as organizational center for French governments. This crucial position has implied its dragon-king status

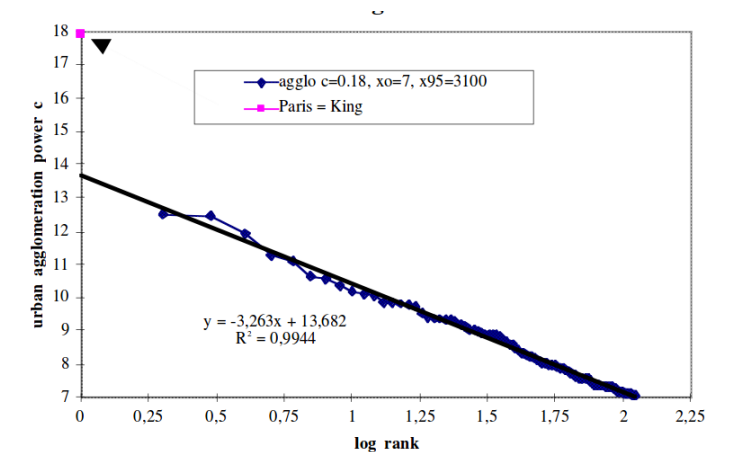


Figure 1.3: **Rank-ordering plot of the population size of French cities as a function of their rank:** the sizes are ordered in decreasing values. For the ordinate, the city size is raised to the power $c = 0.18$ and the abscissa represents the logarithm of the rank. The continuous black line plotted is the exponential distribution $\exp[-(S/S_0)^c]$. The arrow shows the data point for Paris which result to have a size larger than expected. This kind of outlier is called *Dragon King*: it coexists with power laws in the distributions of event sizes. Dragon-kings reveal the existence of mechanisms of self-organization that otherwise is not possible to observe from the distribution of the other events. This image is reproduced from [17].

observed in the statistical distribution of French city sizes. Again London exhibits a similar dragon-king role with respect to the distribution of British city sizes. In conclusion Sornette presents a large number of examples which suggest that the dragon-king status emerges in general from the existence of positive feedbacks, that amplify the role of certain events.

Dragon kings belong to a statistical set of events which have different probability distribution from the nucleus of other events which exhibits the power law distribution. This observation is a consequence of the privileged role covered by dragon kings: their key role is due to a characteristic mechanisms of the analyzed system. Consequently an extreme event cannot be more considered only as a particular event which happens at a specific scale: now it is a dragon king, an outlier which emerges between the other possible events only in its exact collective regime.

More in general, in statistical physics as in complex systems theory the properties of different regimes and their transitions are matter of study. In fact, a large variety of complex systems exhibits qualitative changes of regimes in their characteristics and dynamics under the smooth variations of some order parameters or changing the network topology. Sornette suggests that Dragon kings could cover an interesting role in this context. The presence of a dragon king is strictly related to a collective regime with specific properties. Since different collective organizations are in general associated to completely different regimes, the possibility to relate the appearing of dragon kings to a phase transition cannot be neglected. In particular, Sornette shows as examples of phase transitions characterizable through the presence of dragon kings the crashes of financial bubbles and the acoustic emission recorded as stress on tanks

embarked on rockets [8].

In conclusion dragon-kings are evidences of the existence of mechanisms of self-organization which otherwise is not possible to observe from the distribution of the other events.

This observation involves that extreme events occur much more often than would be predicted or expected from the observations of small, medium and even large events. Thus, dragon kings allow to predict the presence of this kind of mechanisms. Moreover it is possible to use this concept as a parameter characterizing different regimes of a complex system and in order to diagnose its behavior under smooth changes of some control variables.

1.4 Scale-free Networks: the Barabási-Albert model

In the context of complex systems there is a class of complex networks characterized by the existence of a high degree of self-organization. In particular we present the Barabási-Albert model of scale-free networks [18]. This model is inspired from the most important principles shared by real networks: the *growth* and the *preferential attachment*. Starting from a limited number of nodes, real networks usually grow during their entire lifetime. In addition new nodes do not make edges completely random but following some rules. These observations are the basic elements of the Barabási-Albert model. This kind of networks are produced according to the following algorithm: starting from a small number n_0 of nodes, at every time step, the network gains a new node with m edges ($m \leq n_0$) that connect the new nodes with m different nodes already present in the system. These edges are not chosen randomly: a connection between the new node and a node i depends on the degree k_i of the node i according to the following probability:

$$p(k_i) = \frac{k_i}{\sum_j k_j}.$$

Consequently after t time steps, the resulting network will have $n = n_0 + t$ nodes and mt edges. Numerical simulations show that this kind of networks is scale invariant and the probability distribution of the degree of given node i follows a power law with scaling exponent $\gamma_{BA} = 3$. Moreover this last exponent is independent of m , the only parameter of this model.

It is possible to characterize the scale invariance of the Barabási-Albert model analytically with various approaches: the *continuous theory* by Barabási and Albert, developed from the dynamics of the node degree, the *master equation approach* by Dorogovtes, Mendes and Samukhin and the *rate-equation approach* by Krapivsky, Redner and Leyvraz are methods which give satisfactory results [19].

In particular Albert and Barabási characterize numerically the average path length of a scale-free network generated according to their model as a function of the network size N . Barabási-Albert networks show an average path length smaller than random graphs for any N : the heterogeneous scale-free topology results more efficient in bringing the nodes close than an homogeneous topology such as that of random graphs [19]. An analytical by Bollobás and Riordan [20] demonstrate that this average path length increases approximately less than logarithmically with N ,

like $l \sim \ln(N)/\ln\ln(N)$. According to this result it is possible to affirm that scale-free networks are also *small-world* networks in the sense that the average path length grows less than logarithmic increasing N .

Chapter 2

Random Boolean Networks

2.1 Neural Networks

Human brains are made up of about 100 billion neurons. Each neuron is connected to thousands neurons and communicates with electrochemical signals through synapses. A neuron receives continuously signals from these connections: if the sum of its inputs is greater than some threshold value, the neuron generates a voltage and fires a signal. The human brain thus can be described as a biological neural network: interconnected neurons constitute a network where electrical signals and complicated patterns are transmitted.

Artificial Neural Networks are an statistical learning models that are inspired by this kind of biological nervous systems, such as the brain.

The key element of these models is the information processing system: a large number of highly interconnected processing elements, neurons, works together to solve specific problems. These connections are weighed and can be tuned based on experience, making neural networks adaptive to inputs and capable of learning.

In this context it is useful to introduce the model of Random Boolean Networks which has been introduced in order to model certain properties of biological neural networks like gene regulation in organisms.

2.2 Random Boolean Network model

Random Boolean Networks (RBNs) are models developed by Stuart Kauffman in 1969 [7, 21] in order to describe gene regulation.

In living organisms, genes interact with each other via proteins, but since there is a great variety of them, genetic regulation is not completely understood so far. RBNs were originally proposed in order to overcome this kind of problem [22, 23]: the genome thus could be described as a network of interacting genes where one gene influences the functionality of the genes it is connected to in the network. *Escherichia Coli* [24] and yeast [25, 26] are examples of biological systems whose behavior is well described using Random Boolean Networks.

According to this model, the genome is a random dynamic network where each gene is represented by a node and a biological relationship of activation or inhibition between genes is indicated by an edge between two vertices.

The main benefit of using Random Boolean Networks in biological systems is the possibility to study the nature of self-organization and to analyze how a given perturbation to a system can affect its global behavioral properties.

Mathematically a Random Boolean Network is a directed graph $G = (V, E)$, defined by a set $V = \{\sigma_1, \sigma_2, \dots, \sigma_N\}$ of N vertices or nodes together with a set $E = \{(\sigma_i, \sigma_j)\}$ of edges or links, which are ordered pairs of the vertices. Each element σ_i admits one of the two possible boolean states, $\sigma_i \in \{0, 1\}$ $i = 1, \dots, N$. The set of variables which each element σ_i depends on in the dynamics are established by the links between these nodes. The number of ingoing edges that a node receives is called *connectivity*. In general self-connections are allowed.

A Random Boolean Network is fully specified by giving its topology and its dynamical rules [27]. The topology of a graph is completely defined by choosing the number N of its elements, the number of inputs K_i which each element σ_i receives and specifying how the linkage and how these connectivities are assigned to each element. The dynamical rules are boolean functions describing how states of nodes change with time evolution.

Since each node has two possible states, the network has 2^N possible configurations. Thus the system has a finite state space where each configuration can be represented as a boolean string of $\{\sigma_i\}$. The topological properties of the state space will be deeply analyzed in the following sections.

2.3 The Topology of Random Boolean Networks

In the most general case, connectivities K_i vary from one element to another and links are chosen according to certain distribution of probability. Consequently it is useful to define the mean connectivity, $\langle K \rangle$, as a parameter which characterizes the behavior of such networks:

$$\langle K \rangle = \frac{1}{N} \sum_{i=1}^N K_i.$$

The dynamics of this kind of systems depends strongly on the way the edges between nodes are been chosen. Given a node, each element of the graph, including itself, may have the same probability of making up one of the K_i possible edges. This is called an *uniform* assignment. Otherwise, all nodes can be arranged on a regular lattice: the K_i links relative to every nodes may be chosen randomly from the set of the nearest neighbors on the lattice. This is a *lattice* assignment. Obviously various other choices are possible: for example, in a system where linkages are chosen according to a power-law probability distribution, some nodes are linked to far-away elements and others to neighboring elements. This is the case of *scale-free* networks [28].

A Random Boolean Network such that all connectivities are chosen equal to a fixed value K and each element has the same probability to constitute an edge, is called *Kauffman network* or $N - K$ model.

In this chapter, everywhere it is not specified, we will assume to study a Kauffman network.

For a given number of N nodes and a given connectivity K per node, the topology of a Kauffman network is completely defined by choosing the K edges of each

node randomly among all nodes, included the node itself. In this case, these connections are chosen randomly and are quenched: they remain fixed during the entire dynamics. Moreover, since each node can be linked to each other, there are N ways to select the first edge, $N - 1$ ways for the second and $N - K + 1$ for k -th edge. Consequently a Kauffman network can assume

$$\left(\frac{N!}{(N - K)!} \right)^N$$

possible configurations.

The set of all possible graphs topologically different with N and K fixed is called the *ensemble* of the network. All possible topologies which are part of the ensemble can have different degenerations and different statistical weights.

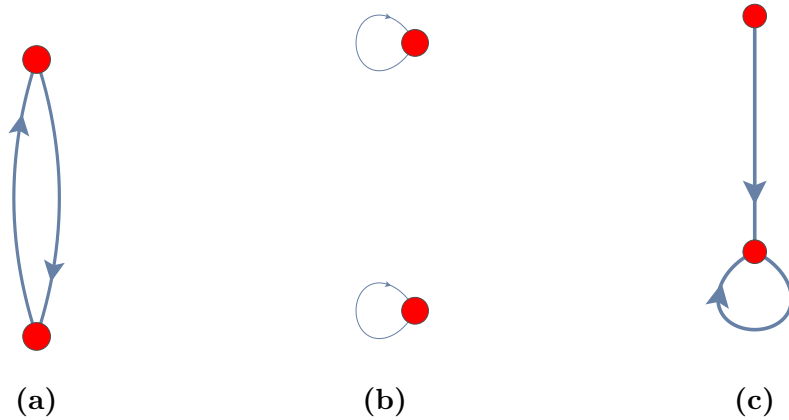


Figure 2.1: **The ensemble of the possible topologies of Kauffman networks for $N = 2$ and $K = 1$:** the set of all possible graphs with fixed N and K which are topologically different is the *ensemble* of a network. In this case there are 4 possible graphs but only 3 possible topologies: (a) and (b) appear only one time in the ensemble and have the same statistical weights $\frac{1}{4}$. Whereas topology (c) has the weight $\frac{1}{2}$ because there are two different ways to chose which node has a self-link. Graphs are plotted with Mathematica [63].

Let us consider as a simple case, the ensemble of Kauffman networks for $N = 2$ and $K = 1$. There are $\left(\frac{2!}{(2-1)!} \right)^2 = 2^2 = 4$ possible graphs but only 3 different topologies are possible (this example is shown in Figure 2.1). Both topologies (a) and (b) appear only one time and have the same statistical weights $\frac{1}{4}$. Whereas topology (c) has the weight $\frac{1}{2}$ because there are two possible graphs with such shape: either of the two nodes can be the one with a self-link.

We now discuss another example, the Kauffman network with $N = 3$, $K = 1$. The set of all possible topologies of this example is shown in Figure 2.2. This kind of networks has $\left(\frac{3!}{(3-1)!} \right)^3 = 3^3 = 27$ graphs but it admits only seven different topologies.

Topologies (a) and (f) have the weight $\frac{3}{27}$ because they have one self-link and either of the three nodes can be the one with it. (b), (c) and (e) have weight $\frac{6}{27}$.

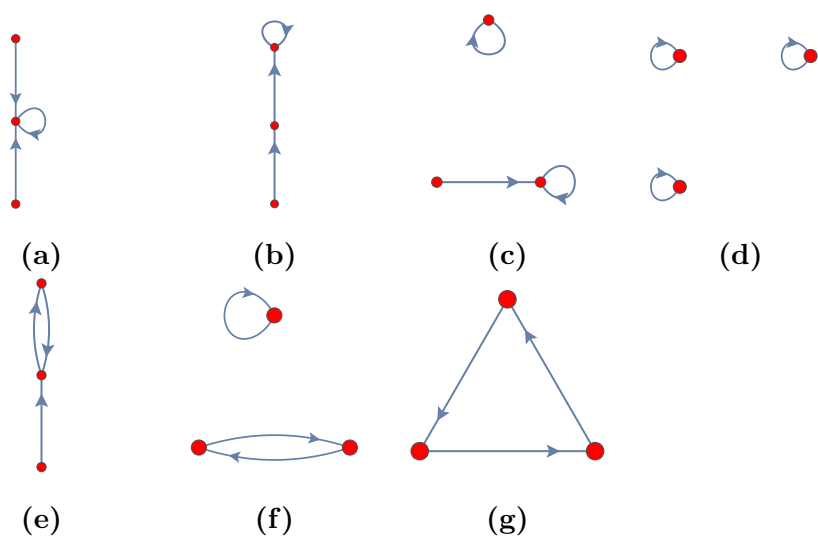


Figure 2.2: **The ensemble of the possible topologies of Kauffman networks for $N = 3$ and $K = 1$.** In this case there are 27 possible graphs but only 7 possible topologies: (a) and (f) have the weight $\frac{3}{27}$ because there are two possible ways to chose which node has a self-link. (b), (c) and (e) have weight $\frac{6}{27}$. Topology (d) appear one time in the ensemble and its statistical weight is $\frac{1}{27}$. Finally (g) is invariant under the contemporaneous change of the direction of all the edges and consequently has a weight of $\frac{2}{27}$. Graphs are plotted with Mathematica [63].

Topology (d) appear one time and its statistical weight is $\frac{1}{27}$. Finally (g) is invariant under the contemporaneous change of the direction of all the edges and consequently has a weight of $\frac{2}{27}$.

Moreover while the number of inputs of each node is fixed by choosing the connectivity K , the number of outgoing links for each node varies between the nodes. The mean number of outputs must be again K , since the total number of outgoing links must be equal to the total number of ingoing links.

In particular a given node become an input of each other nodes with probability $\frac{K}{N}$. the probability distribution of outgoing links thus is a Bernoulli distribution:

$$P_{out}(l) = \binom{N}{l} \left(\frac{K}{N}\right)^l \left(1 - \frac{K}{N}\right)^{N-l}$$

In the thermodynamic limit $N \rightarrow \infty$ the probability tends to a Poisson distribution:

$$P_{out}(l) = \frac{K^l}{l!} e^{-K}.$$

2.4 How to define a dynamics

The dynamical rules of a Random Boolean Network are a crucial topic in this context. The value which each node assumes at time t is determined only by the states of its K inputs $\{\sigma_i\}$ at time $t - 1$:

$$\sigma_i(t) = f_i(\sigma_1(t-1), \sigma_2(t-1), \dots, \sigma_K(t-1)).$$

f_i is a Boolean function, $f_i : \{0, 1\}^K \rightarrow \{0, 1\}$, for the i^{th} element which depends on K arguments. The boolean functions f_i associated to each element σ_i are randomly chosen between all possible functions.

Now let us consider the case of a Kauffman network in detail. In general, a given boolean function of K arguments can take on 2^K different values. It is completely determined by giving, for each of these values of the arguments, a value to the function. Consequently there are 2^{2^K} different boolean functions. As seen before, each node has $\frac{N!}{(N-K)!}$ possible ordered combinations for K different edges. Therefore, given N and K , the number of all possible Kauffman networks is

$$\left(2^{2^K} \frac{N!}{(N-K)!}\right)^N.$$

Note that many of these graphs will be equivalent.

Below boolean functions for some values K will be analyzed.

For $K = 0$, there are two possible functions, the tautology $f = 1$ and the contradiction $f = 0$. Together they constitute the class of the *constant* functions \mathcal{C} .

Input	Class \mathcal{K}		Class \mathcal{R}	
	\mathcal{K}_0	\mathcal{K}_1	\mathcal{R}_I	\mathcal{R}_N
0	0	1	0	1
1	0	1	1	0

Table 2.1: **The Boolean functions of one argument.** The first column lists the possible states of the input, the other columns represent all possible outputs, divided into two classes.

Instead the possible boolean functions with one argument, $K = 1$, are four and are divided into two classes. Table (2.1) shows these functions. The first two functions constitute again the class of constant functions \mathcal{K} such that the resulting state is independent of its input. The other two functions are the identity $f(\sigma) = \sigma$ and the negation $f(\sigma) = -\sigma$. They make up the class of *reversible* functions \mathcal{R} .

		Class \mathcal{K}		Class \mathcal{C}_1				Class \mathcal{C}_2						Class \mathcal{R}					
0	0	1	0	0	1	0	1	1	0	0	0	0	1	1	1	1	1	0	
0	1	1	0	0	1	1	0	0	1	0	0	1	0	1	1	0	1	0	1
1	0	1	0	1	0	0	1	0	0	1	0	1	1	0	1	0	1	0	1
1	1	1	0	1	0	1	0	0	0	0	1	1	1	1	1	0	1	0	0

Table 2.2: **The Boolean functions of two arguments.** The first column lists the four possible states of the input, the other columns represent all possible outputs, divided into four classes.

For $K = 2$ the situation is a bit more complicated. There are four class of these functions. There are again two constant and two reversible functions. Moreover there are twelve *canalizing* functions. A function is canalizing if at least for one of the values of its arguments the results is fixed, independently of the values of the other inputs. These functions are divided in two classes according to the number of

arguments on which they depend. The class of canalizing functions \mathcal{C}_1 which depend on only one of the arguments is made up by functions which simple copy or invert the value of one of the inputs. The second class \mathcal{C}_2 of canalizing functions that depend on the two arguments has only functions with three times 1 or three time a 0 in its output. All these functions are shown in table (2.2).

Every time the functions f_i and the set of connectivities are chosen, a realization of the model is been defined. Given a realization it is possible to define completely a dynamics in order to describe exactly how all the values of each node evolve.

If all elements are updated at the same time, the dynamics is called *synchronous*. Otherwise if the nodes are updated one by one it is called *serial*. Obviously it is possible to choose which element has to been updated using a deterministic sequence or with a proper random algorithm.

Moreover the realization can be fixed for all time step. The model is thus *quenched*. Furthermore it is possible to change the realization after each time step. Now the model is called *annealed*. Obviously intermediate choices are possible.

In Kauffman network, the system is quenched, every boolean functions f_i are been randomly chosen at $t = 0$ and are kept fixed during the entire dynamics. Consequently the dynamics is deterministic. The last consideration gives the possibility to deeply analyze the properties of the state space. Given an initial random state \mathcal{C} , the dynamics updates this state according to the dynamical rules. Since the state space of all possible states is finite (2^N), eventually a state would be repeated. The dynamics exhibits a deterministic behavior, so if the network is a state \mathcal{C}_1 and if it reaches a state \mathcal{C}_2 at the next time step, then this transition will occur every time the system is found to be in \mathcal{C}_1 .

Eventually a state will be repeated. This means that the system has reached an *attractor*. If these two configurations \mathcal{C}_1 and \mathcal{C}_2 are the same state, then the attractor consists of only one state and it is called a point attractor or steady state. Instead if these returning configurations consist of two or more different states, the attractor is called a cycle attractor or state cycle. The entire set of states which evolve in the same attractor is called *attractor basin*.

2.5 Dynamical observables: the Hamming distance and the overlap

Now let us consider how to analyze the behavior of a generic state belong to a Kauffman Network under the action of the dynamics.

Let us consider \mathcal{C}_0 and $\tilde{\mathcal{C}}_0$ two different initial configurations randomly chosen:

$$\mathcal{C}_0 = \{\sigma_1(0), \sigma_2(0), \dots, \sigma_N(0)\} \quad \tilde{\mathcal{C}}_0 = \{\tilde{\sigma}_1(0), \tilde{\sigma}_2(0), \dots, \tilde{\sigma}_N(0)\},$$

which differ in the values of some variables. It is possible to study how these two configurations change through the action of the same dynamics.

It's useful introducing the notion of a distance. For this purpose the Hamming distance $D_{\mathcal{C}_0, \tilde{\mathcal{C}}_0}(t)$ between the two configurations is defined as

$$D_{\mathcal{C}_0, \tilde{\mathcal{C}}_0}(t) = \sum_{i=1}^N (\sigma_i(t) - \tilde{\sigma}_i(t))^2.$$

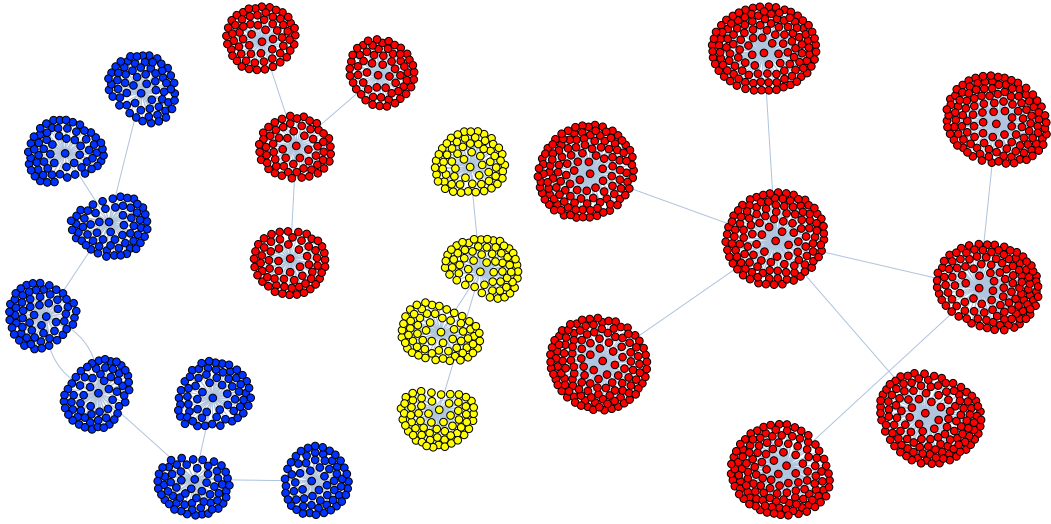


Figure 2.3: **Schematics of Kauffman Networks with $N = 10$ and $K = 1$:** each node corresponds to a configuration and each attractor basin, the set of states which evolve to the same attractor, is colored with a different color. These networks are examples of synchronous and quenched Kauffman networks where dynamical boolean functions are fixed and chosen with equal probability and all nodes are updated at the same time. In this case with $K = 1$, the network exhibits an *ordered* phase. Networks are plotted using IGraph library [64].

If the system is sufficiently chaotic, the information could be transferred over the entire system, thus in the limit of large N , the Hamming distance can diverge for large time. Otherwise if the dynamics is localized, the distance will never grow very large.

Furthermore it is possible to define a quantity which gives a measure of the number of identical spins between two configurations: the normalized overlap $a_{\mathcal{C}_0, \tilde{\mathcal{C}}_0}(t)$ between two configurations $\mathcal{C}_0, \tilde{\mathcal{C}}_0$ is defined as

$$a_{\mathcal{C}_0, \tilde{\mathcal{C}}_0}(t) = 1 - \frac{1}{N} D_{\mathcal{C}_0, \tilde{\mathcal{C}}_0}(t).$$

In the limit $t \rightarrow \infty$, if the overlap is less than unity, the system remembers only a fraction of its input data.

2.6 Order and chaos: phase transition in Random Boolean Networks

Kauffman networks, as well as other dynamical systems, exhibit different behaviors associated to different connectivity K . Three phases can be distinguished: ordered, chaotic and critical.

There are several properties which can be analyzed in order to underline the differences between these phases.

Let us plot the states of a network in a square lattice and let the dynamics act. As an example the dynamics of a Kauffman network with $N = 64$ and different

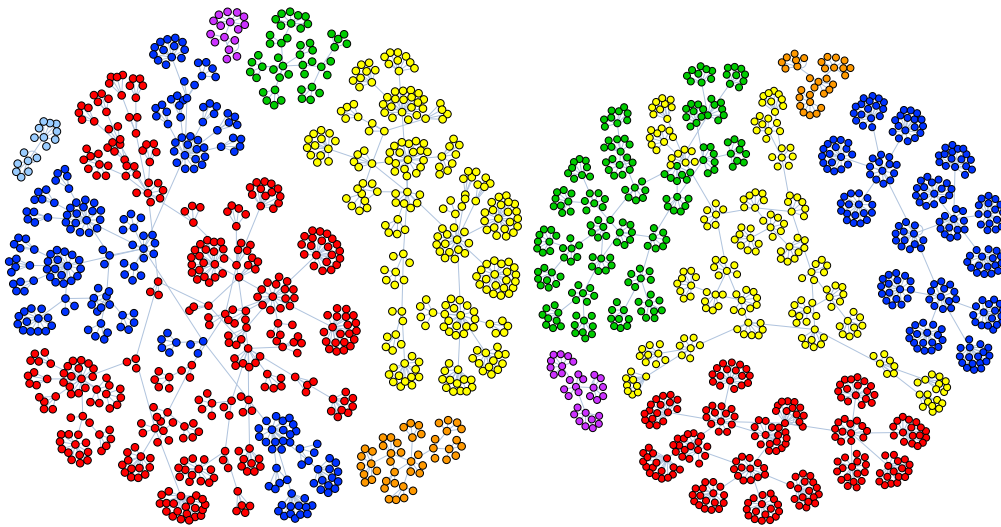


Figure 2.4: **Schematics of Kauffman Networks with $N = 10$ and $K = 2$:** each node corresponds to a configuration and each attractor basin, the set of states which evolve to the same attractor, is colored with a different color. These networks are examples of synchronous and quenched Kauffman networks where dynamical boolean functions are fixed and chosen with equal probability and all nodes are updated at the same time. In this case with $K = 2$, the network exhibits a *critical* phase. Networks are plotted using IGraph library [64].

values of connectivity is shown in Figure (2.6). States with value 1 can be colored with black and 0 states with white. It is possible to study the behavior of the network analyzing which states change and which ones are stable.

Initial states are chosen randomly. Initially many states are changing but quickly the dynamics stabilizes. In the chaotic regime, most of the states are changing at each time step. In the ordered phase there are "strips" of states with only one color stable under the action of the dynamics. The "edge of chaos", the point where the system exhibits the phase transition from the ordered regime to the chaotic phase, occurs when the ordered strips with a definite color breaks into the strips with the other color mixing with one another.

Another approach to describe these different phases is the study of attractors and their topological properties. As seen before, for quenched systems the evolution functions f_i are independent of time. Consequently, for any configuration, the system evolves dynamically to another configuration in a deterministic way and eventually reaches an attractor state or an attractor cycle. The state space is divided in basins of attraction each of which is related to a certain attractor. Each initial configuration will eventually fall in one of these attractors. It is interesting to develop a quantitative description of some observables related to the attractors, like the number of steps the system takes before it falls into an attractor, the *transient* time, or which is the set of initial configurations falling into that attractor. This approach may be analyzed either within a given realization or averaging over realizations.

Consequently the analysis of these properties shows again the different phases

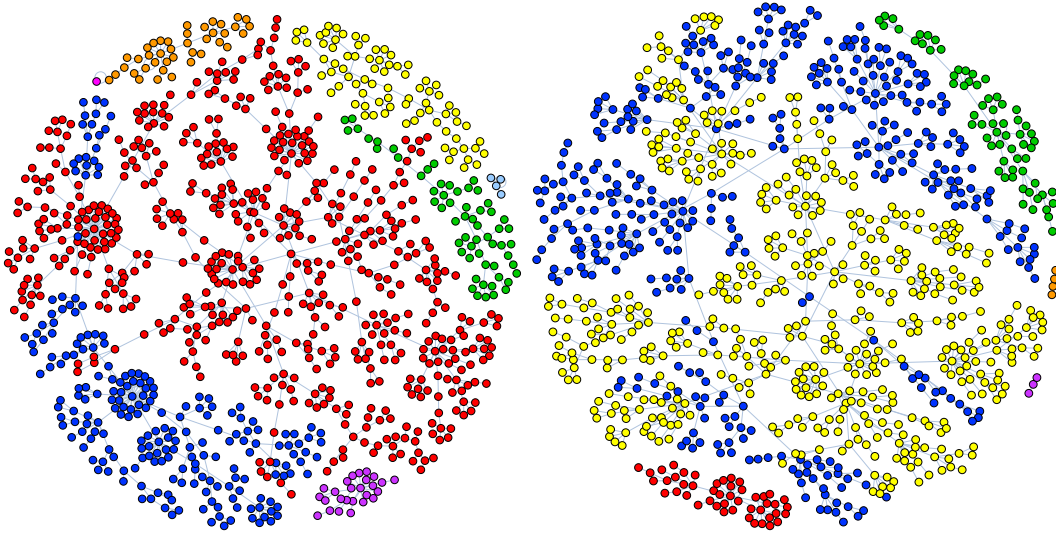


Figure 2.5: **Schematics of Kauffman Networks with $N = 10$ and $K = 5$:** each node corresponds to a configuration and each attractor basin, the set of states which evolve to the same attractor, is colored with a different color. These networks are examples of synchronous and quenched Kauffman networks where dynamical boolean functions are fixed and chosen with equal probability and all nodes are updated at the same time. In this case with $K = 1$, the network exhibits a *chaotic* phase. Networks are plotted using IGraph library [64].

of the system. The chaotic phase is characterized by very long cycles, in which the typical cycle-lengths grow as a power of the size of the state space. In this phase, the transient time is long and exhibit a complex topology. In contrast, the ordered phase tends to have much shorter and simpler cycles, and also shorter transient time which do not grow with the size of the system. The critical phase has a more complex behavior where the number of attractor cycles grows faster than any power law with system size [29].

A third feature of this dynamical behavior is related to the convergence or the divergence of the trajectories in the state space. In the chaotic phase, similar states tend to diverge. In the ordered phase, similar states tend to converge to the same state. At the edge of chaos, nearby states tend to lie on trajectories that neither converge nor diverge in state space. In order to describe this properties the Hamming distance, defined in the previous section, is an useful tool.

Let us consider two different initial states randomly chosen. They have to contain a very large number N of elements:

$$\mathcal{C} = \{\sigma_1, \sigma_2, \dots, \sigma_N\} \quad \tilde{\mathcal{C}} = \{\tilde{\sigma}_1, \tilde{\sigma}_2, \dots, \tilde{\sigma}_N\}$$

The Hamming distance at time zero, $D_{\mathcal{C}, \tilde{\mathcal{C}}}(0)$, is the number of different elements between the two configuration \mathcal{C} and $\tilde{\mathcal{C}}$. On average, a change in a single element will change the argument of K functions. Consequently there will be $K D_{\mathcal{C}, \tilde{\mathcal{C}}}(0)$ functions affected by this change. Each of these functions has the probability one half of changing their value. Thus the Hamming distance after the first time step

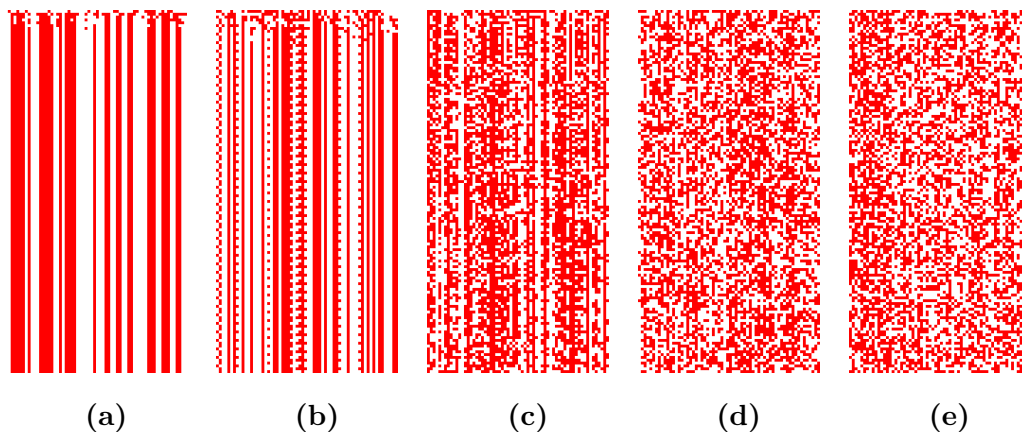


Figure 2.6: **Dynamics of a Kauffman Network in different phases:** Each column represents a different Kauffman network with $N = 64$ and with different connectivities K_i . A line represents the state of the network, each pixel the state of a single node. Initial states are drawn at the top of the columns, time flows downwards. The dynamics is synchronous and quenched: it is defined by boolean functions fixed and randomly chosen with equal probability and all nodes are updated at the same time. (a) ordered phase, $K = 1$. (b) critical phase, $K = 2$. (c), (d) and (e) chaotic phases with $K = 3, 4, 5$.

will be

$$D_{c,\tilde{c}}(1) = \frac{K}{2} D_{c,\tilde{c}}(0).$$

If the set of connectivities and functions f_i are chosen sufficiently random, then at the next time step, the resulting elements and their functions will remain random as well. Then the same equation can be apply again in the following time steps. Since the fraction of changed elements remains small than the dimension of the network and the condition of randomness continues to be valid, the Hamming distance will continue to change by a factor of $K/2$:

$$D_{c,\tilde{c}}(t+1) = \frac{K}{2} D_{c,\tilde{c}}(t).$$

The generic solution for time t results:

$$D_{c,\tilde{c}}(t) = D_{c,\tilde{c}}(0) \exp[t \ln(K/2)]. \quad (2.1)$$

According to the last equation, for $K > 2$ the Hamming distance $D_{c,\tilde{c}}(0)$ grows exponentially, for $K < 2$ it decays exponentially, and for $K = 2$ there are neither exponential growth nor decay, the behavior is substantially influenced by fluctuations.

Thus the behavior of the Kauffman networks can be associated to one of three following phases according to the value of the connectivity K :

- *Ordered* ($K < 2$), picking up a random configuration, it evolves in a few steps to a stable configuration, an attractor, and consequently the Hamming distance decays exponentially with time to a fixed value linked to the various attractors of the dynamics.

- *Chaotic* ($K > 2$), picking up a random configuration, most of the values varies continually, the Hamming distance grows exponentially with time.
- *Critical* or "edge of chaos" ($K_c = 2$), the temporal evolution of the Hamming distance is determined mainly by fluctuations.

In deriving equation (2.1) the functions f_i are assumed to give the values 0 and 1 with the same probability $p = 1/2$.

Let us consider a more general model where the functions f_i give a 0 and an 1 with probabilities p and $1 - p$ respectively. The chaotic, ordered and critical phases are also present: for a given value of p , there is again a critical value $K_C(p)$ of the connectivity below which the system exhibits an ordered phase and above which a chaotic phase. Consequently, for a given connectivity $K \geq 2$, a critical value $p_C(K)$ of the probability separates the chaotic and the ordered phases.

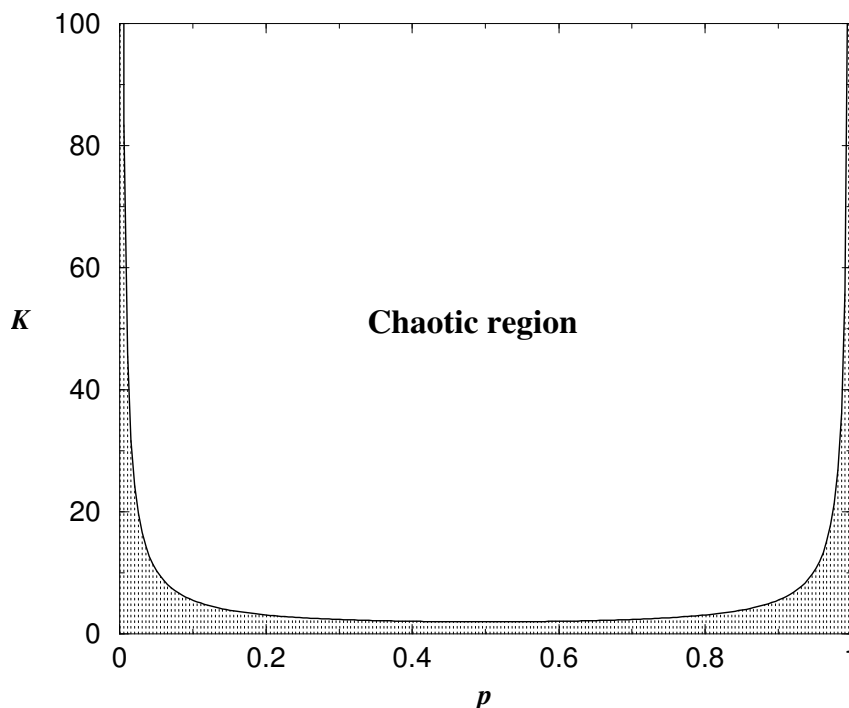


Figure 2.7: **Phase diagram for the Kauffman model.** For a Kauffman model, the outcomes of functions f_i are a 0 and an 1 with probabilities p and $1 - p$ respectively. For each value of p , there is a critical value $K_C(p)$ of the connectivity below which the system exhibits an ordered phase and above which a chaotic phase. In this plot the area with the shadow corresponds to the *ordered phase*, whereas the remaining region corresponds to the *chaotic phase*. The curve separating the two areas is described by equation $K_C = \frac{1}{\lfloor 2p(1-p) \rfloor}$. The last formula is analytically demonstrated in section (2.6.1). This image is reproduced from [22].

In order to obtain an equation for $K_C(p)$ let us consider the behavior of the overlap in the different phases [30]. The overlap between two states \mathcal{C} and $\tilde{\mathcal{C}}$ at time t , $a_{\mathcal{C}_0, \tilde{\mathcal{C}}_0}$, describes the number of elements with the same value in either the

two configurations. Then the probability that the arguments of a function f_i will be the same for either the two configurations is $\left[a_{\mathcal{C}_0, \tilde{\mathcal{C}}_0}(t) \right]^K$. Consequently two configurations \mathcal{C} and $\tilde{\mathcal{C}}$ have $N \left[a_{\mathcal{C}_0, \tilde{\mathcal{C}}_0}(t) \right]^K$ elements with the same inputs and $N \left[1 - \left[a_{\mathcal{C}_0, \tilde{\mathcal{C}}_0}(t) \right]^K \right]$ with different inputs. The spins whose functions f_i have all identical arguments for both the configurations will be the same again at time $t + 1$. On contrary, if one or more arguments are different in the two configurations, the spins have a probability $\frac{1}{2}$ of having the same value and a probability $\frac{1}{2}$ to be different at time $t + 1$ is $1/N$. Therefore:

$$a_{\mathcal{C}_0, \tilde{\mathcal{C}}_0}(t+1) = \left[a_{\mathcal{C}_0, \tilde{\mathcal{C}}_0}(t) \right]^K + \frac{1}{2} \left[1 - \left[a_{\mathcal{C}_0, \tilde{\mathcal{C}}_0}(t) \right]^K \right]$$

which gives:

$$a_{\mathcal{C}_0, \tilde{\mathcal{C}}_0}(t+1) = \frac{1}{2} \left[1 + \left[a_{\mathcal{C}_0, \tilde{\mathcal{C}}_0}(t) \right]^K \right].$$

It is possible to make a generalization: if the function f_i has the different outcomes 0 and 1 weighted with probabilities p and $1 - p$ respectively, like a sort of magnetization bias, then the last equation becomes [31]:

$$a_{\mathcal{C}_0, \tilde{\mathcal{C}}_0}(t+1) = 1 - \frac{1}{K_C} \left[1 - \left[a_{\mathcal{C}_0, \tilde{\mathcal{C}}_0}(t) \right]^K \right], \quad (2.2)$$

where K_C is given as a function of p :

$$K_C = \frac{1}{[2p(1-p)]}. \quad (2.3)$$

This equation will be demonstrate in a following section (2.6.1).

2.6.1 Analytical solution for criticality with the annealed approximation

Following the solution by Derrida and Pomeau [31] it will give an analytical demonstration that the transition occurs at $K_C = 2$. Moreover the equation (2.2) will be obtained.

Given the functions f_i the dynamics is defined:

$$\sigma_i(t+1) = f_i(\sigma_{i_1}(t), \sigma_{i_2}(t), \dots, \sigma_{i_k}(t)).$$

For the Kauffman network these functions are fixed at each time step.

Let us consider 2 configurations \mathcal{C} and $\tilde{\mathcal{C}}$ such that they are at distance $d_{\mathcal{C}, \tilde{\mathcal{C}}} = n$ at $t = 0$. The probability $P_1(m, n)$ that the distance $D_{\mathcal{C}', \tilde{\mathcal{C}}'}(t)$ between their images \mathcal{C}' and $\tilde{\mathcal{C}}'$ at time $t = 1$ is $D_{\mathcal{C}', \tilde{\mathcal{C}}'}(t) = m$.

Let us define the set \mathcal{I} of spin which are identical in \mathcal{C} and $\tilde{\mathcal{C}}$ and \mathcal{D} the set of spins which are different. Set \mathcal{I} contains $N - n$ spins at $t = 0$ while \mathcal{D} contains n spins.

Now the probability $Q(N_0)$ that a configuration has N_0 spins such that all linked nodes are coming from set \mathcal{I} is a Bernoulli distribution:

$$Q(N_0) = \binom{N}{N_0} \left[\left(\frac{N-n}{N} \right)^K \right]^{N_0} \left[1 - \left(\frac{N-n}{N} \right)^K \right]^{N-N_0}$$

where $\left(\frac{N-n}{N} \right)^K$ is the probability that a spin belongs to set \mathcal{I} and $\left(1 - \frac{N-n}{N} \right)^K$ is the probability that a spin belongs to set \mathcal{D} .

These N_0 spins are the same in \mathcal{C}' and $\tilde{\mathcal{C}}'$. Instead the other $N - N_0$ spins are different in \mathcal{C} and $\tilde{\mathcal{C}}$ and each of them has a probability $\frac{1}{2}$ of being the same in \mathcal{C}' and $\tilde{\mathcal{C}}'$ and a probability $\frac{1}{2}$ of being different. Consequently the probability $P_1(m, n)$ is:

$$P_1(m, n) = \sum_{N_0=0}^N Q(N_0) \left(\frac{1}{2} \right)^{N-N_0} \binom{N-N_0}{m}$$

Using $\binom{N}{N_0} \binom{N-N_0}{m} = \binom{N}{m} \binom{N-m}{N_0}$ and substituting $M = N - m$ it results:

$$P_1(m, n) = \frac{1}{2^N} \binom{N}{m} \left[1 - \left(1 - \frac{n}{N} \right)^K \right]^m \sum_{N_0=0}^M \binom{M}{N_0} \left[2 \left(1 - \frac{n}{N} \right)^K \right]^{N_0} \left[1 - \left(1 - \frac{n}{N} \right)^K \right]^{M-N_0}$$

Using the relation $\sum_{k=0}^n \binom{n}{k} p^k q^{n-k} = (p+q)^n$, the final result is

$$P_1(m, n) = \frac{1}{2^N} \binom{N}{m} \left[1 + \left(1 - \frac{n}{N} \right)^K \right]^{N-m} \left[1 - \left(1 - \frac{n}{N} \right)^K \right]^m$$

This formula is the exact probability $P_1(m, n)$ for Kauffman's quenched model if \mathcal{C} and $\tilde{\mathcal{C}}$ are randomly chosen at time $t=0$.

It is more interesting the the probability $P_t(m, n)$ that the two configurations $\mathcal{C}^{(t)}$ and $\tilde{\mathcal{C}}^{(t)}$, obtained as evolutions at time t from \mathcal{C} and $\tilde{\mathcal{C}}$, are at distance m .

In order to calculate $P_t(m, n)$ it is necessary to take in account that for a Kauffman model the functions f_i are fixed: the system is quenched and both the two configurations $\mathcal{C}^{(t)}$ and $\tilde{\mathcal{C}}^{(t)}$, are correlated to the these functions.

$$P_2(m, n) \neq P_2^{annealed}(m, n) = \sum_{q=0}^N P_1(m, q) P_1(q, n)$$

However it is possible to neglect those correlation and to evaluate $P_t(m, n)$ in the *annealed approximation* where the functions and the set of links change randomly at every time step:

$$P_t^{annealed}(m, n) = \sum_{q_1=0}^N \dots \sum_{q_{t-1}=0}^N P_1(m, q_{t-1}) P_1(q_{t-1}, q_{t-2}) \dots P_1(q_1, n)$$

Let us introduce the continuous variables $x = \frac{n}{N}$ and $y = \frac{m}{N}$. $P_1^{annealed}(m, n)$ is very peaked around a well defined value y_1 :

$$y_1 = \frac{1 - (1-x)^K}{2}$$

In a similar way $P_t^{\text{annealed}}(m, n)$ is peaked around a value of $m = Ny_t$, where y_t is defined as:

$$y_t = \frac{1 - (1 - y_{t-1})^K}{2}. \quad (2.4)$$

In conclusion we have demonstrate that given two configurations \mathcal{C} and $\tilde{\mathcal{C}}$ with distance Nx , then, in the limit $N \rightarrow \infty$, the distance between their images at time t is Ny_t with probability 1.

Thus it is necessary to study the behavior of the map (2.4).

For $K \leq 2$, the map has only a fixed point $x = 0$ which results to be attractive. So, for every value x ,

$$\lim_{t \rightarrow \infty} \lim_{N \rightarrow \infty} \frac{d(\mathcal{C}_1^{(t)}, \mathcal{C}_2^{(t)})}{N} = 0 \quad K \leq 2.0$$

For $K > 2$, the map has again a fixed point $x = 0$ which this time results to be unstable. There is also a new fixed point y^* which is attractive (for a numerical value for y^* see [31]). Therefore, for every value x :

$$\lim_{t \rightarrow \infty} \lim_{N \rightarrow \infty} \frac{d(\mathcal{C}_1^{(t)}, \mathcal{C}_2^{(t)})}{N} = y^* \quad K > 0.$$

It is also possible to calculate the mean fluctuations of y around y^* in the limit $t \rightarrow \infty$ using the annealed approximation. This result can be obtained by relating the moments of m to those with n assuming to know the probability distribution of the distances n :

$$\begin{aligned} \langle m \rangle &= \frac{N}{2} \left\langle 1 - \left(1 - \frac{n}{N}\right)^K \right\rangle \\ \langle m^2 \rangle &= \frac{N}{2} + \frac{N(N-1)}{4} \left\langle \left[1 - \left(1 - \frac{n}{N}\right)^K\right]^2 \right\rangle \end{aligned}$$

In the limits $N \rightarrow \infty$ and $t \rightarrow \infty$ the fluctuations result:

$$\begin{aligned} \langle y^2 \rangle - \langle y \rangle^2 &= \frac{\langle m^2 \rangle - \langle m \rangle^2}{N^2} = \frac{\langle n^2 \rangle - \langle n \rangle^2}{N^2} \\ &= \frac{1}{N} \frac{\left[\frac{1}{2} - (y^*)^2\right]}{\left[1 - \frac{K^2}{4} (1 - y^*)^{2K-2}\right]}. \end{aligned}$$

In conclusion we have shown that the critical value $K_C = 2$ for a Kauffman network can be obtained analytically using the annealed approximation.

This solution obtained using the annealed approximation can be extended to a generalization: instead of assuming that the functions f_i give with the same probability the values 0 or 1, it is possibility to assign a weight p or $1 - p$ to the outcomes of these functions. In conclusion equation (2.4) becomes:

$$y_t = \left[1 - (1 - y_{t-1})^K\right] 2p(1 - p).$$

Chapter 3

Spin Glass

The concept of spin glass was originally introduced to describe magnetic alloys which experimentally exhibit a non-periodic freezing of the orientations of the magnetic moments together with slow response and linear low-temperature heat capacity characteristic of conventional glasses.

Spin glasses thus are systems with localized magnetic moments whose interactions are characterized by quenched randomness: each pair of localized moments, or spins, have a given a priori probability of having a ferromagnetic or an antiferromagnetic interaction [32].

The fundamental physical behavior of such systems do not depend heavily on the microscopic interactions but in the competing properties between ferromagnetic and antiferromagnetic interactions. This is the modern approach to spin glass that began with the paper of Edward and Anderson [33]

3.1 The Sherrington Kirkpatrick model

A benchmark for Spin Glass physics is a generalization of the Ising model. It consists of N boolean variables $\sigma_i \in \{+1, -1\}$, $i = 1, \dots, N$ that represent interacting magnetic dipole moments of atomic spins. The interaction among the spins can be ferromagnetic ($J_{ij} > 0$, it tends to align spins) or anti-ferromagnetic ($J_{ij} < 0$, it tends to anti-align spins). The sign and strength of the couplings are supposed to be chosen with a given probability distribution $P(J_{ij})$. The model is described by the Hamiltonian:

$$H_J[\sigma] = - \sum_{1 \leq j < i \leq N} J_{ij} \sigma_i \sigma_j. \quad (3.1)$$

It depends directly on the configuration of spins $\{\sigma_i\}$ and on the random variables $\{J_{ij}\}$ which are seen as parameters at first.

The model is completely defined by choosing the probability distribution $P(J_{ij})$ for the spin-spin interactions. The simplest and more realistic description is an infinite range model defined on a complete graph whose interactions are independent random variables gaussian distributed:

$$P(J_{ij}) = \frac{1}{\sqrt{2\pi J^2}} e^{-\frac{(J_{ij}-J_0)^2}{2J^2}}.$$

This is the Sherrington-Kirkpatrick model (SK)[1]. In this model the disorder is assumed to *quenched*.

3.1.1 Quenched disorder and frustration

Spin Glasses are typically systems where quenched disorder and frustration co-exist. In order to analyze the concept of frustration Parisi, in the introduction of [2], suggests as example the social behavior of three people.

If each person has to choose between two sides and they like each other, they will chose the same side. Then there are two equivalent scenario and the problem exhibits a trivial symmetry. This case is like the ferromagnetic Ising model, where the two possible ground states are characterized by all spins aligned.

Otherwise, in the case where the three persons hate each other the situation is no more naïve. There are three scenarios where two enemy have to be on the same side and consequently they are frustrated. This case is equivalent to the antiferromagnetic triangular Ising model, where the spins on a triangular lattice tend to stay anti-aligned.

The triangular antiferromagnetic displays a large number of ground states but the free energy barriers which separates these configuration are quite low. At nonzero temperature, the system can move easily from one free energy valley to another and the energy landscape displays a network of many ground states connected by small energy barriers [34].

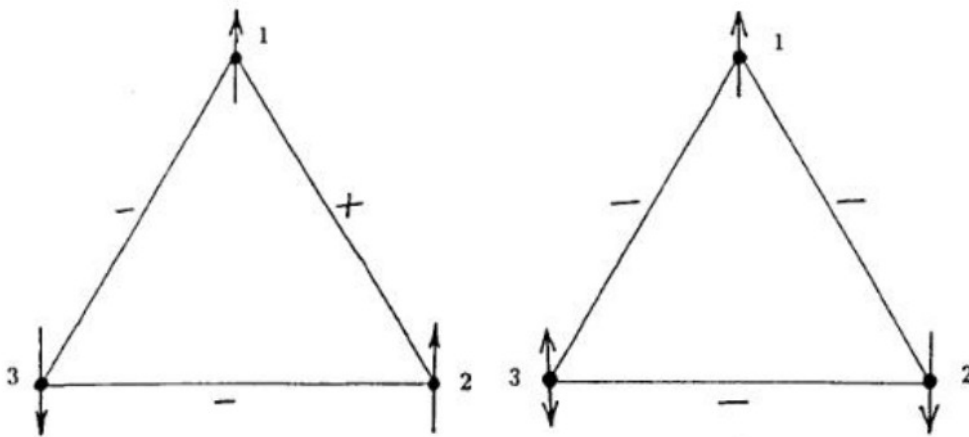


Figure 3.1: **Frustration in a system of three spins:** spin glasses are typically systems where quenched disorder and frustration coexist. In the first image there is no frustration: the spin can find an optimal configuration and the product of the interactions along the triangle is positive. In the second image the product of the interactions along the triangle is negative: the system is frustrated, there is no configurations which can exclude all the unfavorable interactions. This image is reproduced from [34].

On the other hand, the spin glass has a more complex behavior: the Hamiltonian 3.1 exhibits again frustration, indeed it is impossible for the system to find an

optimal configuration such that all the unfavorable interactions are excluded, even in the ground state. The spin glass has a exponential number of low energy states which do not correspond to the ground states. They are separated by high energy barriers. In the thermodynamic limit these barriers diverge and at low temperature, if the system falls in one of these valleys it is not able to go away, the ergodicity consequently is broken.

3.1.2 Quenched, annealed averages and selfaveraging

In general in the spin glass theory the variables which describe the interactions are assumed to quenched [35]. This means that the "disordered" are fixed while spins fluctuates. This condition corresponds to an experimental system where the timescale of the disorder results to be longer than the timescale of the spin fluctuations. This kind of assumption implies that each realization of the disorder is a given sample of the system and the properties of the fluctuations of each sample depends on the single realization.

In the case such that the timescale are comparable, the disorder is *annealed*. Experimentally this situation corresponds to a system where spins and disorder fluctuate together and their statistics depend on the corresponding distributions at the same time.

Let us consider, for example, the thermodynamics of the quenched disorder. Ideally the averages for a given sample can compute using the Boltzmann measure in order to evaluate the equilibrium properties of this sample. Then also the averages over the disorder distribution have to be computed. This procedure is not trivial due to the presence of the disorder. The behavior of extensive observable, such as free energy, do not make any problem since their densities are *selfaveraging* in the thermodynamic limit, they assume the same value for each realization of disorder which has a finite probability.

The free energy of the system, as an extensive observable, is proportional to the volume of the system, for a spin glass system is N . In the thermodynamic limit $N \rightarrow \infty$, the main contribution to the free energy in a macroscopic system is affected by the boundary which usually gives a contribution of order $1/N$. Such macroscopic system could be divided into a macroscopic number of macroscopic subsystems. Therefore the resultant total free energy of the entire system would be the sum of the free energy of each subsystem. If all the interactions in the system are short range, then the contributions from the interactions between the subsystems are like the boundary effects which can be denied in the thermodynamic limit.

Consequently, the total free energy is the sum of a macroscopic number of terms which would be a random quenched quantity since it contains the random spin-spin interactions as parameters next.

The sum of many random quantities can be represented as their averaged value according to the law of large numbers. Therefore, the free energy of a macroscopic system must be selfaveraged over the realizations of the random interactions taking in account their statistical distribution.

Then the free energy is given by the logarithm of the partition function. So, in order to calculate the free energy is necessary to evaluate the average of the logarithm of the partition function over the given distribution of random J_{ij} 's simultaneously

with the calculation of the partition function itself.

Given the free energy density f_J for a given disorder realization J_{ij} :

$$f_J = -\frac{1}{\beta N} \log Z_J = -\frac{1}{\beta N} \log \text{Tr}_{\{\sigma_i\}} e^{-\beta H_J[\sigma]},$$

the average free energy over the disorder distribution is given by

$$f = \int dJ P(J) f_J = \langle \langle f_J \rangle \rangle = -\frac{1}{\beta N} \langle \langle \log Z_J \rangle \rangle$$

where the $\langle \langle \dots \rangle \rangle$ indicates the average over the distribution $P(J)$.

For the annealed average it is necessary a simpler computation, only the average of the partition function is required:

$$f_{an} = -\frac{1}{\beta N} \log \langle \langle Z_J \rangle \rangle = -\frac{1}{\beta N} \log \int dJ P(J) \text{Tr}_{\{\sigma_i\}} e^{-\beta H_J[\sigma]}.$$

In this case the average over the Boltzmann measure and the disorder distribution are performed at the same time.

3.2 The replica method

In order to afford the computation of the logarithm in the quenched average it is useful to explain the replica approach.

For a given realization with a fixed set of quenched variables J_{ij} , the partition function is defined as

$$Z_J = \sum_{\{s\}} \exp \{-\beta H_J[s]\},$$

and the free energy:

$$f_J = -\frac{1}{\beta N} \log Z_J.$$

As seen before the free energy is self-averaging in the thermodynamic limit and we can calculate equivalently as $\langle \langle f_J \rangle \rangle$.

The replica method consists in computing the average free energy as the analytic continuation of the average of the partition function of n uncoupled replicas of the initial system. If n is a real number, in general:

$$\log Z = \lim_{n \rightarrow 0} \frac{Z^n - 1}{n}$$

where this result is a consequence of expansion $A^n \simeq 1 + n \log A$ in the limit $n \rightarrow 0$.

The "replica trick", introduced by Parisi [2] consists in first considering n as an integer and then taking the limit $n \rightarrow 0$ of the result. If n is an integer, the partition function of n uncoupled replicas of the initial system is:

$$\begin{aligned} Z_J^n &= \left(\sum_{\{\sigma_i^a\}_{1 \leq i \leq N}} e^{-\beta H[\{\sigma_i\}]} \right)^n \\ &= \sum_{\{\sigma_i^a\}_{1 \leq a \leq n, 1 \leq i \leq N}} e^{-\beta \sum_{a=1}^n H[\{\sigma_i^a\}]} \end{aligned}$$

i.e. it is possible to rewrite the sum over the configuration of one system to the power n as a sum over the configurations of n replicas of the same system with the same couplings J_{ij} .

The free energy per spin of a system made by n uncoupled replicas is:

$$f_n = -\frac{1}{\beta N n} \log \langle \langle Z_J^n \rangle \rangle$$

where $\langle \langle Z_J^n \rangle \rangle$ is the quenched average of the partition function over the ξ 's.

Then the free energy per spin results:

$$\lim_{n \rightarrow 0} f_n = \langle \langle f \rangle \rangle \equiv f$$

This result is evident considering that:

$$\begin{aligned} \lim_{n \rightarrow 0} f_n &= -\frac{1}{\beta N} \lim_{n \rightarrow 0} \frac{1}{n} \log \langle \langle Z_J^n \rangle \rangle \\ &= -\frac{1}{\beta N} \lim_{n \rightarrow 0} \frac{1}{n} \log \left[\sum_J P(J) Z_J^n \right] \\ &= -\frac{1}{\beta N} \lim_{n \rightarrow 0} \frac{1}{n} \log \left[\sum_J P(J) (1 + n \log Z_J) \right] \\ &= -\frac{1}{\beta N} \sum_J P(J) \log Z_J \\ &= -\frac{1}{\beta N} \langle \langle \log Z_J \rangle \rangle \\ &= \langle \langle f \rangle \rangle. \end{aligned}$$

This approach is general for spin glass systems. In particular, the SK model, which was defined above, has been solved using the replica method and a replica symmetric ansatz. This solution based on a saddle-point solution is approximate and it implies a non physical result: the entropy is negative at zero temperature and it results an unstable solution in a range of low temperature. More satisfactory solutions are obtained taking in account the replica symmetry breaking as proposed by Parisi (for example see [36]) or alternatively considering a mean field analysis which leads to the TAP (Thouless-Anderson-Palmer) equation.

3.3 Phase transition

As in the usual Ising model it is possible to analyze the system using the magnetization as an order parameter in function of the temperature T .

For large T , the system has sufficient thermal energy to occupy any possible configuration and exhibits a paramagnetic state where $\langle m \rangle \rightarrow 0$. The local magnetization would differ from zero only in presence of an external magnetic field

Decreasing the temperature T , In the low temperature phase the spins tend to freeze in energetically favorable positions and the local magnetization can be different from zero even with zero field. The system can exhibits a ferromagnetic

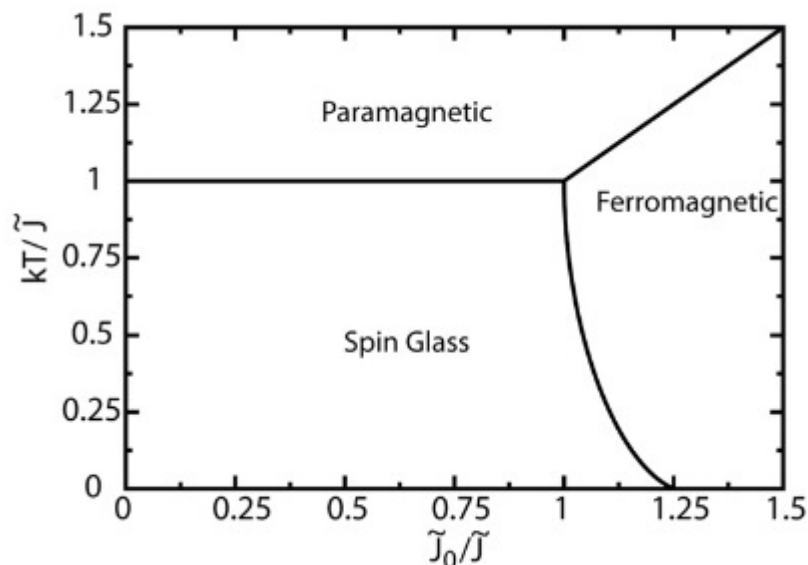


Figure 3.2: **Phase diagram for SK model:** For large T the system is in the paramagnetic phase such that $\langle m \rangle \sim 0$ and $q \sim 0$. For low temperature the system exhibits two phases: when $\tilde{J}_0/\tilde{J} > 1$ there is the ferromagnetic phase, $|\langle m \rangle| \sim 1$ and $q \sim 0$. Otherwise, when $\tilde{J}_0/\tilde{J} < 1$, there is the *spin glass phase* characterized by conditions $\langle m \rangle \sim 0$ and $q \sim 1$.

In the image, the diagram is plotted with normalized variables related to temperature and to the probability distribution of interactions, $P(J_{ij}) = \frac{1}{\sqrt{2\pi J^2}} e^{-\frac{(J_{ij}-J_0)^2}{2J^2}}$: $J = \tilde{J}/\sqrt{N}$ and $J_0 = \tilde{J}_0/N$. This image is reproduced from [37].

phase or a spin glass phase. As usual, the ferromagnetic state is characterized by the alignment of spins, $|\langle m \rangle| \rightarrow 1$. In the spin glass state, some spins could align locally but there is not a long range ordering. The local magnetization depends on the specific choice of J_{ij} and therefore the global magnetization has to be zero even at zero temperature.

According to the phase diagram sketched in figure 3.2, for low T , when $\tilde{J}_0/\tilde{J} > 1$ the system will be in the ferromagnetic phase. On the other hand in the case $\tilde{J}_0/\tilde{J} < 1$, the system is composed by a mixture of ferromagnetic and antiferromagnetic interaction and it results to be energetically frustrated.

In order to characterize these phase transitions the local magnetization is not enough.

A generic equilibrium state can be decomposed as the sum of other equilibrium states with weights w_α . The states which cannot be decomposed in this way, are consequently defined as pure states. It is possible to introduce the overlap between two states α and β :

$$q_{\alpha\beta} = \frac{1}{N} \sum_i m_i^\alpha m_i^\beta. \quad (3.2)$$

In particular, if $q_{\alpha\alpha} = q_{\beta\beta} = q_{EA}$, the overlap of a state with itself, q_{EA} is the

self-overlap or Edward-Anderson order parameter. In the thermodynamic limit q_{EA} doesn't depend on the given realization, J_{ij} and can be used as the order parameter to describe the phase transition from the low temperature and ferromagnetic phase, where $q_{EA} = 0$, to the low temperature and Spin Glass phase such that $q_{EA} \neq 0$.

In order to describe the statistics of all possible overlap it is also useful to define the probability distribution of overlaps:

$$P(q) = \overline{P_J(q)} = \overline{\sum_{\alpha\beta} w_\alpha^J w_\beta^J \delta(q_{\alpha\beta} - q)}, \quad (3.3)$$

where w_α s are the weights for the decomposition of the state in pure states which depend only on its free energy. In other words, the distribution of overlaps $P(q)$ is the probability of finding two state with overlap q weighting each state with its probability of appearing in the ensemble. $P(q)$ is the physical order parameter which can be used for characterizing phase transitions. For example in the ferromagnetic Ising model, under the critical temperature, the distribution shows a bifurcation: it is one delta function at non zero magnetic field, because there is only one equilibrium state, while it contains two delta functions at zero field.

In the SK model the situation is not naive. The ferromagnetic phase is similar to the usual Ising model and the distribution has two delta functions. In the spin glass phase, there are many different equilibrium states at low temperature and the function $P(q)$ is non trivial: between two delta functions at $q = \pm q_{max}(T)$ there is a continuous curve. The $q_{max}(T)$ is the maximum possible overlap which is the "selfoverlap". Since the number of minima of the free energy of the system is macroscopic, their selfoverlap are all equal and the function $P(q)$ exhibits the two delta functions. The existence of the continuous curve between the two delta functions is the result of the continuous process of fragmentation of the valleys of the free energy into the smaller and the smaller one. In the high temperature phase there is only one delta corresponding to $q = 0$ for zero magnetic field. This phase transition is associated with the spontaneous replica symmetry breaking and an analytical solution is been provided using Parisi's approach [2].

Typical properties of the spin glass phase, such as the ground state energy or the number of local minima of the Hamiltonian, are usually difficult to be investigated analytically, even at $T = 0$. Often is necessary to employ numerical methods, especially to determinate finite-size corrections (see for example [38]).

3.4 Complexity in Spin Glass Theory

In this chapter we have seen that Spin Glasses are disordered magnetic systems which exhibit a variety of properties that are characteristic of complex systems like quenched disorder and frustration. These systems exhibit rugged energy landscape and many metastable states, states stable to flips of finite numbers of spins, which are connected to the dynamical features of these systems. This property is characterized through the complexity. The complexity Σ is the entropic contribution due to the exponentially large number of metastable states and it is defined as the logarithm of them, divided by the size of the system [39, 40]. In mean-field disordered models

it can be computed by calculating the number of minima of the Thouless-Anderson-Palmer (TAP) free energy. The TAP equations can be written as $G_i = \partial F / \partial m_i = 0$, $i = 1, \dots, N$, where each G_i is a function of the N variables m_i which denote the local magnetizations, $m_i = \langle \sigma_i \rangle$, at each site, where $\langle \dots \rangle$ denotes thermal averages. The number of solutions of the N equations $G_i = 0$ is given by

$$N_s = \int_{-1}^1 \prod_i dm_i \prod_i \delta(\partial F / \partial m_i) |\det \partial^2 F / \partial m_i \partial m_j|,$$

where the modulus on the determinant is necessary to count each solution only one time. Therefore, N_s corresponds to the number of physical states is justified a posteriori. Then there is a relation which connects the number of solutions to complexity $\langle N_s \rangle_J \sim \exp[N\Sigma]$. The complexity is a function of temperature T : it vanishes at the Spin Glass critical point T_c , while for $T \rightarrow 0$ it approaches the value 0.1992. This matter is still studied [41].

The necessity of finding local minima strictly relates complexity to the problem of global optimization. In Spin Glasses, similarly to a large class of complex systems, finding the ground state corresponds is a NP-hard problem: the number of steps needed to find the ground state grows faster than any power of the system size.

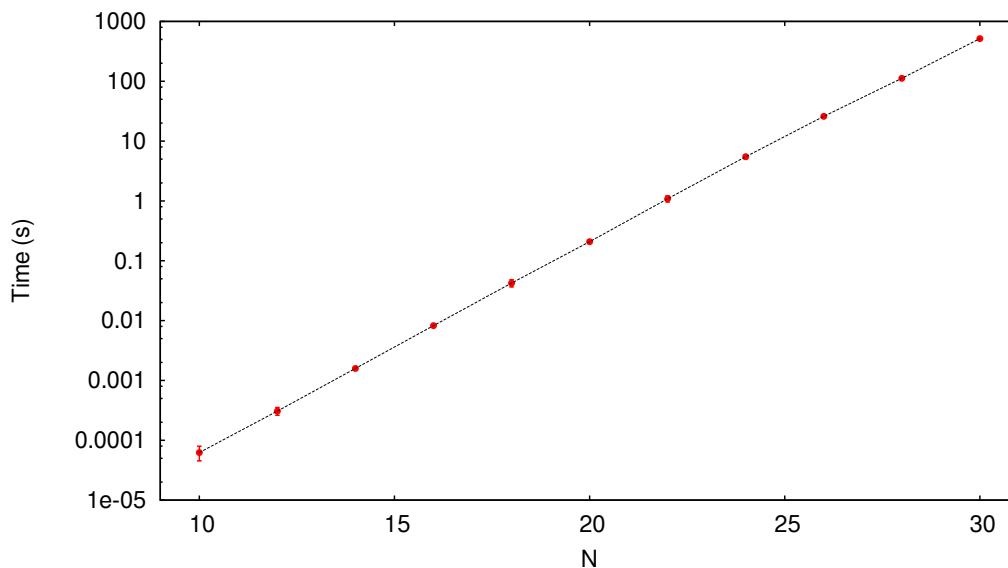


Figure 3.3: **Time of determine the ground state energy as a function of the size N .** Finding the ground state energy for the Sherrington-Kirkpatrick is a NP-hard problem: the number of steps needed to find the ground state grows faster than any power of the system size. This plot shows the time necessary for a recursive algorithm to evaluate the energy of each configurations and to select the minimum.

Many of global optimization methods have been developed for this kind of minimization problem and successfully applied to a variety of computational problems [42]. An example is a Monte Carlo with minimization: a minimization process have been performed starting from N^2 randomly chosen initial configurations until a local

minima has been reached. This kind of algorithm works efficiently only for limited sizes. For example see figure (3.4).

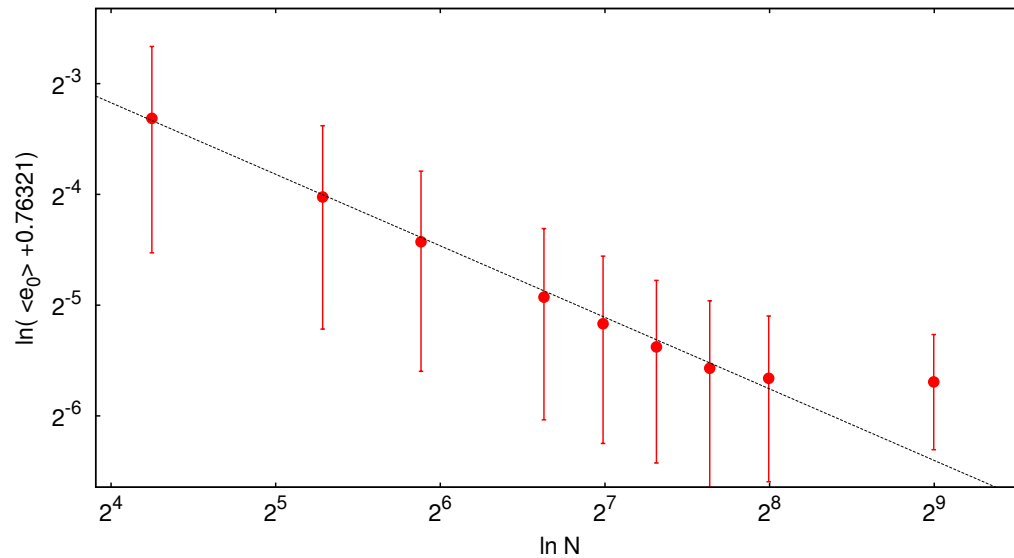


Figure 3.4: **Plot of $\ln(\langle e_N \rangle + \langle e_\infty \rangle)$ as a function of $\ln N$:** For finite-size systems the ground state energy for the Sherrington-Kirkpatrick model depend on N as $\langle e_N \rangle = \langle e_\infty \rangle + aN^{-\omega}$ where $\omega = 0.672$. These results have been obtained through a Monte Carlo with minimization: a minimization process have been performed starting from N^2 randomly chosen initial configurations until a local minima has been reached. For system with limited sizes this algorithm results efficient. In this case it works correctly until systems are bigger than $N = 300$. Indeed the last data for $N = 511$ departs from the expected value.

Chapter 4

The Hopfield Model

The Hopfield model was originally proposed in 1982 by John Hopfield [3] as a simple toy model in order to describe the behavior of the memory in the human brain. Below there will be reported the main results related to this model.

The main viewpoint analyzed by Hopfield was the dynamics: indeed it is a mathematical model aiming to describe a network functioning as an associative memory and it exhibits the property of storing and retrieving informations even if given data are degraded [43]. The statistical mechanics properties were developed by Amit, Gutfreund and Sompolinsky [4] in the context of spin glass theory, in particular with the replicas approach and the replica symmetry breaking which allowed a complete analysis. Moreover an exhaustive study of the dynamics is due to Derrida [44].

The original purpose of the Hopfield model was to describe in a simple way the interactions between two neurons through a synapse. Each neuron is an Ising spin with two possible states, $\sigma_i = 1$ (active) $\sigma_i = -1$ (turned off). The space of the possible configurations of N boolean spins which constitute the network is $S_N = \{-1, +1\}^N$. The strength of a connection between two neurons σ_i and σ_j is described by an interaction variable J_{ij} . Each one of these is defined from a set of p different configurations $\{\xi_i^\mu\}_{1 \leq i \leq N}^{1 \leq \mu \leq p}$:

$$J_{ij} = \begin{cases} \frac{1}{N} \sum_{\mu=1}^p \xi_i^\mu \xi_j^\mu & \forall i \neq j, \\ 0 & \forall i = j. \end{cases}$$

According to this definition, J_{ij} are symmetric, $J_{ij} = J_{ji}$, and every pair of neurons is connected. Each ξ_i^μ is an independent, quenched, random variable assuming the values $+1$ and -1 with probability

$$P(\xi_i^\mu) = \frac{1}{2} \delta(\xi_i^\mu - 1) + \frac{1}{2} \delta(\xi_i^\mu + 1).$$

For a fixed value of μ , the pattern $\{\xi_i^\mu\}_{1 \leq i \leq N}$ is called a *memory*. The network is designed in order to memorize p memories: each pattern ξ^μ results to be associated to any configuration sufficiently close to it: "close" usually means that between a memory and a configuration the Hamming distance is small.

The Hopfield model is described by the Hamiltonian defined on S_N :

$$H[\sigma] = -\frac{1}{2} \sum_{i,j}^N J_{ij} \sigma_i \sigma_j. \quad (4.1)$$

From an historical point of view, the simplest version of this Hamiltonian with $p = 1$ was originally introduced by Mattis [45] in 1976 in order to define a first model of a disordered magnet. It differs from an Ising ferromagnet only by a simple gauge transformation $\sigma_i \rightarrow \sigma'_i = \xi_i \sigma_i$ of spins. Then Luttinger [46] analyzed the case where $p = 2$ and finally Figotin and Pastur [47] develop a generalized model with an arbitrary, but fixed, number of memories p , as a soluble model of spin glass. Therefore, only after the paper by Hopfield, who approaches the above Hamiltonian as a starting point for an autoassociative memory model, the analysis become exhaustive.

This model has the crucial property of storage and retrieval of information if the dynamically stable configurations $\{\sigma_i\}$ are correlated with the memories [48].

The retrieval process is described by a dynamics: a system describes a trajectory in the space of 2^N possible states. In general a discrete-time dynamics is defined so that each neuron change his state in time according to

$$\sigma_i(t+1) = \text{sign} \left(\sum_j^N J_{ij} \sigma_j(t) \right). \quad (4.2)$$

Consequently a configuration $\{\sigma_i\}_{1 \leq i \leq N}$ is a fixed point of this dynamics if and only if

$$\sigma_i \left(\sum_j^N J_{ij} \sigma_j \right) \geq 0 \quad \forall i = 1, \dots, N.$$

This kind of dynamics can be defined in a synchronous or asynchronous way. In the original paper, Hopfield defined an asynchronous dynamics where a randomly chosen neuron changes his state in time. This is nothing but a Monte Carlo dynamic at $T = 0$. A more general case, a non-zero temperature process, can be defined:

$$\sigma_i(t+1) = \begin{cases} \sigma_i(t) & \text{with probability } p_+ = \frac{e^{\beta \sigma_i (\sum_j^N J_{ij} \sigma_j)}}{e^{\beta \sigma_i (\sum_j^N J_{ij} \sigma_j)} + e^{-\beta \sigma_i (\sum_j^N J_{ij} \sigma_j)}} \\ -\sigma_i(t) & \text{with probability } p_- = 1 - p_+ \end{cases}$$

where the parameter $\beta = 1/T$ determines the thermal noise intensity. In this chapter the dynamics defined in equation (4.2) will be used.

4.1 Thermodynamics

The analysis of the thermodynamic properties of the Hopfield model is interesting not only in the context of memory retrieval but also in statistical mechanics as a disordered magnetic system. According to the above Hamiltonian (4.1), this model

can be studied as a particular case of a infinite range spin glass system: it differs from the usual Sherrington Kirkpatrick model for the probability distribution of the quenched disorder. In this case the disorder is due to the quenched patterns $\{\xi_i^\mu\}_{1 \leq i \leq N}^{1 \leq \mu \leq P}$ and not for the spin couplings J_{ij} themselves.

The random probability measure of a given configuration $\{\sigma_i\}_{1 \leq i \leq N}$ in the S_N space is the Gibbs measure:

$$\mathcal{G}_{N,\beta}[\sigma] \equiv \frac{1}{Z_{N,\beta}} e^{-\beta H_N[\sigma]}$$

where $Z_{N,\beta}$ is the partition function. Then the free energy per spin is:

$$f_{N,\beta} \equiv -\frac{1}{\beta N} \log Z_{N,\beta}.$$

The parameter β is the usual inverse temperature, N the size of the system. The aim of the following analysis is to study the behavior of this model in the thermodynamic limit, where N tends to infinity.

An useful parameter to characterize the behavior of such system is the overlap of a state with the ν th pattern:

$$m_\nu = \frac{1}{N} \sum_{i=1}^N \langle \sigma_i \rangle \xi_i^\nu$$

where $\langle \dots \rangle$ is the thermal average. Using the last equation and the previous definition for J_{ij} , the average energy can be expressed as a function of the overlap:

$$\begin{aligned} H &= -\frac{1}{2} \sum_{i,j} J_{ij} \sigma_i \sigma_j = -\frac{1}{2} \sum_{i,j} \left(\frac{1}{N} \sum_{\mu=1}^p \xi_i^\mu \xi_j^\mu - \frac{p}{N} \delta_{ij} \right) \sigma_i \sigma_j \\ &= \frac{p}{2} - \frac{N}{2} \sum_{\mu=1}^p \left(\frac{1}{N} \sum_{i=1}^N \xi_i^\mu \sigma_i \right) \left(\frac{1}{N} \sum_{j=1}^N \xi_j^\mu \sigma_j \right). \end{aligned}$$

Then the expected value of the energy results:

$$E = \langle H \rangle = \frac{\alpha}{2} N - \frac{N}{2} \sum_{\mu=1}^p (m^\mu)^2.$$

The Hopfield model exhibits different behaviors in in two different regimes [2]. Then there are two two analytical which will be analyzed in the following pages:

- the *unsaturated* limit, $\frac{p}{N} \rightarrow 0$ as $N \rightarrow \infty$.

In this case p is finite whereas the size of system grows to infinity. At $T = T_C = 1$ the system exhibits a second order phase transition, from a disordered phase to an ordered phase. Below T_C , there are $2p$ equilibrium states, which are minima of the free energy. They are connected to *Mattis states*. Each one of these states are correlated to one of the learned patterns $\{\xi_i^\mu\}_{1 \leq i \leq N}$.

This regime can be studied without the replicas [48] and even the dynamics for simultaneous synchronous updating can be solved.

- the finite α limit, $\frac{p}{N} \rightarrow \alpha$ when $N \rightarrow \infty$.

In this case there are two phase transitions increasing α . For $\alpha \leq \alpha_{crit_1} \approx 0.05$ all stored memories result to correspond to ground states of the free energy. This is the ordered phase. For $\alpha \geq \alpha_{crit_2} \approx 0.15$ there is a so-called spin glass phase: there is a total collapse of the capabilities of the memory. The only ground state is the spin glass state. Replica symmetry is broken and as a consequence each state has the fine structure of a full ultrametric tree. In addition $\alpha_{crit_1} \leq \alpha \leq \alpha_{crit_2}$ the spin glass state is the ground state but the retrieval is still efficient. In this regime the replicas approach is necessary and only the statistical equilibrium can be analyzed.

4.2 The limit of finite p

The Hopfield model will be studied in the limit $N \rightarrow \infty$ and finite p [48]. The free energy density is given by

$$f_\beta = -\frac{1}{\beta} \lim_{N \rightarrow \infty} \left[\frac{1}{N} \langle \langle \log \text{Tr}_\sigma e^{-\beta H[\sigma]} \rangle \rangle \right],$$

the $\langle \langle \dots \rangle \rangle$ is the average over the distribution of patterns $\{\xi_i^\nu\}_{1 \leq \nu \leq s}^{1 \leq i \leq N}$. For a given realization of ξ 's, the partition function can be written as

$$\begin{aligned} Z &= \text{Tr}_\sigma e^{-\beta H} \\ &= e^{-\frac{\beta p}{2}} \text{Tr}_\sigma \exp \left[\frac{\beta}{2N} \sum_{\mu=1}^p \left(\sum_{i=1}^N \sigma_i \xi_i^\mu \right)^2 \right] \\ &= (N\beta)^{\frac{p}{2}} e^{-\frac{\beta p}{2}} \int \prod_{\mu=1}^p \frac{dm_\mu}{2\pi} \exp \left[-\frac{N\beta \vec{m}^2}{2} + \sum_{i=1}^N \log \left[2 \cosh \left(\beta \vec{m} \cdot \vec{\xi}_i \right) \right] \right], \end{aligned}$$

\vec{m} and $\vec{\xi}$ are the vector notation for the p components of m_μ and ξ_i^μ and the last line is obtained using the property of gaussian integral and evaluating the average over the spins σ_i . For definition, p is finite, then the integral over m can be evaluated with a saddle point approximation:

$$-\frac{1}{N\beta} \log Z = \frac{1}{2} \vec{m}^2 - \frac{1}{N\beta} \sum_{i=1}^N \log \left[2 \cosh \left(\beta \vec{m} \cdot \vec{\xi}_i \right) \right],$$

By the saddle point equation,

$$\frac{\partial \log Z}{\partial m_\mu} = 0,$$

the solution for the order parameter \vec{m} is obtained:

$$\vec{m} = \frac{1}{N} \sum_{i=1}^N \vec{\xi}_i \tanh \left(\beta \vec{m} \cdot \vec{\xi}_i \right).$$

This result depends explicitly on the given realization $\{\xi_i^\nu\}_{1 \leq \nu \leq s}^{1 \leq i \leq N}$. As discussed for the SK model in the previous chapter, $\log Z$ is a selfaveraging observable, therefore

the sums $(1/N) \sum_i$ can be replaced by the averages over the patterns [49]. The consequences are the mean field equations:

$$f_\beta = \frac{1}{2} \bar{m}^2 - \frac{1}{\beta} \left\langle \left\langle \log \left[2 \cosh \left(\beta \bar{m} \cdot \vec{\xi} \right) \right] \right\rangle \right\rangle, \quad (4.3)$$

$$\bar{m} = \left\langle \left\langle \vec{\xi} \tanh \left(\beta \bar{m} \cdot \vec{\xi} \right) \right\rangle \right\rangle. \quad (4.4)$$

\bar{m} is the average overlap between the local magnetization and the ξ 's:

$$m_\mu = \left\langle \left\langle \sigma_i \xi_i^\mu \right\rangle \right\rangle$$

where

$$\langle \sigma_i \rangle = \tanh(\beta \bar{m} \cdot \xi_i)$$

is the thermal average of the i -th spin. The properties of the solutions of equation (4.4) depends of the correlations between the thermal averages $\langle \sigma_i \rangle$ and the quenched patterns $\{\xi_i^\nu\}_{1 \leq \nu \leq s}$.

4.2.1 Low temperature phase

At low temperature, the system exhibits $2p$ equilibrium states, which are minima of the free energy. Now we demonstrate that they are connected to Mattis states and correlated to one of the learned patterns $\{\xi_i^\mu\}_{1 \leq i \leq N}$.

Let us consider the case where the distribution of ξ_i 's is

$$P(\{\xi_i^\mu\}) = \prod_{\mu, i} p(\xi_i^\mu)$$

and, seen before,

$$p(\xi_i^\mu) = \frac{1}{2} \delta(\xi_i^\mu - 1) + \frac{1}{2} \delta(\xi_i^\mu + 1).$$

The free energy obtained above,

$$f_\beta = \frac{1}{2} \bar{m}^2 - \frac{1}{\beta} \left\langle \left\langle \log \left[2 \cosh \left(\beta \bar{m} \cdot \vec{\xi} \right) \right] \right\rangle \right\rangle,$$

can be expanded in powers of \bar{m} in order to obtain:

$$f = -T \log 2 + \frac{1}{2} (1 - \beta) \bar{m}^2 + O(\bar{m}^4)$$

and

$$m_\mu = \beta m_\mu + \frac{2}{3} \beta^3 (m_\mu)^3 - \beta^3 m_\mu \bar{m}^2 + O(\bar{m}^4).$$

These equations, above $T = 1$, have only one solution, the paramagnetic state characterized by $\bar{m} = 0$ and $f = -T \log 2$. But this solution is unstable below $T_C = 1$: under this condition solutions with nonzero m start to appear.

Let us denote the number of nonzero components of \bar{m} as n . From the previous equation, permuting m_μ or changing the sign of each component generates equivalent solutions. It is possible to consider only the solutions such that the first n components are positive and the others are zero without loss of generality.

For $n = 1$, the remaining factors are:

$$f = \frac{1}{2} (m_1)^2 - \frac{1}{2} \log [2 \cosh (\beta m_1)]$$

$$m_1 = \tanh (\beta m_1).$$

These are the mean field solutions for the usual Ising model. Moreover this solution implies that the local magnetization is

$$\langle \sigma_i \rangle = \xi_i^1 \tanh (\beta m_1).$$

This state is equivalent to a ferromagnetic state under a gauge transformation $\sigma_i \rightarrow \sigma'_i = \xi_i^1 \sigma_i$ of spins. Consequently, there are 2^p equivalent states related to different memories and different signs of m : there are the Mattis states. These states are the global of free energy in the neighborhood of $T = 0$ and $T = 1$ and probably at all $T < 1$. In the limit $T \rightarrow 0$, for $n = 1$:

$$E(T = 0) = -\frac{1}{2},$$

$$\vec{m}(T = 0) = (1, 0, 0, \dots, 0)$$

and in general, for all values of n :

$$E = -\frac{1}{2} \vec{m}^2,$$

$$\vec{m} = \left\langle \left\langle \vec{\xi} \text{sign} (\vec{m} \cdot \vec{\xi}) \right\rangle \right\rangle.$$

In this phase, the equilibrium states are fully correlated to the learned patterns. These states give the main contribute to the thermodynamic of the system but also the solutions with $n > 1$ have an important role if they are the local minima of the free energy.

Let us consider the of solutions of equations (4.3) and (4.4) such that all n nonzero components have the same module:

$$\vec{m} = m_n (1, 1, \dots, 1, 0, 0, \dots, 0),$$

where the first n components have unitary values and the others $p - n$ components are zeros. There are

$$2^n \binom{p}{n}$$

possible solutions which are equivalent to the previous solution. These states exist for all temperature $T < 1$. The mean field equations for the symmetric states are then

$$f_n = \frac{n}{2} m_n^2 - \frac{1}{\beta} \langle \langle \log [2 \cosh (\beta m_n z_n)] \rangle \rangle$$

$$m_n = \frac{1}{n} \langle \langle z_n \tanh (\beta m_n z_n) \rangle \rangle$$

where

$$z_n^i = \sum_{\mu=1}^n \xi_i^\mu.$$

considering the probability distribution of each ξ_i^μ , the distribution of z_n^i is then

$$p(z_n) = \frac{1}{2^n} \binom{n}{\frac{(z_n+n)}{2}}.$$

$\frac{(z_n+n)}{2}$ is the number of positive ξ_i^μ which contributes to z_n^i .

It is possible to evaluate the behavior of such solutions expanding the previous functions at $T = 1$ and $T = 0$ (see [48] for details). At $T = 1$ the averages give:

$$\begin{aligned} \langle\langle f_n \rangle\rangle &\simeq -\frac{3n(T-1)^2}{4(3n-2)}, \\ m_n^2 &\simeq \frac{3(1-T)}{3n-2} \end{aligned}$$

$T = 1$ is the critical temperature for the appearance of all symmetric solutions. The equation relative to the free energy exhibits a monotonically increasing with n . This condition implies that for $n = 1$ the free energy assumes the lowest values, like the Mattis states:

$$\begin{aligned} \langle\langle f_1 \rangle\rangle &\simeq -\frac{3(T-1)^2}{4}, \\ m_n^2 &\simeq 3(1-T) \end{aligned}$$

At $T = 0$ the expansion gives two different results which differ if n is even or odd. For odd n :

$$\begin{aligned} \langle\langle f_{2k+1}(T=0) \rangle\rangle &= -\frac{2k+1}{2^{4k+1}} \binom{2k}{2}^2, \\ m_{2k+1}^2(T=0) &= \frac{1}{2^{2k}} \binom{2k}{2} \end{aligned}$$

and for even n :

$$\begin{aligned} \langle\langle f_{2k}(T=0) \rangle\rangle &= -\frac{2k}{2^{4k+1}} \binom{2k}{2}^2, \\ m_{2k}^2(T=0) &= \frac{1}{2^{2k}} \binom{2k}{2} \end{aligned}$$

All the functions of the sequence f_n is limited between $f_1 = -\frac{1}{2}$ and $f_2 = -\frac{1}{4}$. Moreover the sequence for even n is monotonically decreasing with k while the sequence with odd n is monotonically increasing, both with the limiting value $-\frac{1}{\pi}$ for $k \rightarrow \infty$ which coincides with the ground state energy per spin for a gaussian distribution of ξ^μ .

The difference between is evident analyzing the low temperature behavior of the Edwards Anderson order parameter:

$$q_n = \left\langle\left\langle \langle \sigma_i \rangle^2 \right\rangle\right\rangle = \left\langle\left\langle \tanh^2(\beta m_n z_n) \right\rangle\right\rangle.$$

If n is odd, the minimum value of $|z|$ is 1, then

$$q_n \simeq 1 - 2p(z_n = 1) e^{-2\beta m_n} \rightarrow 1$$

as $T \rightarrow 0$ For even n , the parameter at $T = 0$ is

$$q_n \simeq 1 - p(z_n = 0).$$

The solutions are obtained as solutions of saddle point equation:

$$\vec{m} = \frac{1}{N} \sum_{i=1}^N \vec{\xi}_i \tanh(\beta \vec{m} \cdot \vec{\xi}_i).$$

The local stability of these solutions is studied analyzing the eigenvalues of the Hessian matrix of the free energy:

$$H^{\mu\nu} = \frac{\partial^2 f}{\partial m^\mu \partial m^\nu}.$$

A detailed analysis (see again [48]) of these mean field solutions shows that the Mattis states are the only stable solutions near $T = 1$. At lower temperature the behavior is different: below a certain temperature $0 < T_n < 1$ (Numerical solutions: $T_3 = 0.461$, $T_5 = 0.385$ and $T_7 = 0.345$) some of the odd- n symmetric solutions became locally stable while all the even- n symmetric solutions are unstable for all T . At $T = 0$ all the odd- n solutions are stable and order fully.

When the temperature increases, some odd- n solutions change its stability in a certain direction. It does not usually exchange stability with another existing saddle point which lie in that direction. Instead, an asymmetric saddle point between the two existing saddle point appears. This situation is verified since the temperature is $T \simeq 0.575$ when the $n = 2$ symmetric solution $\vec{m} = (m, m, 0, 0, \dots, 0)$ became unstable due to the mixing of more memories.

4.3 Limit of finite α : from the retrieval to Spin Glass phase

Let us proceed with the analysis of properties of the equilibrium statistical mechanics of the Hamiltonian (4.1) in the limit of finite α [4, 50].

In this case, in the low temperature phase the random overlaps with most of patterns will be weak, typically of order $\frac{1}{\sqrt{N}}$. However, one, or a finite number of overlaps, could condense macroscopically, in other words, they will assume fixed and finite values as $N \rightarrow \infty$. In order to consider this possibility it is useful to introduce external fields, aligned to a finite number of patterns ($\{\xi_i^\nu\}_{1 \leq \nu \leq s}$). Then Hamiltonian will have a new term due to the presence of such external fields:

$$H[\sigma]_h = -\frac{1}{2} \sum_{i,j} J_{ij} \sigma_i \sigma_j - \sum_{\nu=1}^s h^\nu \sum_{i=1}^N \xi_i^\nu \sigma_i.$$

This approach is known as the Bogolyubov's method of quasiaverages.

Moreover the replica method is necessary to proceed the analysis. As seen in details for spin glasses in the previous chapter, it consists in computing the average free energy from the analytic continuation of the average of the partition function of

n uncoupled replicas of the initial system. Then the "replica trick" consists in first considering n as an integer and then taking the limit $n \rightarrow 0$ of the result.

This method is useful to evaluate the average free energy, in particular:

$$\lim_{n \rightarrow 0} f_n = -\frac{1}{\beta N} \lim_{n \rightarrow 0} \frac{1}{n} \log \langle \langle Z^n \rangle \rangle = -\frac{1}{\beta N} \langle \langle \log Z \rangle \rangle = \langle \langle f \rangle \rangle.$$

This property let compute the average of the free energy over the distribution of patterns without evaluate the average of $\log Z$ which is an approach technically difficult to deal with. The only function which is necessary to be averaged is the partition function.

The partition function of the n replicas is thus:

$$\begin{aligned} \langle \langle Z^n \rangle \rangle = & \left\langle \left\langle \sum_{\{\sigma_i^a\}_{\substack{1 \leq a \leq n \\ 1 \leq i \leq N}}} \exp \left[\frac{\beta N}{2} \sum_{a=1}^n \sum_{\mu=1}^p \left(\frac{1}{N} \sum_{i=1}^N \xi_i^\mu \sigma_i \right) \cdot \left(\frac{1}{N} \sum_{j=1}^N \xi_j^\mu \sigma_j \right) \right. \right. \\ & \left. \left. - \frac{\beta \alpha n}{2} N + \beta \sum_{\nu=1}^s h^\nu \sum_{i=1}^N \sum_{a=1}^n \xi_i^\nu \sigma_i^a \right] \right\rangle \right\rangle \end{aligned} \quad (4.5)$$

where a is the replica index over the n copies of the systems and h^ν are external fields coupled to the projections of the configurations on the first s pattern. Note that it is assumed that $s \ll p$.

Using the well-known property of gaussian:

$$\int_{-\infty}^{+\infty} dx e^{-\frac{k}{2}x^2 + Jx} = \sqrt{\frac{2\pi}{k}} e^{\frac{J^2}{2k}},$$

and setting the various parameters as:

$$J = \frac{1}{N} \sum_{i=1}^N \xi_i^\mu \sigma_i, \quad k = \frac{1}{\beta N}, \quad x = m_\mu^a N \beta,$$

then, the first term of the exponential in the above equation can be expressed as:

$$\begin{aligned} & \prod_{a=1}^n \prod_{\mu=1}^p \exp \left[\frac{\beta N}{2} \left(\frac{1}{N} \sum_{i=1}^N \xi_i^\mu \sigma_i \right) \cdot \left(\frac{1}{N} \sum_{j=1}^N \xi_j^\mu \sigma_j \right) \right] = \\ & \prod_{a=1}^n \prod_{\mu=1}^p \left\{ \int_{-\infty}^{+\infty} \left(\sqrt{\frac{N\beta}{2\pi}} dm_\mu^a \right) \exp N\beta \left[-\frac{1}{2} (m_\mu^a)^2 + m_\mu^a \frac{1}{N} \sum_{i=1}^N \xi_i^\mu \sigma_i^a \right] \right\}. \end{aligned}$$

Substituting this result in equation (4.5) we obtain:

$$\begin{aligned} \langle\langle Z^n \rangle\rangle &= \left\langle \left\langle e^{-\frac{\beta\alpha}{2}nN} \sum_{\{\sigma_i^a\}_{\substack{1 \leq a \leq n \\ 1 \leq i \leq N}}} \int \prod_{a=1}^n \prod_{\mu=s+1}^p \left(\sqrt{\frac{N\beta}{2\pi}} dm_\mu^a \right) \right. \right. \\ &\quad \left. \exp \left[N\beta \sum_{\mu=s+1}^p \sum_{a=1}^n \left(-\frac{1}{2} (m_\mu^a)^2 + m_\mu^a \frac{1}{N} \sum_{i=1}^N \xi_i^\mu \sigma_i^a \right) \right] \right. \\ &\quad \left. \int \prod_{a=1}^n \prod_{\nu=1}^s \left(\sqrt{\frac{N\beta}{2\pi}} dm_\nu^a \right) \right. \\ &\quad \left. \exp \left[N\beta \sum_{\nu=1}^s \sum_{a=1}^n \left(-\frac{1}{2} (m_\nu^a)^2 + (m_\nu^a + h^\nu) \frac{1}{N} \sum_{i=1}^N \xi_i^\nu \sigma_i^a \right) \right] \right\rangle \right\rangle. \end{aligned}$$

The sums and the products over ν and μ are respectively over the first s patterns and over the remaining $p - s$ patterns. The average over the first s ξ_i^ν 's describes the fact that these random variables are discrete while the average over the infinite number of other pattern (remember the limit $N \rightarrow \infty$ implies $p \rightarrow \infty$) become an average over a gaussian measure.

Then the average over ξ_i^μ 's is now made explicit:

$$\begin{aligned} \langle\langle Z^n \rangle\rangle &= e^{-\frac{\beta\alpha}{2}nN} \sum_{\{\sigma_i^a\}_{\substack{1 \leq a \leq n \\ 1 \leq i \leq N}}} \int \left(\prod_{i=1}^N \prod_{\mu=1}^p P(\xi_i^\mu) d\xi_i^\mu \right) \\ &\quad \int \prod_{a=1}^n \prod_{\mu=s+1}^p \left(\sqrt{\frac{N\beta}{2\pi}} dm_\mu^a \right) \exp \left[N\beta \sum_{\mu=s+1}^p \sum_{a=1}^n \left(-\frac{1}{2} (m_\mu^a)^2 + m_\mu^a \frac{1}{N} \sum_{i=1}^N \xi_i^\mu \sigma_i^a \right) \right] \\ &\quad \int \prod_{a=1}^n \prod_{\nu=1}^s \left(\sqrt{\frac{N\beta}{2\pi}} dm_\nu^a \right) \exp \left[N\beta \sum_{\nu=1}^s \sum_{a=1}^n \left(-\frac{1}{2} (m_\nu^a)^2 + (m_\nu^a + h^\nu) \frac{1}{N} \sum_{i=1}^N \xi_i^\nu \sigma_i^a \right) \right]. \end{aligned}$$

Let us focus on first member of the last equation, in particular let us now perform the average of the first exponential, over $p - s$ patterns. As seen before, the probability of each random variable ξ_i^μ is $P(\xi_i^\mu) = \frac{1}{2}\delta(\xi_i^\mu - 1) + \frac{1}{2}\delta(\xi_i^\mu + 1)$:

$$\begin{aligned} &\int \left(\prod_{i=1}^N P(\xi_i^\mu) d\xi_i^\mu \right) \exp N\beta \sum_{a=1}^n \left[-\frac{1}{2} (m_\mu^a)^2 + m_\mu^a \frac{1}{N} \sum_{i=1}^N \xi_i^\mu \sigma_i^a \right] \\ &= e^{-\frac{N\beta}{2} \sum_{a=1}^n (m_\mu^a)^2} \prod_{i=1}^N \left(\int P(\xi_i^\mu) d\xi_i^\mu \exp \beta \sum_{a=1}^n m_\mu^a \xi_i^\mu \sigma_i^a \right) \\ &= e^{-\frac{N\beta}{2} \sum_{a=1}^n (m_\mu^a)^2} \prod_{i=1}^N \cosh \left[\beta \sum_{a=1}^n m_\mu^a \sigma_i^a \right] \end{aligned}$$

Now it is useful to rescale the integration variables:

$$m_\mu^a \rightarrow \frac{m_\mu^a}{\sqrt{N}},$$

then the part of the first member relative to sums and products over μ results to be:

$$\int \prod_{a=1}^n \prod_{\mu=s+1}^p \left(\sqrt{\frac{\beta}{2\pi}} dm_\mu^a \right) \exp \sum_{\mu=s+1}^p \left[-\frac{\beta}{2} \sum_{a=1}^n (m_\mu^a)^2 + \sum_{i=1}^N \ln \cosh \left(\frac{\beta}{\sqrt{N}} \sum_{a=1}^n m_\mu^a \sigma_i^a \right) \right].$$

In the thermodynamic limit, $N \rightarrow \infty$, the function $\ln[\cosh(ax)]$ can be expanded as $\frac{(ax)^2}{2}$:

$$\int \prod_{a=1}^n \prod_{\mu=s+1}^p \left(\sqrt{\frac{\beta}{2\pi}} dm_\mu^a \right) \exp \sum_{\mu=s+1}^p \left[-\frac{\beta}{2} \sum_{a=1}^n (m_\mu^a)^2 + \frac{\beta^2}{2N} \sum_{i=1}^N \sum_{a=1}^n \sum_{b=1}^n m_\mu^a \sigma_i^a m_\mu^b \sigma_i^b \right].$$

Moreover the integration over m_μ^a gives:

$$\begin{aligned} & \left[\int \prod_{(a,b)} \delta \left(q_{ab} - \frac{1}{N} \sum_{i=1}^N \sigma_i^a \sigma_i^b \right) dq_{ab} \right] \times \\ & \prod_{\mu=s+1}^p \left[\int \prod_{a=1}^n \left(\sqrt{\frac{\beta}{2\pi}} dm_\mu^a \right) \exp \left[-\frac{\beta}{2} (1-\beta) \sum_{a=1}^n (m_\mu^a)^2 + \frac{\beta^2}{2} \sum_{a \neq b=1}^n m_\mu^a m_\mu^b q_{ab} \right] \right] \\ & = \left[\int \prod_{(a,b)} \delta \left(q_{ab} - \frac{1}{N} \sum_{i=1}^N \sigma_i^a \sigma_i^b \right) dq_{ab} \right] \times \\ & \prod_{\mu=s+1}^p \left[\int \left(\frac{\beta}{2\pi} \right)^{\frac{n}{2}} d\vec{m}_\mu \exp \left[-\frac{\beta}{2} (1-\beta) \vec{m}_\mu^T \mathbb{1} \vec{m}_\mu + \frac{\beta^2}{2} \vec{m}_\mu^T \mathbb{Q} \vec{m}_\mu \right] \right] \\ & = \left[\int \prod_{(a,b)} \delta \left(q_{ab} - \frac{1}{N} \sum_{i=1}^N \sigma_i^a \sigma_i^b \right) dq_{ab} \right] \prod_{\mu=s+1}^p \left[\frac{1}{\det [(1-\beta) \mathbb{1} - \beta \mathbb{Q}]} \right]^{\frac{1}{2}} \\ & = \int \prod_{(a,b)} dq_{ab} \exp \left[-\frac{p}{2} \text{Tr} \log [(1-\beta) \mathbb{1} - \beta \mathbb{Q}] \right] \times \\ & \prod_{(a,b)} \delta \left(q_{ab} - \frac{1}{N} \sum_{i=1}^N \sigma_i^a \sigma_i^b \right). \end{aligned}$$

The products over the couple (a, b) are over two replicas indexes such that $a < b$. \mathbb{Q} is the $n \times n$ matrix of overlap q_{ab} which has only $n(n-1)/2$ independent variables (remember that the overlap is symmetric: $q_{ab} = q_{ba}$). The last two lines are obtained using the property of gaussian integral in n -dimensional:

$$\begin{aligned} \int e^{-\frac{1}{2} \sum_{i,j=1}^N A_{ij} x_i x_j + \sum_{i=1}^N J_i x_i} d^N x &= e^{-\frac{1}{2} \vec{x}^T A \vec{x} + \vec{J}^T \vec{x}} d^N x \\ &= \frac{(2\pi)^{\frac{N}{2}}}{\sqrt{\det A}} e^{\frac{1}{2} \vec{J}^T A^{-1} \vec{J}} \\ &= \frac{(2\pi)^{\frac{N}{2}}}{\sqrt{\det A}} e^{\frac{1}{2} \sum_{i,j=1}^N A_{ij}^{-1} J_i J_j}. \end{aligned}$$

Now it is useful to write the delta function in another way in order to rewrite the last term as:

$$\int \prod_{(a,b)} dr_{ab} \int \prod_{(a,b)} dq_{ab} \exp \left[-\frac{p}{2} \text{Tr} \log [(1 - \beta) \mathbb{1} - \beta \mathbb{Q}] \right] \times \\ \exp \frac{N}{2} \left[-\alpha \beta^2 \sum_{a \neq b} r_{ab} q_{ab} + \frac{\alpha \beta^2}{N} \sum_{a \neq b} \sum_{i=1}^N r_{ab} \sigma_i^a \sigma_i^b \right].$$

Finally after the average over the $\{\sigma_i^a\}_{1 \leq a \leq n, 1 \leq i \leq N}$ and the quenched average, the partition function of the n replicas in (4.3) results to be:

$$\langle \langle Z^n \rangle \rangle = e^{-\frac{\beta \alpha}{2} n N} \int \prod_{(a,b)} dq_{ab} dr_{ab} \int \prod_{\nu}^s dm_{\nu}^a \times \\ \exp N \left[-\frac{1}{2} \beta \sum_a \sum_{\nu} (m_{\nu}^a)^2 - \frac{1}{2} \alpha \text{Tr} \log [(1 - \beta) \mathbb{1} - \beta \mathbb{Q}] - \alpha \beta^2 \sum_{a \neq b} r_{ab} q_{ab} \right] \times \\ \exp \left[\left\langle \left\langle \log \text{Tr}_{\{\sigma_i^a\}_{1 \leq a \leq n, 1 \leq i \leq N}} \exp \left[\frac{1}{2} \alpha \beta^2 \sum_{a \neq b} \sum_{i=1}^N \sigma_i^a \sigma_i^b + \beta \sum_a \sum_{\nu} (m_{\nu}^a + h^{\nu}) \xi^{\nu} \sigma_i^a \right] \right\rangle \right\rangle_{\xi} \right].$$

As $N \rightarrow \infty$, the integrals are dominated by the saddle point. Physically the parameters m_{μ}^a , q_{ab} and r_{ab} have meaning as a consequence of the saddle point equations.

m_{μ}^a is the overlap with a learned pattern:

$$m_{\mu}^a = \frac{1}{N} \left\langle \left\langle \sum_{i=0}^N \xi_i^{\mu} \langle \sigma_i^a \rangle \right\rangle \right\rangle,$$

q_{ab} is the Edwards-Anderson order parameter:

$$q_{ab} = \frac{1}{N} \left\langle \left\langle \sum_{i=1}^N \langle \sigma_i^a \rangle \langle \sigma_i^b \rangle \right\rangle \right\rangle,$$

and r_{ab} is the Lagrange multiplier:

$$r_{ab} = \frac{1}{\alpha} \sum_{\mu > s}^p \left\langle \left\langle \left[\frac{1}{N} \sum_{i=1}^N \xi_i^{\mu} \langle \sigma_i^a \rangle \right] \cdot \left[\frac{1}{N} \sum_{i=1}^N \xi_i^{\mu} \langle \sigma_i^b \rangle \right] \right\rangle \right\rangle \\ = \frac{1}{\alpha} \sum_{\mu=s+1}^{\alpha N} \left\langle \left\langle m_{\mu}^a m_{\mu}^b \right\rangle \right\rangle.$$

Then, after having evaluated the integrals with the saddle point, the free energy per spin in the limit $n \rightarrow 0$ results:

$$f_n = \frac{\alpha}{2} + \frac{1}{2n} \sum_{\nu=1}^s \sum_{a=1}^n (m_{\nu}^a) + \frac{\alpha}{2\beta n} \text{Tr} \log [(1 - \beta) \mathbb{1} - \beta \mathbb{Q}] + \frac{\alpha \beta}{2n} \sum_{a \neq b}^n r_{ab} q_{ab} - \frac{1}{n\beta} \langle \langle \log \mathbb{Z} \rangle \rangle$$

where

$$Z_0 = \text{Tr}_{\{\sigma_i^a\}_{\substack{1 \leq a \leq n \\ 1 \leq i \leq N}}} \exp \left(\frac{\alpha\beta^2}{2} \sum_{a \neq b}^n r_{ab} \sigma_i^a \sigma_i^b + \beta \sum_a \sum_\nu (m_\nu^a + h^\nu) \xi^\nu \sigma_i^a \right)$$

4.3.1 Symmetric replica solutions

Now the analysis continue using the replica symmetric ansatz. According to this approach, the possible free energies are restricted considering that all the replica of the system are thus equivalent and it is possible to set all the parameters equals:

$$\begin{aligned} m_\mu^a &= m_\mu^b & \forall \mu \\ q_{ab} &= q & a \neq b \\ r_{ab} &= r & a \neq b. \end{aligned}$$

Then, after having substituted these parameters in equation (4.6), we have to conclude the replica method computing the limit $n \rightarrow 0$. In order to make this computation let us consider the limit for single parts of equation (4.6).

1) Let us consider the matrix $(1 - \beta) \mathbb{1} - \beta \mathbb{Q}$. It has one eigenvalue $1 - \beta - (n - 1)q\beta$ and $n - 1$ eigenvalues $1 - \beta - q\beta$. Then the limit $n \rightarrow 0$ implies:

$$\begin{aligned} \lim_{n \rightarrow 0} \frac{1}{n} \text{Tr} \log [(1 - \beta) \mathbb{1} - \beta \mathbb{Q}] &= \lim_{n \rightarrow 0} \frac{1}{n} [\log (1 - \beta - (n - 1)q\beta) \\ &\quad + (n - 1) \log (1 - \beta - q\beta)] \\ &= \log (1 - \beta + q\beta) - \frac{q\beta}{(1 - \beta + q\beta)}. \end{aligned}$$

2) Then, the sum:

$$\lim_{n \rightarrow 0} \frac{1}{n} \sum_{a \neq b}^n r_{ab} q_{ab} = -qr.$$

3) The limit $n \rightarrow 0$ of the average over the distribution of pattern can be exchanged and can be seen as the average of the limit $n \rightarrow 0$:

$$\begin{aligned} &\lim_{n \rightarrow 0} \frac{1}{n} \left\langle \left\langle \log \left[\text{Tr}_{\{\sigma_i^a\}_{\substack{1 \leq a \leq n \\ 1 \leq i \leq N}}} e^{\left(\frac{\alpha\beta^2}{2} r \sum_{a \neq b}^n \sigma_i^a \sigma_i^b - \frac{1}{2} n \alpha \beta^2 r \right)} e^{(\beta \sum_a \sum_\nu (m_\nu^a + h^\nu) \xi^\nu \sigma_i^a)} \right] \right\rangle \right\rangle \\ &= -\frac{1}{2} \alpha \beta^2 r \\ &\quad + \lim_{n \rightarrow 0} \frac{1}{n} \left\langle \left\langle \log \int \frac{dz}{\sqrt{2\pi}} \left[-\frac{z^2}{2} + n \log 2 \cosh \left[\beta \sqrt{\alpha r} z + \beta (\vec{m} + \vec{h}) \cdot \vec{\xi} \right] \right] \right\rangle \right\rangle_\xi \\ &= -\frac{1}{2} \alpha \beta^2 r + \int \frac{dz}{\sqrt{2\pi}} e^{-\frac{z^2}{2}} \left\langle \left\langle \log 2 \cosh \left[\beta \sqrt{\alpha r} z + \beta (\vec{m} + \vec{h}) \cdot \vec{\xi} \right] \right\rangle \right\rangle_\xi. \end{aligned}$$

In conclusion, the resulting free energy per spin is:

$$\begin{aligned} f &= \frac{\alpha}{2} + \frac{1}{2} \sum_{\nu=1}^s (m_\nu) + \frac{\alpha}{2\beta n} \left[\log (1 - \beta + q\beta) - \frac{q\beta}{(1 - \beta + q\beta)} \right] + \frac{\alpha\beta}{2} r (1 - q) \\ &\quad - \frac{1}{\beta} \int \frac{dz}{\sqrt{2\pi}} e^{-\frac{z^2}{2}} \left\langle \left\langle \log 2 \cosh \left[\beta \sqrt{\alpha r} z + \beta (\vec{m} + \vec{h}) \cdot \vec{\xi} \right] \right\rangle \right\rangle_\xi. \end{aligned}$$

Then at the saddle points, obtained as the stationary states which minimize the last equation, the parameters m_μ^a , q_{ab} and r_{ab} are respectively:

$$m_\nu = \left\langle \left\langle \xi^\nu \tanh \left[\sqrt{\alpha r} z + (\vec{m} + \vec{h}) \cdot \vec{\xi} \right] \right\rangle \right\rangle, \quad (4.7)$$

$$q = \left\langle \left\langle \tanh^2 \left[\beta \sqrt{\alpha r} z + \beta (\vec{m} + \vec{h}) \cdot \vec{\xi} \right] \right\rangle \right\rangle, \quad (4.8)$$

$$r = \frac{q}{(1 - \beta + q\beta)^2}. \quad (4.9)$$

The average $\langle \langle \dots \rangle \rangle$ now is the combined average over the ξ^ν 's and over the gaussian noise z .

The results exhibit two components: a ferromagnetic contribute $\vec{m} \cdot \vec{\xi}$, due to the s condensed overlaps and a spin glass part $\sqrt{\alpha r} z$ due to the random overlap with the remaining patterns.

Equations (4.7), (4.8) and (4.9) have two kind of solutions: a solution such that $\vec{m} = 0$, $q, r \neq 0$, which is a Spin Glass state characterized by none macroscopic overlap. It does not contribute to associative memory. The other possibility is a ferromagnetic solutions which have also $\vec{m} \neq 0$: the system, when these solutions are verified, exhibits, for small α , associative memory.

4.3.2 Ferromagnetic solutions at $T = 0$

Ferromagnetic solutions are characterized by macroscopic overlap with a single learned pattern. These solutions have $2N\alpha$ degenerate solutions. In the limit $\alpha \rightarrow 0$ they approach the Mattis states as seen for finite p .

In the limit of zero temperature, $\beta \rightarrow \infty$,

$$\begin{aligned} \int \frac{dz}{2\pi} e^{-\frac{z^2}{2}} \tanh(\beta \sqrt{\alpha r} + \beta x) &= \sqrt{\frac{2}{\pi}} \int_0^{\frac{x}{\sqrt{\alpha r}}} dz e^{-\frac{z^2}{2}} + O\left(\frac{1}{\beta}\right) \\ &= \text{erf}\left(\frac{x}{\sqrt{2\alpha r}}\right) + O\left(\frac{1}{\beta}\right), \end{aligned}$$

equation (4.7) becomes:

$$m^\nu = \left\langle \left\langle \xi^\nu \text{erf} \left[\frac{1}{\sqrt{2\alpha r}} (\vec{m} + \vec{h}) \cdot \vec{\xi} \right] \right\rangle \right\rangle_\xi$$

where the average is over the discrete distribution of ξ_ν , $\nu = 1, \dots, s$.

The parameters result:

$$\begin{aligned} q &= 1 - CT \\ r &= \frac{1}{(1 - C)^2} \end{aligned}$$

where

$$C = \left(\frac{2}{\pi r \alpha} \right)^{\frac{1}{2}} e^{-\frac{m^2}{2r\alpha}}.$$

The parameters have always the solution with $m = 0$ which is the Spin Glass (SG) solution, with no macroscopic overlaps with any patterns. For $\alpha > \alpha_C = 0.138$

there is not other solutions with $m \neq 0$. Instead, for $\alpha < \alpha_C$, there are also the ferromagnetic solutions where $m \neq 0$. There are $2p$ of such kind of solutions. They appear at $\alpha = \alpha_C$ with an overlap $m = 0.967$.

In particular, the ferromagnetic solutions have macroscopic overlaps with the condensed patterns: these overlaps are close to unity and they exhibit associative memory. Moreover, while there is a macroscopic overlap with these patterns, they have very small overlaps with the other patterns and they are randomly distributed and of order $\frac{1}{\sqrt{N}}$.

The average energy per spin when the system exhibits a macroscopic overlap m with one of the learned patterns is:

$$\begin{aligned} E &= \left\langle \left\langle -\frac{1}{2N^2} \sum_{\mu=1}^p \sum_{ij} \xi_i^\mu \xi_j^\mu \sigma_i \sigma_j \right\rangle \right\rangle + \frac{\alpha}{2} \\ &= -\frac{m^2}{2} + \frac{\alpha}{2} (1 - r) \end{aligned}$$

At $\alpha = \alpha_C$, $E = -0.5014$, whereas as $\alpha \rightarrow 0$, for finite m , $E \rightarrow -0.5$. For finite α the system is able to slightly lower its energy by relaxing a small fraction of the spins, to accommodate for fluctuations in the overlap of the other patterns.

4.3.3 Spin Glass solutions at $T = 0$

Let us focus on the spin glass solution, where $m = 0$ and $q, r \neq 0$. As seen before, these conditions imply that:

$$r = \left[1 + \left(\frac{2}{\pi\alpha} \right)^{\frac{1}{2}} \right]^2$$

Moreover, using this last result, the energy of the spin glass state is equal to:

$$E = -\frac{1}{\pi} - \left(\frac{\pi\alpha}{2} \right)^{\frac{1}{2}}$$

In the limit $\alpha \rightarrow 0$, $E \rightarrow -\frac{1}{\pi}$ and $C = \sqrt{\frac{2}{\pi\alpha r}} \rightarrow 1$. This limit coincides with the value of E of the symmetric solutions in the p -finite case, where the state mix n patterns, in the limit $n \rightarrow \infty$. This implies that, as $p \rightarrow \infty$, the numerous states which mix many patterns merge to form the present spin glass phase. Comparing the energy of the spin glass and ferromagnetic states, the spin glass energy results to be lower in the range $0.051 < \alpha < 0.138$, whereas the ferromagnetic states becomes the absolute minimum below 0.051. Then at $\alpha = \alpha_C$ the spin glass state is definitely the ground state of the system.

Even for $\alpha > \alpha_C$ there are states with nonzero m which are stable to single spin flip. The number of these states will decay at finite T much faster than the thermodynamically stable or metastable ferromagnetic states below α_C , which are surrounded by barriers of order N .

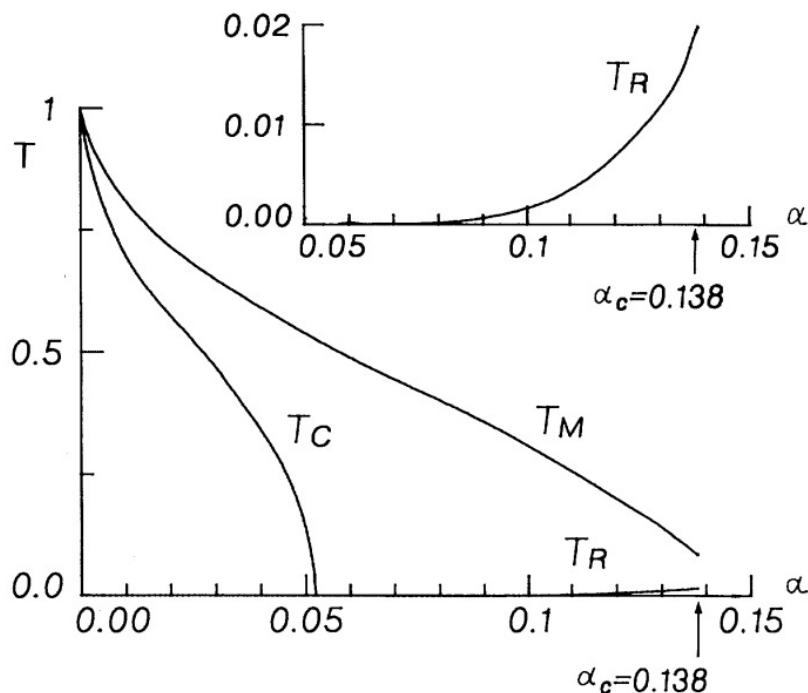


Figure 4.1: **Phase diagram for the Hopfield model.** The system exhibit three different phases. Under the curve T_C the phase is ferromagnetic: the states with $m \neq 0$ are the global minima of the free energy. In the limit $T \rightarrow 0$ the ferromagnetic phase persists since $\alpha < 0.051$. Above the T_M the system has a spin glass behavior: $m = 0$ and $q, r \neq 0$. In the limit $T \rightarrow 0$ the spin glass phase persists since $\alpha > 0.138$. Between T_C and T_M there is a "mixture" phase: there are also ferromagnetic states but they are only metastable states. In this phase the spin glass state is again the global minima of the free energy. The phase transition at T_C is a first-order transition at which the ferromagnetic states becomes global minima. These states start to appear under T_M in a discontinuous way. The curve T_R in the main plot is the instability temperature for replica symmetric solutions. In the upper box the instability temperature for broken replica symmetric solutions is plotted. This image is reproduced from [50].

4.3.4 Finite temperature solutions

The spin glass phase appears as T decreases via a second order transition. The expansions of equations (4.7) and (4.8) for $\vec{m} = \vec{h} = 0$ in powers of q and r gives the transition temperature T_g :

$$T_g = 1 + \sqrt{\alpha}.$$

Moreover, above $T = 1$ and below T_g there are only spin glass solutions for any α . For $\alpha < \alpha_C$, there are the ferromagnetic states with a single macroscopic overlap m . They appear as T decreases below $T_M(\alpha)$ but in a discontinuous way. The minimum value of T_M is 0.07, at $\alpha = \alpha_C$. As α goes to zero, T_M increases to the $T = 1$ and $m(T_M)$ go to zero, thus approaching the continuous transition of the

p -finite case. Near T_M , the ferromagnetic states are metastable. If $\alpha < 0.051$, these states become the global minima of f below a temperature $T_C(\alpha)$. At $T_C(\alpha)$, there is a thermodynamic first order transition from a spin glass to a ferromagnetic phase characterized by a discontinuous jump in m , q and r and by a latent heat.

$T_C(\alpha)$ varies increasing monotonically from 0 at $\alpha = 0.051$ to unity at $\alpha = 0$. Others ferromagnetic solutions appear for sufficiently small α and T . These solutions are characterized by \vec{m} with more than one nonzero components. As seen before, some of these "mixture" states are metastable but any of them is an absolute minimum at any T . This happened starting below $\alpha = 0.03$ where a locally stable solution with three symmetric overlaps appears.

So far we have assumed that replica symmetry is unbroken. This is clearly wrong at $T = 0$, where the entropy per spin is

$$S = -\frac{1}{2}\alpha \left[\log(1 - C) + \frac{C}{1 - C} \right]$$

with $C = \beta(1 + q)$. This is negative for all replica symmetric solutions and then is unphysical.

Moreover the condition of stability of the replica symmetric solutions is connected to the "eigenvalue"

$$\lambda = [1 - \beta(1 + q)]^2 - \alpha\beta \left\langle \left\langle \text{sech}^4 \left[\beta(r\alpha)^{\frac{1}{2}} z + \beta\vec{m} \cdot \vec{x}_i \right] \right\rangle \right\rangle.$$

The solutions are stable if this eigenvalue is positive. We find that $\lambda < 0$ in the spin glass solution, for $T < T_g$. On the other hand, the ferromagnetic solutions result to be stable in a finite temperature regime $T_R < T < T_M$. The instability temperature $T_R(\alpha)$ is shown in figure 4.1 for the states with single overlaps. It decreases very rapidly to zero with α as

$$T_R(\alpha) \sim \left(\frac{8\alpha}{9\pi} \right)^{\frac{1}{2}} e^{-\frac{1}{2\alpha}}.$$

It is possible to expand this analysis using the broken replica symmetry (see [2] for a general approach to broken replica symmetry). This approach is not expected to give substantial differences and it will not be presented there. For a detailed analysis about the broken replica symmetry see [4].

Chapter 5

Topological characterization of a Spin Glass transition

Nowadays the dynamical properties of Spin Glass systems are still of great interest for their peculiar characteristics. In general Spin Glasses exhibit energy landscapes characterized by the existence of many rugged valley structures due to the inherent frustration in the system: the free energy presents an exponential number of minima separated by free-energy barriers [51] which make difficult to approach the analysis of the dynamics. These properties make computationally expensive a complete simulation with a Monte Carlo approach or an exact evaluation.

In this chapter we will present an alternative approach to overcome these problems and to understand this complex dynamics inspired from studies of the energy landscape of glassy systems [5].

5.1 The Inherent Structure Approach

The starting point is to model a complex system as a network [6, 52, 53]. This kind of approach results intriguing: according to this kind analysis, a large number of complex systems from very different fields exhibit analogous emergent properties.

The main idea is to combine the methods taken from networks analysis to the usual techniques of complex system theory in order to outline the global structure of potential energy landscapes.

For a continuous system, the potential energy landscape is a multi-dimensional configuration space where the dependence of the potential energy is a function of the positions of all the atoms of the system. The landscape of a system with many atoms will present a complex topography with higher-dimensional minima, saddles and barriers. The topology of the landscape is thus strictly connected to the thermodynamics and to the dynamics of the system. In this context, the inherent structure approach of Stillinger and Weber [5] allows to simplify the analysis of such surface: the landscape is partitioned into basins of attraction surrounding each minima. In other words a basin of attraction is the set of every configurations which a local minimization of the potential energy maps to the same minimum. See figure (5.1) as example of the inherent structure approach for a Lennard-Jones system [6].

This partition provides a natural way to investigate the intrinsic properties of

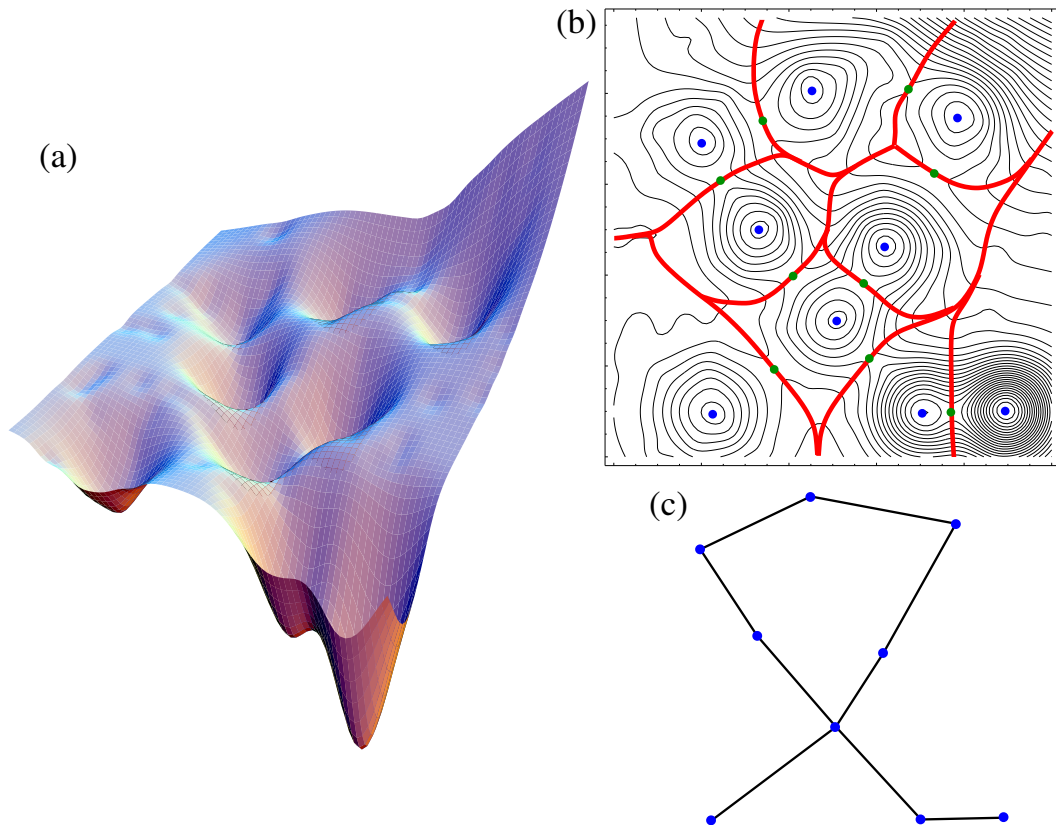


Figure 5.1: **Inherent structure approach for representing the potential energy landscape of a Lennard-Jones system.** (a) A two-dimensional energy surface. (b) The inherent structure partition. According to this approach, the landscape is partitioned into basins of attraction surrounding each minima. A basin of attraction is the set of every configurations which a local minimization of the potential energy maps to the same minimum. The basin boundaries are delimited by red lines, the minima and transition states by blue and green points. (c) The inherent structure network (ISN). The energy landscape can be represented as a network where the nodes are the basins and the edges are the saddles connecting them and the interminima dynamics can then be represented as a walk on this network. This image is reproduced from [6].

the potential energy landscape and to describe the dynamics of the system: if the temperature is low enough, a system spends most of the time around a minimum and only occasionally jumps to a different minimum by passing over a transition state. According to the latter approach the energy landscape can be represented as a network where the basins are nodes and the edges link those basins which are connected by a transition state. The interminima dynamics which describes the effect of a nonzero temperature on the system, can then be represented as a walk on this network. This kind of network is called *inherent structure network* (ISN).

The inherent structure approach can be a very useful tool to study the cooperative behavior of complex systems and gives enthusiastic results in contexts where configuration spaces are continuous [6]. An example of this approach for a Lennard-

Jones systems is presented in figure (5.1)).

Spin Glass models, like Sherrington-Kirkpatrick and Hopfield, analyzed in the previous chapters, present configuration spaces which are no more continuous: these spaces are discrete, they are a boolean hypercube. In this kind of spin systems definitions of saddles or transition states are not well defined and the inherent structure approach we have just presented is not easily applicable and it is necessary to develop a more general approach.

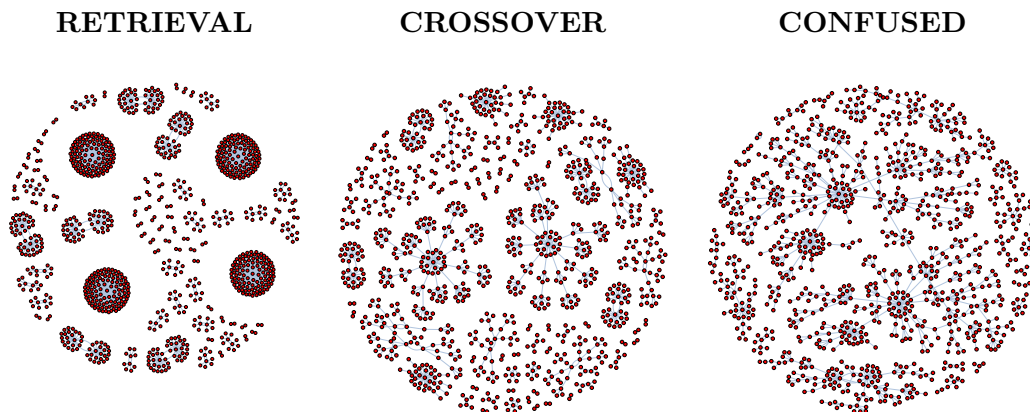


Figure 5.2: **Network schematic of Boolean Hopfield Networks with $N = 10$.** These networks are obtained from the Hopfield model with zero temperature synchronous dynamics. They are the complete graph of a single realization of p fixed memories. Topological properties in different phases can be directly observed. (a) $p = 2$, *retrieval phase*: the initial memories are the global minima of the system indeed the network exhibits $2p$ evident basin of attractions. Other attractors are metastable states or local minima. (b) $p = 3$, *crossover*: the dynamics is no more dominated only by memories attractors and glass states became to emerge. (c) $p = 10$, *confused phase*: the attractors of the dynamics are no more memories: now the attractors are the Spin Glass states and the number of basins of attraction grows exponentially with the size of the system. Networks are plotted using IGraph library [64].

5.2 Zero temperature synchronous dynamics: from Hopfield model to Boolean Hopfield Networks

The dynamical properties of random networks and disordered systems like glasses exhibit several qualitative features in common, for example the randomness of the topology of the energy landscape.

As seen before, the Hopfield model describes a network working as an associative memory and it exhibits the property of storing and retrieving informations even if given data are degraded. The system is defined by a set of boolean variables $\{\sigma_i\}$, neurons, that constitute the vertices of a complete graph with the same Hamiltonian:

$$H = -\frac{1}{2} \sum_{j \neq i} J_{ij} \sigma_i \sigma_j,$$

where the couplings are defined by choosing the set of p initial memories $\{\xi_i^\mu\}_{1 \leq \mu \leq P, 1 \leq i \leq N}$. For the present analysis the dynamics is a synchronous dynamics at $T = 0$ [58], each

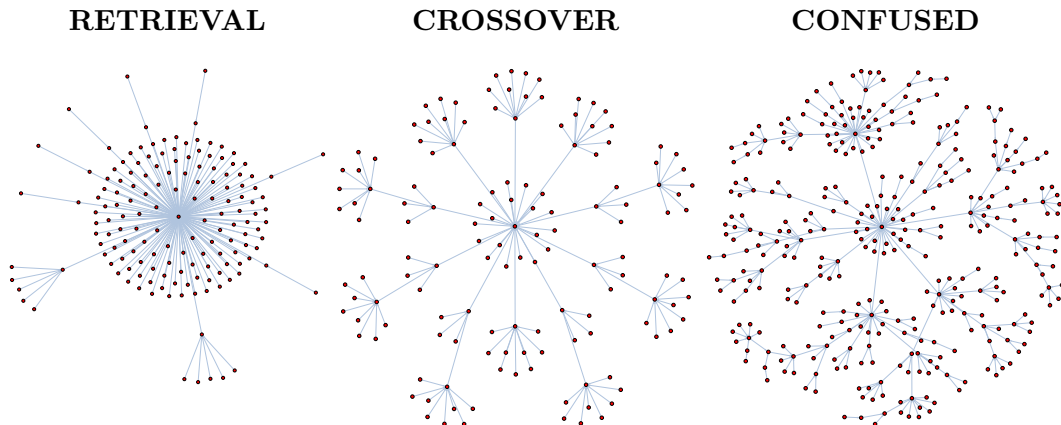


Figure 5.3: **Network schematic of Boolean Hopfield Networks with $N = 10$.** These networks are obtained from the Hopfield model with zero temperature synchronous dynamics. They are the main subgraph of a single realization of p fixed memories. Topological properties and the distribution of the number of incoming vertexes in different phases can be directly observed. (a) $p = 2$, *retrieval phase*: the initial memories are the global minima of the system. Indeed the others configurations tend to evolve into the memory. (b) $p = 3$, *crossover*: the dynamics is no more dominated only by memories attractors and glass states became to emerge. (c) $p = 10$, *confused phase*: the attractors of the dynamics are no more memories: now the attractors are the Spin Glass states and the number of basins of attraction grows exponentially with the size of the system. Networks are plotted using IGraph library [64].

neuron is updated at the same time according to the relation:

$$\sigma_i(t+1) = \text{sign} \left(\sum_j^N J_{ij} \sigma_j(t) \right). \quad (5.1)$$

If the sum results zero, the spin does not flip.

The Hopfield model equipped with this synchronous dynamics provide a natural cross-over between Spin Glass theory and Random Boolean Network.

As shown before for RBNs, it is possible to build a network starting from a synchronous dynamics: each configuration at time t is a node which is directly connected through an edge to the configuration in which evolves. In this case, for a given realization of memories, the dynamics is completely deterministic and consequently a topology can be univocally defined. This process gives rise to a new class of Random Boolean networks, generalizing the ones introduced by Kauffman, characterized by peculiar properties which would be linked to the original Hopfield phase transition which can be called *Boolean Hopfield networks*. Examples of this kind of networks for various number of memories corresponding to different phases of the Hopfield model are plotted in figure (5.2).

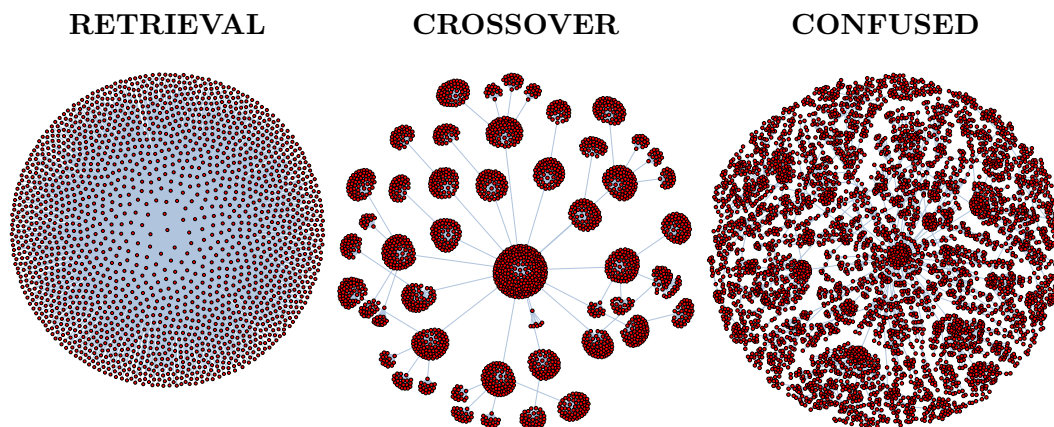


Figure 5.4: **Network schematic of Boolean Hopfield Networks with $N = 14$.** These networks are obtained from the Hopfield model with zero temperature synchronous dynamics. They are the main subgraph of a single realization of p fixed memories. Topological properties and the distribution of the number of incoming vertexes in different phases can be directly observed. (a) $p = 2$, *retrieval phase*: the initial memories are the global minima of the system. Indeed the others configurations tend to evolve into the memory. (b) $p = 3$, *crossover*: the dynamics is no more dominated only by memories attractors and glass states became to emerge. (c) $p = 14$, *confused phase*: the attractors of the dynamics are no more memories: now the attractors are the Spin Glass states and the number of basins of attraction grows exponentially with the size of the system. Networks are plotted using IGraph library [64].

Boolean Hopfield Networks exhibit a general behavior which is strictly related to the properties of the original Hopfield model. In order to investigate the hypotheses presented in the last statement it is useful to observe the distribution of configurations obtained through the spin dynamics. In figure (5.5) the probability that a randomly chosen configuration evolves into one of the p memories is plotted. This probability is computed through exact enumerations of the number of configurations evolving in memories and is the result of averages of various realizations over initial patterns (10000 realizations for systems with $N \leq 25$ and 100 for ones with $N = 30$). The restricted range of systems is due to the time of computation: the number of configurations of a given realization grows as a power of 2 increasing the dimension of the system and similarly the computation time since every evolve has to be valued. A single realization of a network with $N = 30$ spins needs 30 minutes while for $N = 35$ more than 8 hours.

5.3 Topological observables: a phase transition from compact to scale free networks

Thus the inherent structure approach gives an inspiration for studying the Hopfield model as a random boolean network: for a given realization of initial memories, the dynamics described by equation (5.1) defines univocally a topology on the phase

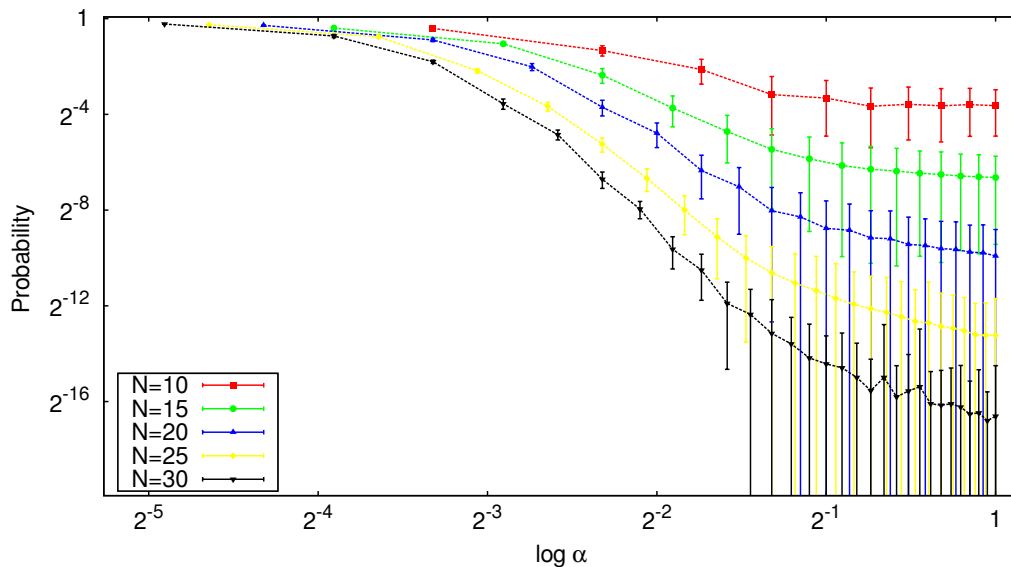


Figure 5.5: **Probability that a random configuration in a Boolean Hopfield Network evolves in one of the p memories as a function of $\alpha = p/N$.**

This probability is computed through exact enumerations of the number of configurations evolving in memories and is the result of averages over various realizations of initial patterns (10000 for $N \leq 25$ and 100 for $N = 30$). The errors are estimate with standard deviation. The restricted range of systems is due to the time of computation: the number of configurations of a given realization grows as a power of 2 increasing the dimension of the system and similarly the computation time since every evolute has to be obtained. A single realization for a network of $N = 30$ need 30 minutes while for $N = 35$ more than 8 hours. Both axes of this plot are in logarithmic scale.

space which can be well characterized through topological properties arising from such networks like the number of incoming connections of each node, the *indegree*, a parameter describing the weight of each node compared to the entire network, and the probability distribution of finding each configuration during the dynamical process. In the following sections we will present results concerned to this context.

5.3.1 Indegree: from compact support distributions to power laws

A network can exhibit an extraordinary complex structure and the connections among the nodes can constitute a range of complicated patterns. It is possible to characterize complex networks studying the degree of their nodes: the degree is defined as the number of edges linking other nodes, included itself. Since Boolean Hopfield Networks are built through a dynamics, they are directed. A direct network has two different degrees, the *indegree*, which is the number of incoming edges, and the *outdegree*, which is the number of outgoing edges. The synchronous dynamics defined by equation (5.1) is deterministic: each configuration evolves in the same state every time. Consequently all nodes of a Boolean Hopfield network has always outdegree 1. Indeed the distribution of indegree emphasizes the collective properties

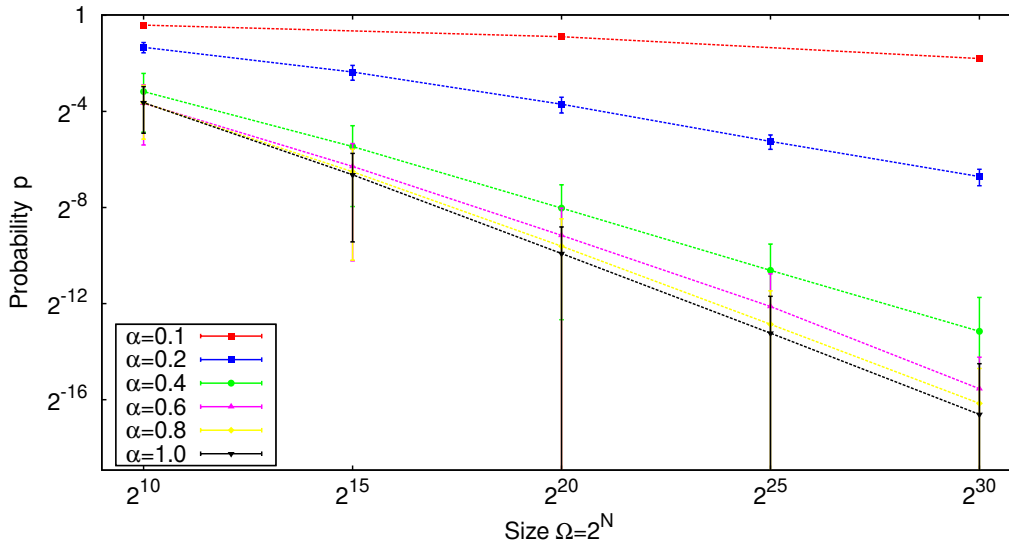


Figure 5.6: **System finite size scaling of the probability that a random configuration evolves in a memory.** The probabilities are plotted as a function of the size of system, 2^N , with $\alpha = p/N$ fixed in logarithmic scales. The errors are estimate with standard deviation. The property of retrieval is not a feature which depends on the number of memories p but it depends on the ratio between p and the number N of spins α . The validity of the last statement is qualitatively suggested by this plot. It is impossible to obtain more accurate results due to the fact that memories are discrete variables.

of networks.

The distribution of indegree in Boolean Hopfield Networks depends on the realization of initial memories: some results relative to a single realization are plotted in figure (5.7) for various numbers of memories. The average distributions computed over 1000 networks are presented in figure (5.9) for various numbers of memories. These graphics are obtained with a logarithmic binning in base 2 on both axes.

The results are relative to finite systems with limited sizes for computational reasons: a configuration is described as a string of N boolean variables and it can be represented efficiently as a binary number, an integer variable. Each integer variable in C++ allocates 4 bytes. A vector containing all 2^N possible configurations of a system will occupy 2^{2N} bytes. For example, exact simulations of a system of only $N = 30$ spins will need 4 gigabytes of RAM.

The distribution of the indegree shows clearly different properties varying the number of memories of the system.

Let us consider the details of the distributions for a single realization varying α .

A system built with only one memory has pathologic behavior: the distribution of indegree exhibits two deltas, one corresponding to indegree 0, which represents configurations which evolve in the memories, one to indegree $2^{N-1} - 1$, representing the memory and its symmetric: the \mathbb{Z}_2 symmetry of the Hopfield model effects

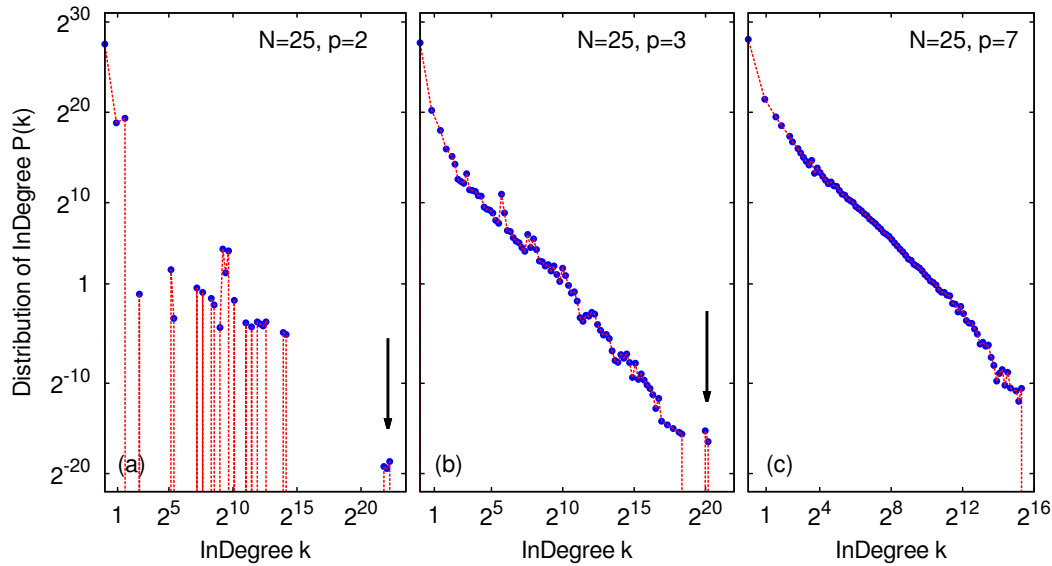


Figure 5.7: **Distributions of *indegree* of a single realization of systems with $N = 25$.**

The distribution of the indegree shows clearly different properties varying the number of memories of the system.

(a) *Retrieval* regime, $p=2$: in the few memories case the distribution exhibits two deltas corresponding configurations with zero indegree and memories with an huge indegree. Moreover there are other deltas with intermediate values of indegree: they are due to the presence of nodes with nonzero indegree in the memories basins of attraction which eventually evolve in memories in a few steps.

(b) *Crossover* regime, $p = 3$: the distribution for intermediate number of memories is a power law overlapping two deltas like in the few memories regime. In this case memories are anyway attractors of the dynamics but now saddles points and Spin Glass states are emerging from the spin glass phase.

(c) *Confused* regime, $p = 7$: increasing the memories the distribution is clearly a power law. The complex behavior of the dynamics is reflexed in the network topology: memories are no more the attractors and the basins of attractions depend on the Spin lass solutions in the Hopfield model.

These graphics are obtained with a logarithmic binning in base 2 on both axes.

Boolean Hopfield Networks too. The dynamical behavior is clear: all configurations evolve in the memory and its symmetric. This kind of characterization depends strictly on the parity of the number of spins: the are two deltas in system where N is even but when N is odd indegree distributions have the same appearance as for few memories systems. The case characterized by a few number of memories exhibits again two deltas corresponding to configurations with zero indegree and memories with an huge indegree. Moreover the distribution has other deltas with intermediate values of indegree. As an example see plot (a) of figure (5.7). The dynamical process is a bit complicated: there are also nodes with nonzero indegree belonging to the basins of attraction of the memories. They eventually evolve in memories in a few

steps. The opposite case is characterized by a big number of memories. As an example see plot (c) in figure (5.7). The distribution is clearly a power law: this kind of Boolean Hopfield Networks are *scale free*. This statement means that they contain multiple groups of nodes with more edges within a group and less connections among groups. The complex behavior of the dynamics is reflexed in the network topology: memories are no more the attractors and the basins of attractions depend on the Spin Glass solutions of the Hopfield model.

Between these two cases there is a crossover regime which contains peculiarities from both previous cases. See plot (b) in figure (5.7). The distribution is again a power law merging with the two deltas like in the few memories regime: memories are again the dynamical attractors but now saddles points and Spin Glass states are emerging from the Spin Glass phase.

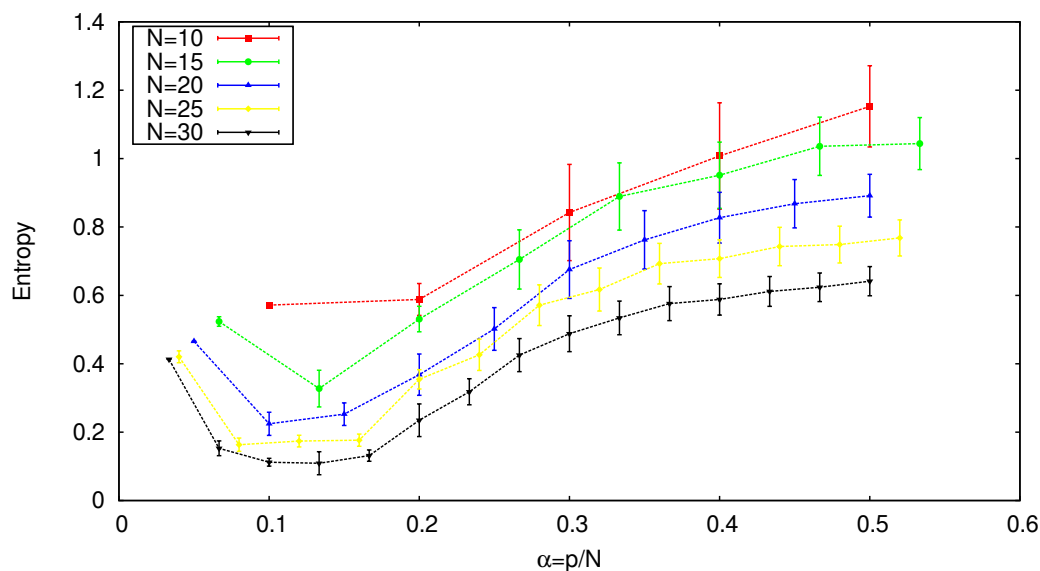


Figure 5.8: **Averaged entropy of the indegree distributions.** The entropy constitutes a measure of randomness of the distribution of indegree. There the averaged entropy is plotted as a function of $\alpha = p/N$ for various sizes. The averages are over 1000 realizations for $N \leq 25$ and 300 for $N = 30$ and the errors are estimate with standard deviation. The entropy exhibits the analogous behavior for different sizes. It is possible to observe a qualitative change of the slope of the curves in different regimes like seen with distributions of indegree: the entropy assumes his minimum values in the few memories phase and seems to tend to a maximum value in the Confused phase. The restricted sizes of networks do not allow to determinate carefully this trend. In addition Hopfield networks defined from one memory have different values bigger than the few memories regime. This property is due to the pathological distributions of indegree characterized by only two deltas.

In Boolean Hopfield Networks, the distribution of indegree depends strictly on the initial p memories which define the coupling constants of the original Hopfield model. It is useful to introduce a notion of probability in order to generalize the properties analyzed so far. The probability p that a node has indegree k can be

defined from its frequency, the ratio between number of configurations which have indegree k and the total number of states 2^N , $p : [0, 2^N] \rightarrow [0, 1]$,

$$p : k \mapsto \frac{\#(k)}{2^N}$$

such that $\sum_{k=0}^{2^N} p(k)$. Then it is possible to define the *entropy* function for a realization of initial memories:

$$S_J(p) = - \sum_{k=0}^p (k) \ln(k).$$

This definition of entropy is strictly related to the initial memories and constitutes a measure of randomness of the distribution of indegree. In figure (5.8) the averaged entropy is plotted for various sizes of the system as a function of $\alpha = p/N$ for various sizes. The entropy exhibits the same behavior for different sizes: the trends corresponding to the few memories regime and to the Confused phase show clearly how the general properties of entropy do not depend on the size. Consequently the qualitative changes of regimes are the same seen in distributions of indegree: the entropy assumes his minimum values in the few memories phase and seems to tend to a maximum value in the Confused phase. The restricted sizes of networks do not allow to determinate carefully this trend. In addition Boolean Hopfield networks defined from one memory have different values bigger than the few memories regime. This property is due to the pathological distributions of indegree characterized by only two deltas.

The averaged distributions of indegree exhibits again three regimes varying the number of memories of the system (see figure 5.9).

Again the average distributions of systems built from only one memory are pathologic: every realizations have the same distribution with two deltas and so it is for the average. In the phase characterized by a few number of memories (for example see plot (a) in figure 5.9) the averaged distribution exhibits a coexistence of a compact support distribution and a peak. This kind of outlier is called *Dragon King*: as we have seen in chapter on complex systems, according to Sornette the presence of Dragon Kings reveal the existence of mechanisms of self-organization that otherwise is not possible to observe from the distribution of the other events and could be associated to phase transitions. In this particular class of Random Boolean Network, the peak in the distribution of indegree is a consequence of a condensation of configurations which converge to a limited number of configurations, which results to be memories. This Dragon King is present only at this stage and is reabsorbed by increasing the memories until it disappears completely in the full Confused phase. The regime characterized by a big number of memories (see plot (c) in figure 5.9) presents an averaged distribution which is a power law. Again the Spin Glass solutions of the Hopfield model prevail and affect the topology of Boolean Hopfield networks: memories are no more the attractors. The crossover regime contains peculiarities from both previous cases. See plot (b) in figure (5.9). The averaged distribution is again a power law overlapping the two deltas like in the few memories regime: the Dragon King suggests that memories are again the

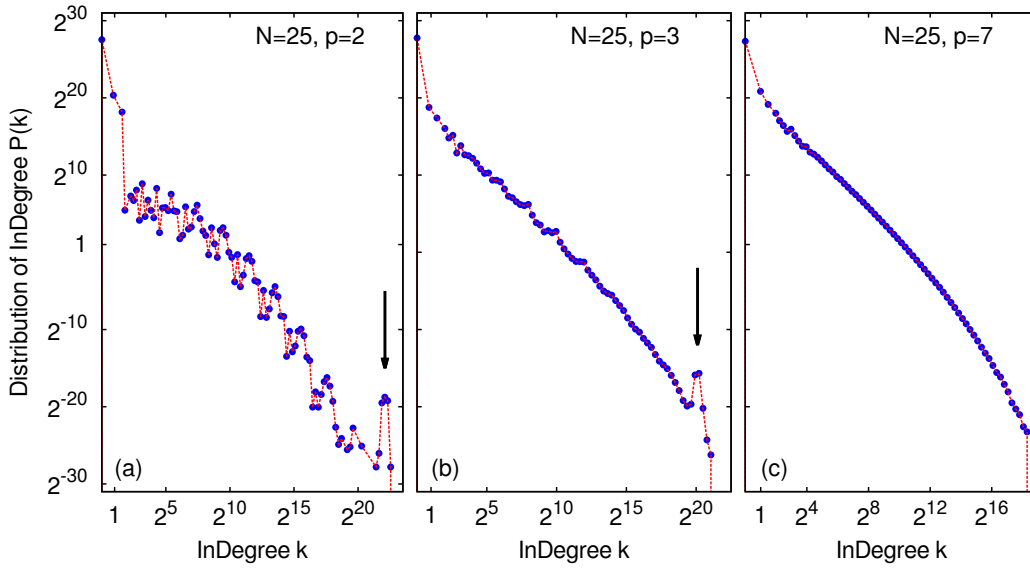


Figure 5.9: **Averaged distributions of indegree for systems with $N = 25$.**

Averaged distributions of the indegree show clearly different peculiarities varying the number of memories of the system.

(a) *Retrieval* regime, $p=2$: in the few memories case the averaged distribution exhibits a coexistence of a compact support distribution and a peak. This kind of outlier is called *Dragon King*: this peak is a consequence of a condensation of configurations which converge to a limited number of configurations, which results to be memories. This Dragon King is present only at this stage and is reabsorbed by increasing the memories until it disappears completely.

(b) *Crossover* regime, $p = 3$: the distribution for intermediate number of memories is a power law overlapping two deltas like in the few memories regime. The Dragon King suggests that memories are again the dynamical attractors but now saddles points and Spin Glass states are emerging from the Spin Glass phase.

(c) *Confused* regime, $p = 7$: increasing the memories the averaged distribution is a power law. Again the Spin Glass solutions of the Hopfield model prevail and affect the topology of Hopfield networks: memories are no more the attractors.

These graphics are obtained averaging over 1000 realizations and plotted with a logarithmic binning in base 2 on both axes.

dynamical attractors but now saddles points and Spin Glass states are emerging from the Confused phase.

The averaged distribution of indegree allows to characterize qualitatively the transitions through the various regimes described so far. The distributions varies clearly and the phase transition can be described as a transition from a compact network, for the few phase memories, to a *scale free* network, in Confused phase. The presence of Dragon Kings which is reabsorbed by increasing the memories completes the peculiarities of this topological observable.

The scaling exponent, which determines the power laws of the averaged distributions of indegree, can be considered as a parameter to characterize more quan-

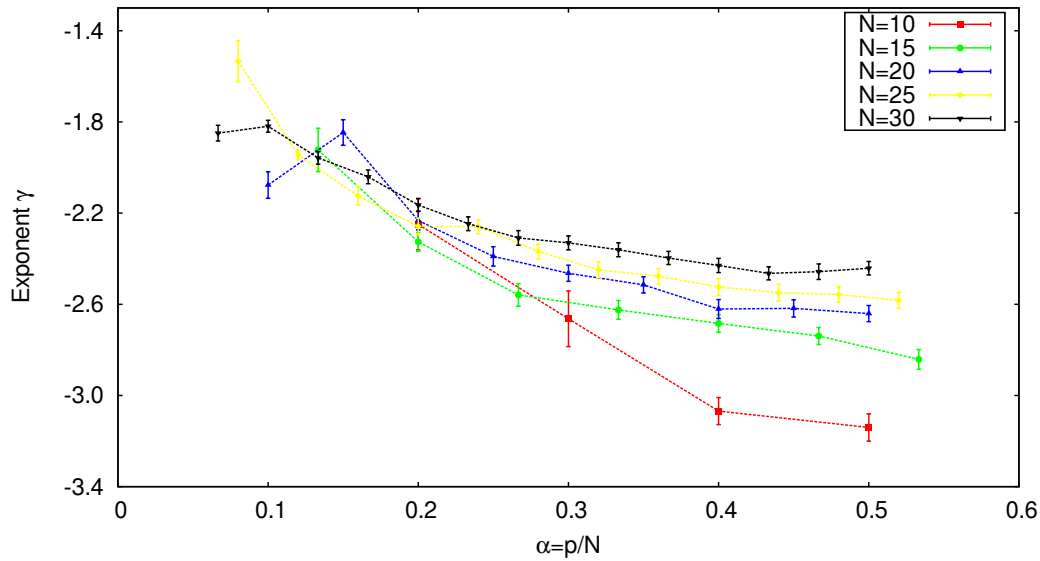


Figure 5.10: **Scaling exponent of the averaged distribution of indegree.**

The scaling exponent, which describes the power laws of the averaged distributions of indegree, can be considered as a parameter to characterize more quantitatively the transition. The scaling exponents exhibit similar behaviors for different sizes and shows clearly different peculiarities corresponding to the few memories regime and to Confused phase. The power laws has been fitted with the distribution $p(k) = Ck^{-\gamma}$ through the maximum likelihood estimator as seen in the previous section about power laws. Every lines corresponds to the exponent as a function of α for a different sizes of the system.

The averages are over 1000 realizations for $N \leq 25$ and 300 for $N = 30$.

tatively the transition. In the chapter on complex systems we have studied the power law probability distribution $p(k) = Ck^{-\gamma}$ and how to fit this kind of functions through the maximum likelihood estimator. In figure 5.10 the scaling exponents are plotted as a function of $\alpha = p/N$ for various sizes. The scaling exponents exhibit similar behaviors for different sizes and again shows clearly different peculiarities corresponding to the few memories regime and to Confused phase. The results give support to the hypotheses that the scaling exponent has a universal form which seems to independent of the size. The exponent of the power law, $\gamma \approx 2.6$, is similar to other scale-free networks [59]. The cause of the random-graph like scaling of the average separation is thus the scale-free topology of the ISN. The network is extremely heterogeneous with a few hubs that have a very large number of connections, but with the majority of nodes only connected to a relatively small number of other minima.

The finite systems which can be exactly investigated give only a weak indications of the transition in Boolean Hopfield Networks, it is necessary to continue the analysis with a numerical approach.

5.3.2 Google Rank: a numerical approach

The results presented so far are interesting but confined due to the limited sizes. As seen before, an exact analysis for systems bigger than $N = 30$ is not realizable because it requires excessive processing resources since configuration spaces dimensions grow as 2^N . Consequently it is necessary a numerical approach.

A naive method could be the computation of the probability distribution of finding each configuration during the dynamical process with a trivial Monte Carlo method. For example the sampling could consist of picking N random configurations $\{\sigma_i\}$ and computing evolve configurations through the spin dynamics. Unfortunately this kind of approach underrate the sampling space and it is not interesting at all.

A more effective tool of network theory is the Google Rank.

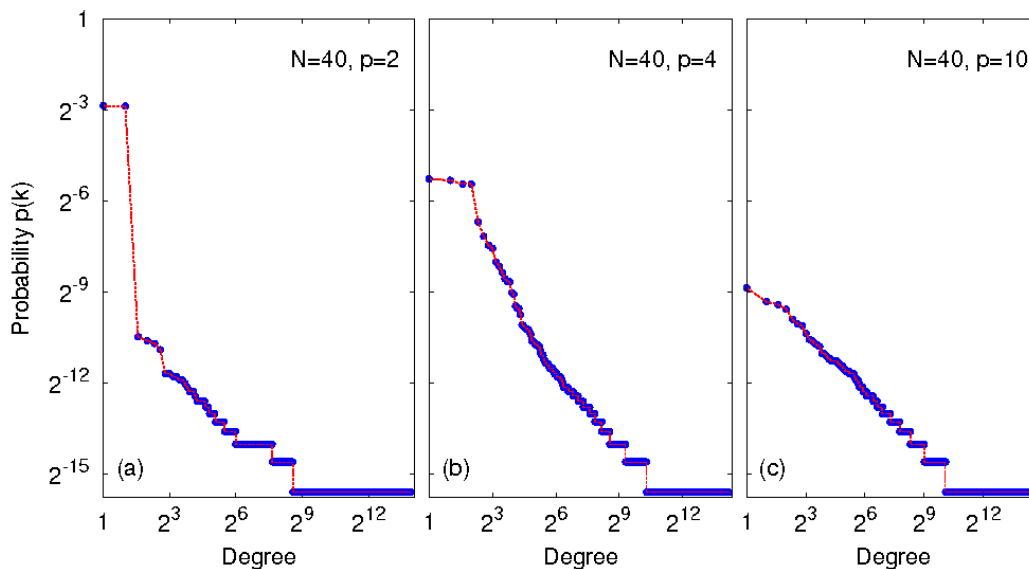


Figure 5.11: **Google Rank Plot of a single Boolean Hopfield Network with $N = 40$.**

The Google Rank algorithm has been performed with $d = 2$ deterministic steps and with 10000 random jumps. In this case the \mathbb{Z}_2 symmetry is taken in account: a configuration and its symmetric contribute in the same way. It is possible to identify again three regimes.

(a) *retrieval* phase, $p = 2$: there is a compact step distribution which exhibits a plateau associated to the memories. The number of configuration of this plateau are exactly the number of memories.

(b) *critical* phase, $p = 4$: the distribution is now a power law. The plateau is reabsorbed by increasing the memories.

(c) *spin-glass* phase, $p = 10$: the distribution is simply a power law.

The growing World-Wide Web requires effective ranking methods in order to optimize the web search. The Google Rank algorithm was originally developed as a quantitative method for analyze connectivities in this context. Interesting results with Google Rank have been obtained in ecology [54] and in the citation network in

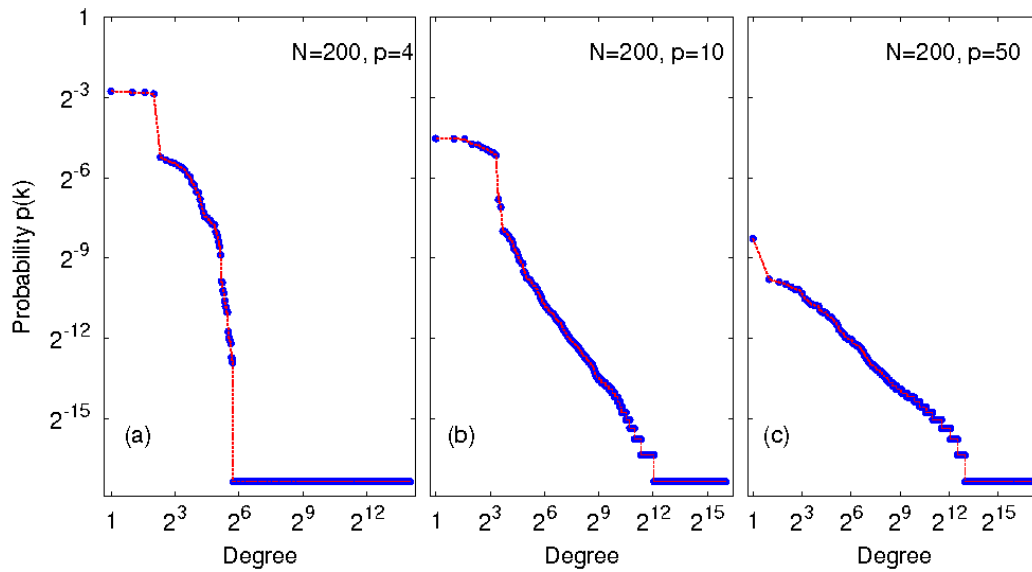


Figure 5.12: **Google Rank Plot of a single Boolean Hopfield Network with $N = 200$.** The Google Rank algorithm has been performed with $d = 16$ deterministic steps and with 10000 random jumps. In this case the \mathbb{Z}_2 symmetry is taken in account: a configuration and its symmetric contribute in the same way. For a bigger three regimes can be easily identified. (a) *retrieval* phase, $p = 4$: there is a compact step distribution which exhibits a plateau associated to the memories. The number of configuration of this plateau are exactly the number of memories. (b) *critical* phase, $p = 10$: the distribution is now a power law. The plateau is reabsorbed by increasing the memories. (c) *spin-glass* phase, $p = 50$: the distribution is simply a power law.

papers of American Physical Society [55].

In the following topic we will use a variant of the algorithm. The Google Rank has been developed in order to quantify numerically the relative importance of an element of network within the network itself. In this case, a surfer is placed on a randomly chosen vertex of the network. Then its position is changed according to the following dynamics: for d times the surfer jumps to the neighboring vertex according to the synchronous spin dynamics. Then the surfer gets bored and starts again from a randomly selected vertex. Consequently the Google Rank gives higher weight to configurations that are the evolutes of configurations and have higher indegree and also weights configurations which are the attractors of the spin dynamics. Because of these attributes, this method identifies a large number of special configurations which are the most outstanding in Boolean Hopfield Networks.

The Google Rank is thus applied to Boolean Hopfield Networks.

In figures (5.11) and (5.12) are shown the Google Rank for single realizations with various sizes as a function of the rank, a number associated to each configuration ordered decreasing the corresponding Google Rank. Analogous analysis have been performed averaging over the possible memories. Results are plotted in figures (5.13) and (5.14) with different sizes.

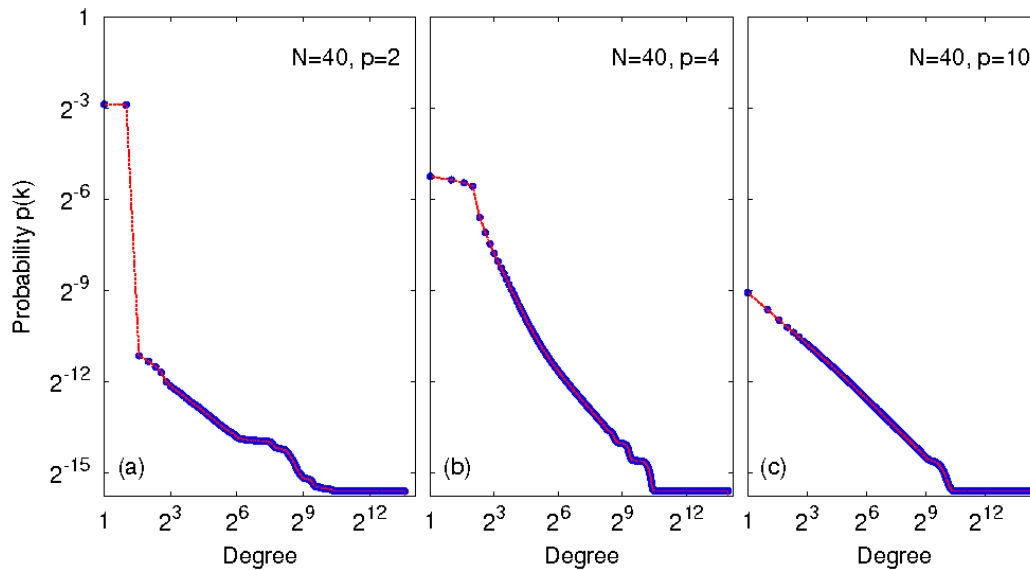


Figure 5.13: **Averaged Google Rank Plot of Boolean Hopfield Networks with $N = 40$.** The Google Rank algorithm has been performed with $d = 2$ deterministic steps and with 10000 random jumps. In this case the \mathbb{Z}_2 symmetry is taken in account: a configuration and its symmetric contribute in the same way. For a bigger three regimes can be easily identified. (a) *retrieval* phase, $p = 2$: there is a compact distribution which exhibits a plateau associated to the memories. The number of configuration of this plateau are exactly the number of memories. (b) *critical* phase, $p = 4$: the distribution is now a power law. The plateau is reabsorbed by increasing the memories. (c) *spin-glass* phase, $p = 10$: the distribution is simply a power law.

Even the Google Rank suggests the presence of a collective behavior characterized by the phase transitions described so far with indegree distributions. Again, in the phase characterized by a few number of memories, the *retrieval regime*, the Google Rank exhibits an overlap of a distinct plateau consisting of configurations corresponding to memories, and a distribution with compact support. Examples are plotted in (a) in figures (5.13) and (5.14). This kind of plateau is directly linked to Dragon Kings seen in distributions of indegree: the plateau is present only at this stage and is reabsorbed by increasing the memories until it disappears completely. Indeed, confirming this statement, the plateau is less defined in the critical regime, as can be seen in plots (a) of figures (5.13) and (5.14).

The scale-free topology of the Spin Glass phase in Boolean Hopfield Networks suggests a reflection on global optimization, the task of locating the global minimum. In the Spin Glass phase attractors are also the minima of the Hopfield Hamiltonian and searching the global minimum is a NP-hard problem. NP-hard in computational complexity theory is a class of problems that are at least as hard as the hardest problems in which proof are verifiable in polynomial time by a deterministic Turing machine. This kind of systems, although the number of minima increases exponentially with the size of the system, as a class of scale-free networks, has also the

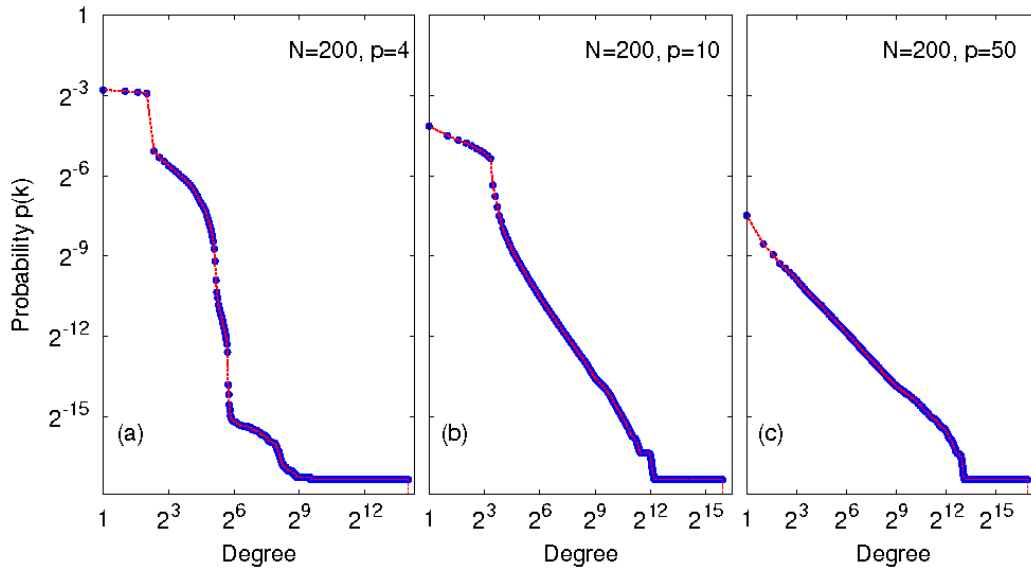


Figure 5.14: **Averaged Google Rank Plot of Boolean Hopfield Networks with $N = 200$.** The Google Rank algorithm has been performed with $d = 16$ deterministic steps and with 10000 random jumps. In this case the \mathbb{Z}_2 symmetry is taken in account: a configuration and its symmetric contribute in the same way. For a bigger three regimes can be easily identified. (a) *retrieval* phase, $p = 4$: there is a compact distribution which exhibits a plateau associated to the memories. The number of configuration of this plateau are exactly the number of memories. (b) *critical* phase, $p = 10$: the distribution is now a power law. The plateau is reabsorbed by increasing the memories. (c) *spin-glass* phase, $p = 50$: the distribution is simply a power law.

property of small-world: their diameter increases logarithmically with the number of vertices [62]. Consequently they have to present an average number of steps in the shortest path to the global minimum which grows sublinearly with system size. Of course, finding the shortest path is not obvious: the process which determines this path is not trivial and required information about the global energy landscape, whereas a global optimization algorithm usually takes a step based on only local information. Some methods which aim to find the shortest path to efficiently navigate scale-free networks have been suggested using the property that most of the shortest paths pass through highly-connected hubs [60, 61].

In Spin Glass phase there is a connection between the topology of a Boolean Hopfield Network and the energy landscape which could provides an additional advantageous strategy in global optimization. The increasing number of links as the energy decreases can be seen in figure (5.17) for a single realization of initial memories. This dependence results to be a power law.

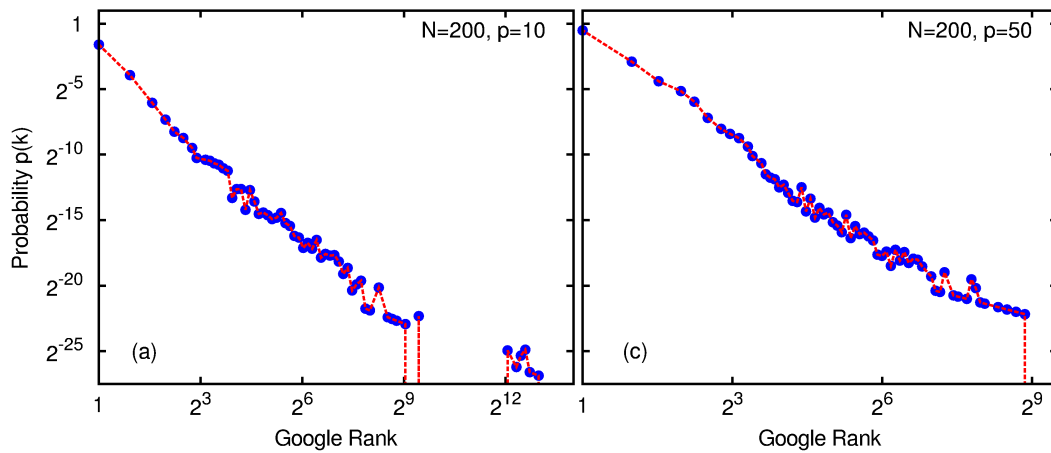


Figure 5.15: **Probability distribution of Google Rank Plot of a single realization of Boolean Hopfield Networks with $N = 200$.** The Google Rank algorithm has been performed with $d = 16$ deterministic steps and with 10000 random jumps. In this case the \mathbb{Z}_2 symmetry is taken in account: a configuration and its symmetric contribute in the same way. (a) *critical* phase, $p = 10$: the distribution is now a power law. A delta is linked to memories as in the indegree distribution. (b) *spin-glass* phase, $p = 50$: the distribution is simply a power law.

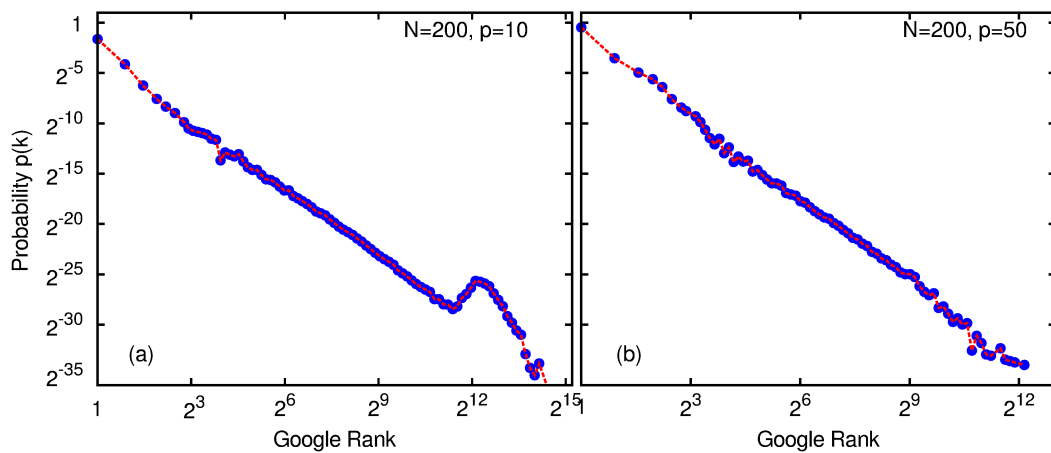


Figure 5.16: **Averaged probability distribution of Google Rank Plot of Boolean Hopfield Networks with $N = 200$.** The Google Rank algorithm has been performed with $d = 16$ deterministic steps and with 10000 random jumps. The average is over 250 realizations. In this case the \mathbb{Z}_2 symmetry is taken in account: a configuration and its symmetric contribute in the same way. (a) *critical* phase, $p = 10$: the distribution is now a power law. A delta is linked to memories as in the indegree distribution. (b) *spin-glass* phase, $p = 50$: the distribution is simply a power law.

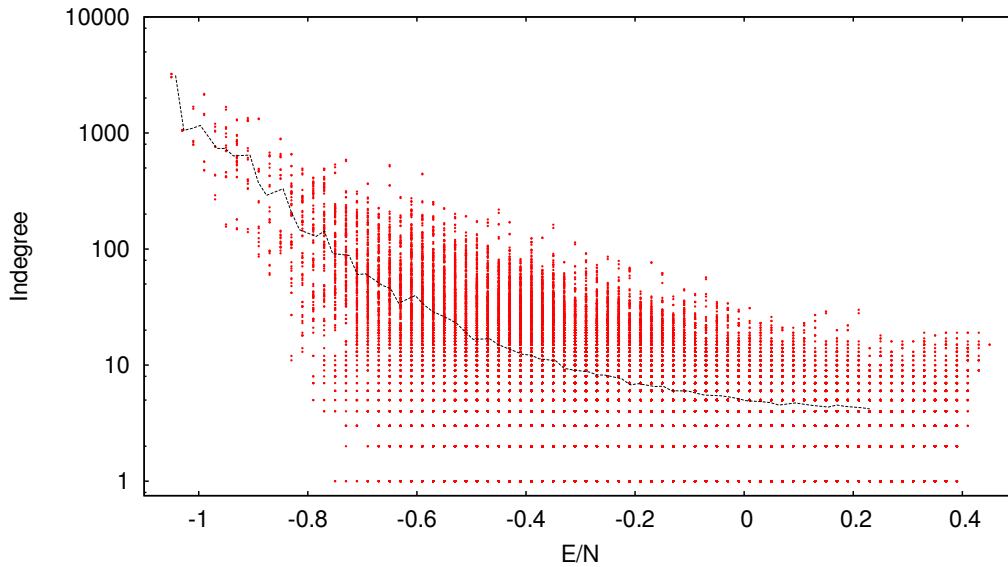


Figure 5.17: **The dependence of the indegree of a node on the energy of corresponding configuration for a system with $N = 20$ spins and 20 memories.** The data points are for each node of a relation and the solid line is a binned average. The indegree is plotted in logarithmic scale.

5.4 Conclusions

The main results are related to the Hopfield model with a zero temperature synchronous dynamics. This dynamics, according to the method inspired from the Inherent Structure Approach, generates a new class of Random Boolean Networks that we called *Random Hopfield Network*. This approach allows to define univocally a topology on the phase space which can be characterized through topological properties arising from such networks like the number of incoming connections of each node, the *indegree*, a parameter describing the weight of each node compared to the entire network, and the probability distribution of finding each configuration during the dynamical process.

It is fundamental to underline how geometric these considerations are sufficient to characterize these phase transitions in the context of Random Boolean Networks as an alternative to the standard approach using overlap between configuration and local magnetization as order parameters. We have presented strong evidences of phase transition in the context of networks theory: Boolean Hopfield Networks exhibit a transition from compact networks in the regime of few memories to scale free networks in the Spin Glass phase. This transition can be characterized in terms of the distributions of connectivities: the properties of such systems change substantially varying α , the rate between the number of memories p and of spins N . The collective behavior originating from Hopfield model emerges clearly also in this approach of network analysis: transitions from compact distributions to power law distributions which are present both for indegrees and for Google Ranks are fundamental mainstay of this work. Dragon Kings in indegree distributions and

plateaus obtained with Google Rank complete the description of the few memories phase: networks condenses to a regime where the most of configurations converges to a limited number of configurations, the memories. Memories are definitively the attractors of the dynamics and coincide to the absolute minima of the Hamiltonian.

For what concerns the spin glass phase, it would be interesting to understand if the scale free network is a feature peculiar to Hopfield model, or more in general (as we suspect), is a general characteristic of spin glass models. We have preliminary evidences that the same scale free graph is also obtained in the SK and K-sat models.

Bibliography

- [1] D. Sherrington, S. Kirkpatrick, *Solvable Model of a Spin-Glass*, Phys. Rev. Lett. 35, 1792 (1975)
- [2] M. Mezard, G. Parisi, M. A. Virasoro, *Spin Glass Theory and Beyond*, World Scientific (1987)
- [3] J. J. Hopfield, *Neural networks and physical systems with emergent collective computational abilities*, Proc. Natl. Acad. Sci. USA, 79, 2554 (1982)
- [4] D. J. Amit, H. Gutfreund, H. Sompolinsky, *Statistical Mechanics of Neural Networks near Saturation*, Ann. Phys. 173, 30-67 (1987)
- [5] F. H. Stillinger, T. A. Weber, *Packing Structures and Transitions in Liquids and Solids*, Science 225, 983 (1984)
- [6] J. P. K. Doye, *network topology of a potential energy landscape: a static scale-free network*, Phys. Rev. Lett. 88, 238701 (2002)
- [7] S. A. Kauffman, *Metabolic Stability and Epigenesis in Randomly Constructed Genetic Nets*, J. Theoret. Biol. 22, 437-467 (1969)
- [8] D. Sornette, *Dragon-Kings, Black Swans and the Prediction of crises*, International Journal of Terraspace Science and Engineering <http://arxiv.org/abs/0907.4290> (2009)
- [9] P. W. Anderson, *More is different*, Science, 177, 393-396 (1972)
- [10] N. Goldenfeld, L. P. Kadanoff, *Simple Lessons from Complexity*, Science, 284, 87-89 (1999)
- [11] D. Sornette, *Probability Distributions in Complex Systems*, <http://arxiv.org/abs/0707.2194> (2009)
- [12] A. Clauser, C. R. Shalizi, M. E. J. Newman, *Power-law distributions in empirical data*, <http://arxiv.org/abs/0706.1062> (2007)
- [13] D. Sornette, *Critical Phenomena in Natural Sciences*, Springer, Berlin (2006)
- [14] J. Bouchaud, *Weak ergodicity breaking and aging in disordered systems*, J. Phys. I, 2, 1705-1713 (1992)

-
- [15] M. E. J. Newman, *Power laws, Pareto distributions and Zipf's law*, <http://arxiv.org/abs/cond-mat/0412004> (2004)
- [16] N. N. Taleb, *The Black Swan: The Impact of the Highly Improbable*, Random House (2007)
- [17] J. Laherrère, D. Sornette, *Stretched exponential distributions in nature and economy: Fat tails with characteristic scales*, *European Physical Journal B*, 2, 525-539 (1999)
- [18] A. Barabási, R. Albert, *Emergence of Scaling in Random Networks*, *Science*, 286, 5439, 509-512 (1999)
- [19] R. Albert, A. Barabási, *Statistical mechanics of complex networks*, *Rev. Mod. Phys.* 74, 47 (2002)
- [20] B. Bollobás, O. Riordan, *The diameter of a scale-free random graph*, *Random Structures Algorithms* 18, 279-290 (2001)
- [21] S. A. Kauffman, *The Origins of Order: Self-Organization and Selection in Evolution*, Oxford University Press (1993)
- [22] M. Aldana, S. Coppersmith, L. Kadanoff, *Boolean Dynamics with Random Couplings*, *Nonlinear Sciences archive* <http://arxiv.org/abs/nlin/0204062> (2002)
- [23] C. Gershenson, *Introduction to random Boolean networks*, <http://arxiv.org/pdf/nlin/0408006.pdf> (2004)
- [24] S. A. Kauffman, C. Peterson, B. Samuelsson, C. Troein, *Genetic networks with canalizing Boolean rules are always stable*, *Proc Natl Acad Sci USA*, 101(49), 17102–17107 (2004)
- [25] S. A. Kauffman, C. Peterson, B. Samuelsson, C. Troein, *Random Boolean network models and the yeast transcriptional network*, *Proc Natl Acad Sci USA*, 100(25), 14796–14799 (2003)
- [26] F. Li, T. Long, Y. Lu, Q. Ouyang, C. Tang, *The yeast cell-cycle network is robustly designed*, *Proc Natl Acad Sci USA*, 101(14), 4781–4786 (2004)
- [27] B. Drossel, *Random Boolean Networks* <http://arxiv.org/abs/0706.3351> (2007)
- [28] S. H. Strogatz, *Exploring Complex Networks* *Nature*, 410, 268-276 (2001)
- [29] B. Samuelsson, C. Troein, *Superpolynomial Growth in Number of Attractors in Kauffman Networks*, *Phys. Rev. Lett.* 90, 098701 (2003)
- [30] B. Derrida, G. Weisbuch, *Evolution of overlaps between configurations in random Boolean networks*, *Journal de Physique*, 47 (8), 1297-1303 (1986)
- [31] B. Derrida, Y. Pomeau, *Random networks of automata: a simple annealed approximation*, *Europhys. Lett.* 1, 45 (1986)
-

-
- [32] D. L. Stein, *Spin Glasses: Still Complex After All These Years?*, De-coherence and Entropy in Complex Systems, Springer (2004)
- [33] S. F. Edwards, P. W. Anderson, *Theory of spin glasses*, J. Phys. F: Met. Phys. 5 965 (1975)
- [34] V. Dotsenko, *An introduction to the theory of spin glasses and neural networks*, World Scientific (1994)
- [35] C. De Dominicis, I. Giardinà, *Random Fields and Spin Glasses, a Field theory Approach*, Cambridge University Press (2006)
- [36] G. Parisi, *Order parameter for spin-glasses*, Phys. Rev. Lett. 50, 1206 (1983)
- [37] P. C. Whitford, K. Y. Sanbonmatsu, J. N. Onuchic, *Biomolecular dynamics: order-disorder transitions and energy landscapes*, Rep. Prog. Phys. 75, 076601 (2012)
- [38] S. Kim, S. J. Lee, J. Lee, *Ground-state energy and energy landscape of the Sherrington-Kirkpatrick spin glass*, Phys. Rev. B 76, 184412 (2007)
- [39] A. Crisanti, L. Leuzzi, G. Parisi, T. Rizzo, *Spin-Glass Complexity*, Phys. Rev. Lett., 92, 127203 (2004)
- [40] T. Aspelmeier, A. J. Bray, M. A. Moore, *The Complexity of Ising Spin Glasses*, Phys. Rev. Lett. 92, 087203 (2004)
- [41] A. Cavagna, I. Giardinà, G. Parisi, *Numerical Study of Metastable States in Ising Spin Glasses*, Phys. Rev. Lett., 92, 120603 (2004)
- [42] S. Kim, S. J. Lee, J. Lee, *Ground-state and energy landscape of the Sherrington-Kirkpatrick spin glass*, Phys. Rev. B, 76, 184412 (2007)
- [43] J. Feng, B. Tirozzi, *Capacity of the Hopfield model*, J. Phys. A: Math. Gen. 30, 3383–3391 (1997)
- [44] B. Derrida, H. Flyvbjerg, *Multivalley structure in Kauffman's model: analogy with spin glasses*, J. Phys. A: Math. Gen. 19, L1003 (1986)
- [45] D.C. Mattis, *Solvable Spin Systems with Random Interactions*, Phys. Lett. A 56, 421 (1976)
- [46] J. Luttinger, *Exactly Solvable Spin-Glass Model*, Phys. Rev. Lett. 37, 778 (1976)
- [47] L. A. Pastur, A. L. Figotin, *Exactly soluble model of a spin glass*, Sov. J. Low Temp. Phys. 3 (6), 378-383 (1977)
- [48] D. J. Amit, H. Gutfreund, H. Sompolinsky, *Spin-glass models of neural networks*, Phys. Rev. A, 32, 1007 (1985)
- [49] J. P. Provost, G. Vallee, *Ergodicity of the Coupling Constants and the Symmetric n -Replicas Trick for a Class of Mean-Field Spin-Glass Models*, Phys. Rev. Lett. 50, 598 (1983)
-

-
- [50] D. J. Amit, H. Gutfreund, H. Sompolinsky, *Storing infinite numbers of patterns in a spin-glass model of neural networks*, Phys. Rev. Lett., 55, 1530 (1985)
- [51] A. Cavagna, I. Giardina, G. Parisi, *Numerical Study of Metastable States in Ising Spin Glasses*, Phys. Rev. Lett. 92, 120603 (2004)
- [52] L. Angelani, G. Parisi, G. Ruocco, and G. Viliiani, *Connected Network of Minima as a Model Glass: Long Time Dynamics*, Phys. Rev. Lett. 81, 4648 (1998).
- [53] S. Carmi, S. Havlin, C. Song, K. Wang, H. A. Makse, *Energy-landscape network approach to the glass transition*, <http://arxiv.org/abs/0808.2203>
- [54] S. Allesina, M. Pascual, PLoS Comput Biol 5(9) (2009) *Googling Food Webs: Can an Eigenvector Measure Species' Importance for Coextinctions?*
- [55] S. Maslov, S. Redner, *Promise and Pitfalls of Extending Google's PageRank Algorithm to Citation Networks*, The Journal of Neuroscience, 28 (44) (2008)
- [56] D. J. Watts, S. H. Strogatz, *Collective dynamics of 'small world' networks*, Nature, 393, 440 (1998)
- [57] R. Albert, H. Jeong, A. L. Barabasi, *Diameter of the world wide web*, Nature, 401, 130 (1999)
- [58] E. Gardener, B. Derrida, P. Mottishaw, *Zero temperature parallel dynamics for infinite range spin glasses and neural networks*, J. Physique 48, 741 (1987)
- [59] R. Albert, A. L. Barabasi, *Statistical Mechanics of Complex Networks*, Rev. Mod. Phys. 74, 47 (2002)
- [60] L. A. Adamic, R. M. Lukose, A. R. Puniyani, B. A. Huberman, *Search in Power-Law Networks*, Phys. Rev. E 64, 046135 (2001)
- [61] B. J. Kim, C. N. Yoon, S. K. Han, H. Jeong, *Path finding strategies in scale-free networks*, <http://arxiv.org/abs/cond-mat/0111232> (2001)
- [62] L. A. N. Amaral, A. Scala, M. Barthélemy, H. E. Stanley, *Classes of small-world networks*, Proc Natl Acad Sci USA, 97(21), 11149–11152 (2000)
- [63] Wolfram Research, Inc., Mathematica, Version 10.0, Champaign, IL <http://www.wolfram.com/mathematica/> (2014)
- [64] *IGraph reference manual for Python*, <http://igraph.org/python>
-